Structural and functional analyses of polycystins

Dissertation

zur Erlangung des Doktorgrades
der Naturwissenschaften (Dr. rer. Nat.) der Fakultät für Biologie und
vorklinische Medizin der Universität Regensburg

Vorgelegt von
Katrin Brunner, geb. Pohl
aus Pfarrkirchen

Regensburg, 2021

Das Promotionsgesuch wurde eingereicht am:

Die Arbeit wurde angeleitet von: Prof. Dr. Ralph Witzgall

Unterschrift:

Contents

Abstract

The autosomal-dominant polycystic kidney disease (ADPKD) is the most common monogenic disorder with a prevalence of 1:400-1:1000. This inherited multisystem disease is characterized by renal and extrarenal fluid-filled cysts which are progressively growing during a patient's course of disease. In approximately 70 % patients suffer from end-stage renal disease (ESRD) at a mean age of 58 years making it the fourth leading cause of ESRD globally. This disease can arise by mutations in the genes *PKD1* (85 %) or *PKD2* (15 %). Both genes encode for the proteins polycystin-1 and polycystin-2 respectively. The membrane protein polycystin-1 comprises a huge extracellular N-terminus with different repetitive motifs like the PKD domains. Those domains are present in 16 copies but only little information about their functional relevance is known yet. Polycycystin-1 can interact by its C-terminal domain with the second relevant membrane protein polycystin-2 which was suggested to be a calcium conducting cation channel present in the endoplasmic reticulum and in the primary cilia. In recent years, contradicting results were published about the calcium conduction so that this was questioned intensively. In this thesis, two subprojects were investigated in the context of ADPKD concerning 1) the function of the first PKD domain as a representative of the 16 domains in putative ligand-binding and 2) the conduction properties of polycystin-2 by comparing the wild-type protein with an established functional mutant protein with an exchanged pore region. Regarding the first aim, comparison of NMR spectra of expressed and purified ^{15}N-labeled *PKD1* PKD domain 1 that was measured before and after incubation with urine of an ADPKD patient or with urine of a control person did not show alterations in the detected peaks. This suggests that compounds of the urine does not bind to the PKD domain 1 implying that this domain is not involved in ligand binding. In terms of aim 2, *in vitro* and *in vivo* measurements revealed that the mutant protein polycystin-2$^{\text{poreL1}}$ showed higher intracellular calcium levels compared to the wild-type protein after stimulation with vasopressin or ATP agreeing with the recent doubts of a calcium conductivity of polycystin-2 rather suggesting a passive role in calcium homeostasis. The presented data contribute to better understand the complex cellular processes proceeding in ADPKD to encourage research for making this disease more endurable for patients.

1 Introduction

The human body is a very complex system where synthesis, maintenance and removal of substances is of high importance to keep up a healthy running state. To ensure correct procedures in all the different metabolic pathways contributing to this healthy state, the body is compartimentalized into organs to have areal segregation with specialized functions. All of these organs have their tasks to maintain a physiological condition and one very important organ is the kidney. A kidney is a paired organ consisting of two bean-shaped parts symmetrically located below the rib cage. The blood passes the kidney about 300 times every day and thereby, toxins produced in the body are filtered out and extra fluid is removed to maintain a healthy balance of water, salts and minerals. Approximately 170 L of primary urine are thereby produced that further concentrate to ~1.7 L of urine after the organ's filtration and reabsorbtion processes. Organs are further segregated into sub-areas where different sub-tasks can be performed. Also the kidney shows a high complexity where different segments are responsible for many specialized purposes (Schmidt et al., 2011).

1.1 Anatomical, physiological and structural basics

There are several diseases where functions of the different kidney segments are disturbed finally leading to an end-stage renal disease with a kidney transplant as the only chance for the patients to escape. Since this is a very drastic way out, researchers all over the world are interested in investigating the disease-causing genes and the encoded proteins located in the complex structures of the kidney and the pathways taking place to find an alternative to an organ transplant.

In the following subsections, more details are shown on the kidney development and anatomy with its very complex composition contributing to the proper function of the organ. Not only the tubular system will be described but also a structure which is suggested to be important for maintaining this system will be specified.

1.1.1 Kidney development and anatomy

Kidney development, also known as 'nephrogenesis', proceeds in mammals similarly but certain time points of developmental steps vary among species, all comprising an interaction of epithelial, mesenchymal and stromal cells. In humans, metanephrogenesis starts in week five of gestation, when an interaction between the ureteric bud and the metanephrogenic mesenchyme occurs. With this epithelial transformation a polarization and a *de novo* lumen formation begins induced by the ureteric bud when it starts to grow, differentiate and branch into the upper urinary tract. The growing cranial end of the ureteric bud is evolving in further branching events to the collecting duct system and thereby, also the major and minor calyces and the renal pelvis are formed. Around each tip of a ureteric bud branch, mensenchymal cells condensate and form vesicles that are further progressing into comma-shaped bodies. From this, S-shaped bodies arise that further progress to a capillary loop stage and by clustering of endothelial cells, a glomerolus is finally formed. By further elongation and growing, the whole tubular system arises and in week 35 after gestation, nephrogenesis and kidney vasculature is completed with about 1'000'000 nephrons (see Fig. 1.1) (Langman, 1975). Since the tubular structures arising during nephrogenesis have to be defined carefully, a regulatory circuit is speculated to be involved in the adjustment of tubular diameters but exact processes and components of this regulation remain elusive.

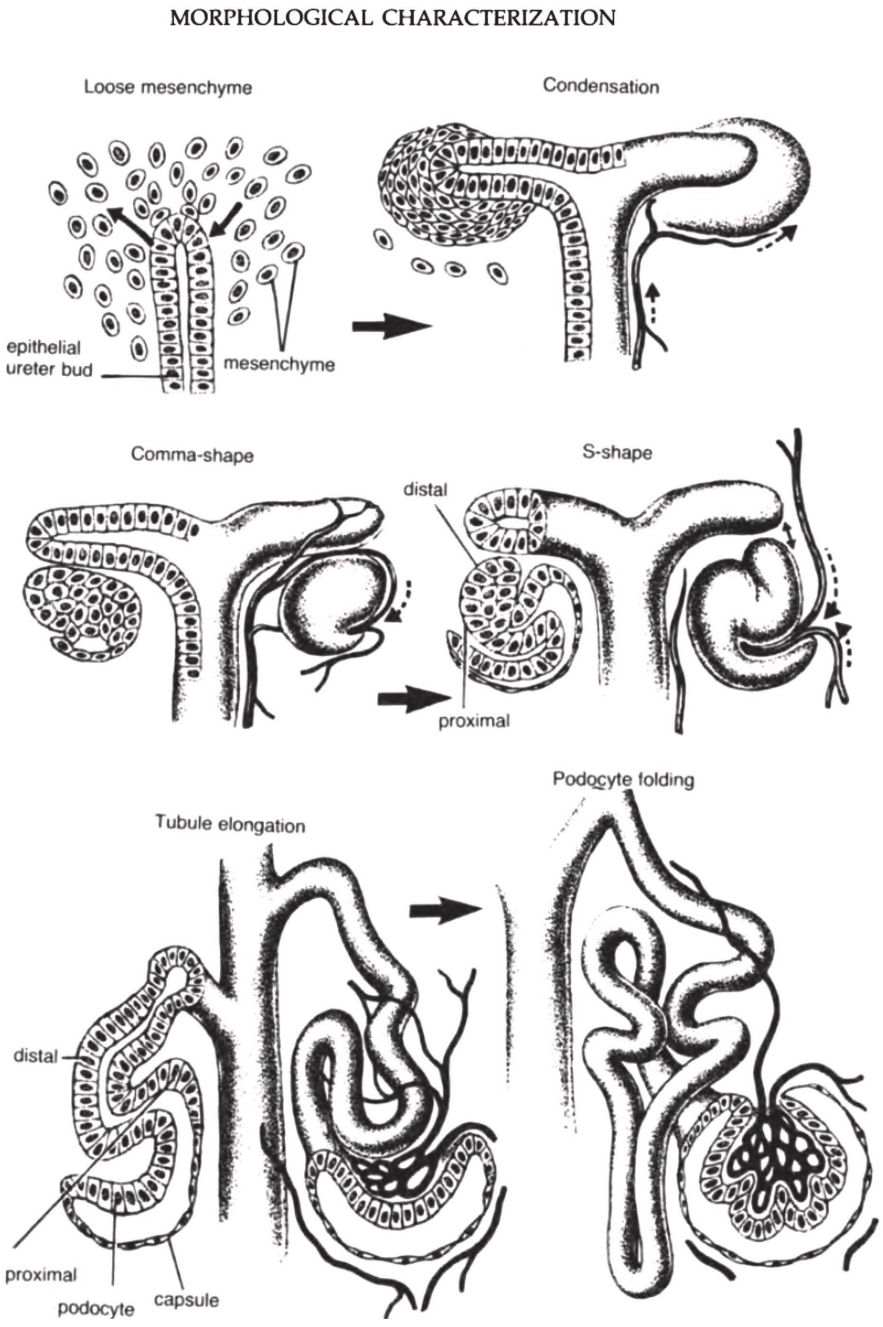

Figure 1.1: **Development of the human nephrotubular system in a schematic overview.** The interaction of the branching ureteric bud with the methanephrogenic mesenchyme induces the mesenchyme to evolve into polarized epithelium and after ongoing condensation and growth, the s-shaped tubule stage follows and the collecting duct epithelium further fuses with the newly formed epithelium, hence establishing the kidney tubular system (modified from Zoetis and Hurtt, 2003).

The kidney is a paired organ with exocrine and endocrine functions and is situated in the retroperitoneal space surrounded by a fibrous capsule. It can be divided into two major regions: the outer renal cortex and the inner medulla which are spanned by the small functional units - nephrons. Cortex and medulla can be separated into renal lobes that contain 8-10 pyramid-shaped structures in the medulla. The papilla is lying conical in the minor calyx and several minor calyces further form major calyces that give rise to the renal pelvis from which the ureter originates (see Fig. 1.2).

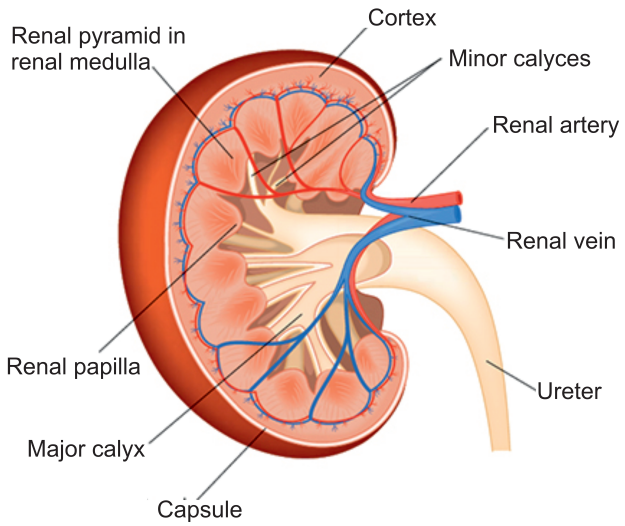

Figure 1.2: **Longitudinal section of the kidney.** The kidney can be separated into cortical and medullary regions with pyramidal structures in the medulla comprising the papilla on the tip. Papillae fuse into minor calyces that further pass over into a major calyx from where the ureter arises (modified from McLafferty et al., 2014).

Glomeruli are localized in the cortex where they filter blood, thereby retaining cells and macromolecules to generate the primary urine, whereas the tubular system consisting of the proximal convoluted tubule located in the cortex, the loop of Henle that descends from the cortex or outer medulla into the inner medulla and the distal convoluted tubule which can be found in cortical regions reabsorb the majority of the filtrate, minerals, toxins and transport the urine along the connecting tubule into the water-reabsorbing collecting duct, which spans the cortex and medulla and are finally fusing at the papilla (see Fig. 1.3) (Witt, 2007).

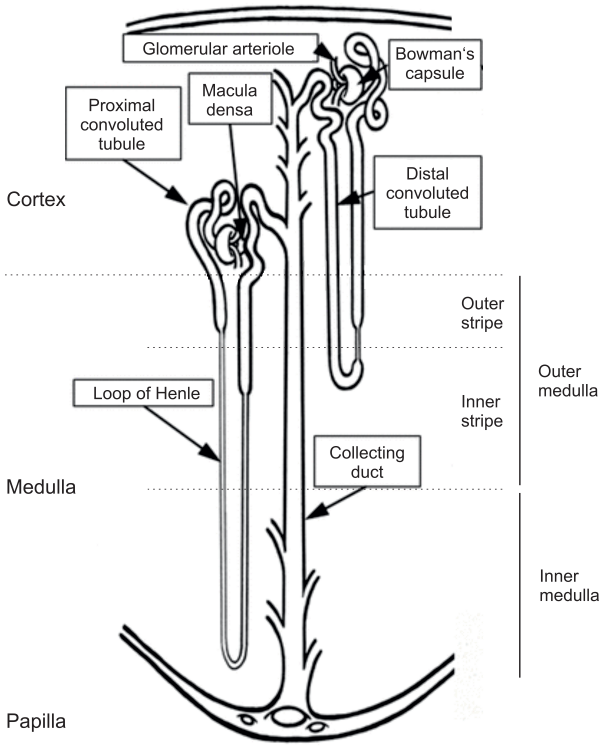

Figure 1.3: **Schematic overview of the nephron organization.** Nephron segments are illustrated with their localization in the kidney regions (modified from Rayner et al., 2015).

1.1.2 The primary cilium

Epithelial cells in the tubular system of the kidney show a specialized structure that is known as the primary cilium. A primary cilium is a microtubule-based organelle protruding from the cell surface of many mammalian cell types during growth arrest. Its three key components are the axoneme, the basal body and the transition zone. The axoneme is a cylindric structure based on nine pairs of microtubules that connects the ciliary tip with its base and serves as the regulatory station for trafficking proteins by the intraflagellar transport machinery. Cilia can be distinguished into two groups - motile and immotile cilia. Motile cilia have a broad range of functions in different organs - e.g. in the respiratory tract, the transport of mucus across the mucous layer is established by metachronal beating of cilia (Wanner et al., 1996) - and stages of embryogenesis - e.g. in mammalian fertilization, sperm motility has to be guaranteed which is also driven by a functional motile cilium (Baccetti and Afzelius, 1976) - to name just a few functions.

Whereas motile cilia have an additional pair of central microtubules (9+2), radial spokes and dynein arms, immotile primary cilia lack those structures and the central pair of

microtubules is also missing (9+0) (see Fig. 1.5) (Haimo and Rosenbaum, 1981). Attached to the plasma membrane by transition fibers, the basal body provides a platform that anchors the primary cilium in the cell body. The transition zone is composed of several protein complexes and its structure is stabilized by linkers that together with transition fibers are suggested to control the entrance and exit of ciliary proteins (Pedersen et al., 2011).

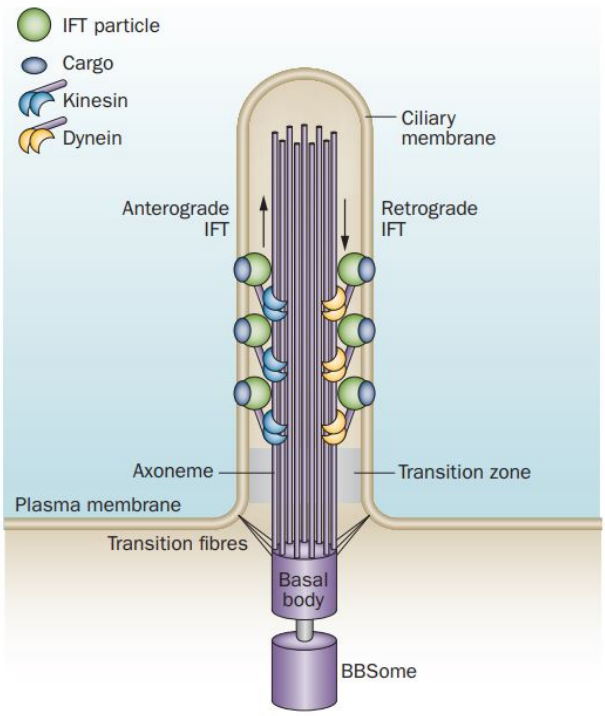

Figure 1.4: **Structural composition of primary cilia**. The axoneme serves as core structure consisting of microtubules where cargo proteins are transported by anterograde (with kinesin motorproteins) and retrograde (with dynein motorproteins) intraflaggelar transport (IFT). The transition zone is stabilized by transition fibers and is important for trafficking of ciliary proteins. The BBSome complex is critical for ciliogenesis and regulates the assembly and functioning of the IFT machinery (adapted from Valente et al., 2013).

Even though first described by Anton van Leeuwenhoek in 1676, primary cilia only became a focus of interest again in the 20th century when scientific techniques such as electron microscopy and immunocytochemistry made it possible to further investigate the ciliary structure and composition (Davis et al., 2006). One exception of primary cilia are the nodal cilia that also lack the central pair of microtubules (9+0) but are motile. Their importance becomes evident during embryogenesis, where synchronized clockwise beating of nodal cilia determine the left-right axis in the body which is important for the arrangement

of asymmetric organs (Nonaka et al., 1998).

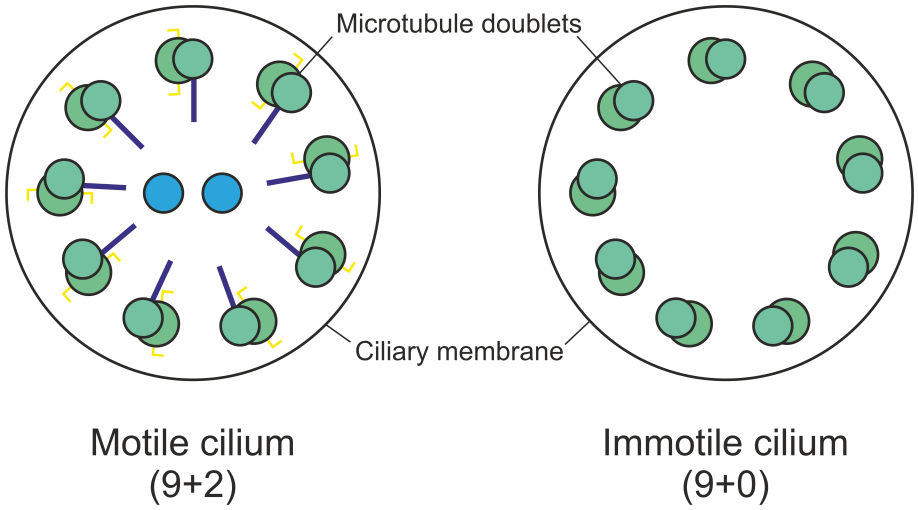

Figure 1.5: **Cross-sectional view of a motile (9+2) and immotile (9+0) cilium.** Microtubule doublets (green) are parietally arranged in a circular manner with (left) or without (right) an additional central pair of microtubules (light blue). Radial spokes are shown in dark purple and dynein arms in yellow.

In the past years, it was elucidated that immotile cilia act as sensory antennae receiving signals from the extracellular space that are then translated into intracellular signaling pathways, but the nature of the signal which is sensed is controversially discussed. In 2001, Praetorius and Spring described the primary cilia as mechanosensors situated on the surface of tubular epithelial cells where they measure fluid flow which is then transmitted into the cell to release intracellular calcium but in recent years, this was cast into doubt and latest publications are refuting a calcium-responsive mechanosensory function of the primary cilium (Delling et al., 2016). However, the role as a general chemosensor has been confirmed by several studies investigating different pathways, e.g. Wnt, Shh, FGF, Notch, mTor, PDGF, and Hippo (Wallingford and Mitchell, 2011; Aanstad et al., 2009; Rohatgi et al., 2007; Hong and Dawid, 2009; Ezratty et al., 2011; Boehlke et al., 2010; Schneider et al., 2005; Habbig et al., 2011). Different proteins involved in those pathways localize to the primary cilium and are discussed to be important for ciliary sensing and/or transmitting and a mislocalization of those proteins often lead to ciliopathies as reviewed in Hildebrandt et al. (2011). Two proteins that are recently often discussed to be important for ciliary sensing and transmitting are polycystin-1 (PC1) and polycystin-2 (PC2), which can lead to a very common ciliopathy called autosomal-dominant polycystic kidney disease (ADPKD).

1.2 Autosomal-dominant polycystic kidney disease

Genetics and pathophysiology

Autosomal-dominant polycystic kidney disease is the most common monogenic disorder with a prevalence of 1:400-1:1000. This disease is the fourth leading cause of end-stage renal disease (ESRD) (Collins et al., 2012) causing severe cyst development arising from all nephron segments, although a remarkable fraction of cysts is arising from collecting ducts (Niemczyk et al., 2009; Verani and Silva, 1988). On a cellular level, not only increased apoptosis events but also higher mitosis rates can be detected in the cyst surrounding epithelium (Gallagher et al., 2006).

It is a systemic disease that can have an onset in adulthood and sometimes as well *in utero* (Gabow, 1993; Shamshirsaz et al., 2005). At the first two decades of an affected individual, only few focally and sporadic renal cysts are occurring. In the later course of the disease, fluid filled cysts can then expand in size to a four to eight-fold expansion of kidney volume thereby causing kidney failure over time - normally in the fourth decade of a patient's life (Roitbak et al., 2004). Disease progression strongly depends on the gene that is mutated. In 85 % patients exhibit a mutation in *PKD1* resulting in a faster progression of the disease compared to the course of the disease in the remaining 15 % of the patients that carry a mutation in the *PKD2* gene. Extrarenal manifestations in patients of ADPKD comprise cysts in other epithelial organs like liver and pancreas. Furthermore, hypertension is a very common symptom and connective tissue defects such as intracranial aneurysms, cardiac valve abnormalities, aortic dissection and abdominal wall hernias can also occur (Yoder, 2002; Hughes et al., 1995).

Due to the fact that there is only sporadic cyst formation in the kidney at the beginning of ADPKD, Reeders speculated in 1992 that the disease involves a "two-hit" process causing loss of heterozygosity. Inactivation of both copies of one of the *PKD* genes by germline and additional somatic mutations within an epithelial cell might lead to growth advantages for it to proliferate clonally into a cyst. In the following years, human as well as knock-out mouse studies were verifying this assumption. By developing a technique to isolate patient cyst-lining cells from the contaminating stromal cells, it was shown that cystic epithelia are of monoclonal nature (Brasier and Henske, 1997). In mice, heterozygous inactivation of one of the *Pkd* genes caused focal renal and extrarenal cyst formation during late adult life, whereas homozygous inactivation of *Pkd1* and *Pkd2* was associated with severe polycystic kidney disease and embryonic or perinatal lethality (Lu et al., 1997; Wu et al., 1998). By breeding mice to create animals with one *Pkd2* null allele ($Pkd2^{-}$) and one instable *Pkd2* allele ($Pkd2^{WS25}$) that can produce either a wild-type or a null allele by intra- or intergenic

somatic recombination into mice, it was shown that mice that have undergone biallelic *Pkd2* inactivation by somatic recombination ($Pkd2^{-/WS25}$) had the most severe cyst progression followed by $Pkd2^{WS25/WS25}$, $Pkd2^{+/-}$and $Pkd2^{WS25/+}$ mice. This strongly supports the "two-hit" theory that another recombination event or mutation is necessary for individual cyst formation in ADPKD (Wu et al., 1998).

Aside from the fact that the disease is often an incidental finding, pre-symptomatic diagnosis of ADPKD is made by ultrasonography when patients have a positive family history and by the compilation of age-dependent ultrasound diagnostic criteria by Ravine *et al.* in 2009, both diagnosis and disease exclusion can be established (Pei et al., 2008). ADPKD progression can be monitored through changes in the estimated glomerular filtration rate (eGFR), that is defined by the filtered volume of a glomerulus per time indicating kidney malfunction when values are low, and in serum creatinine levels indicating organ failure when values are high. Unfortunately, this provides only limited information in early stages of the disease because in three to five decades before loss of kidney function, serum creatinine levels usually do not rise and eGFR is still showing normal values. Measurement of total kidney volume (TKV) is another common bio marker for disease progression because high values include proteinuria, microalbuminuria, hypertension, gross hematuria and progressive loss of kidney function (Grantham et al., 2006). Even though there are several indicators for disease progression, the development of medication for reducing TKV and repressing cyst growth thereby prolonging an ESRD is in the making and ADPKD is still incurable. Different signaling pathways have been discussed to contribute to the pathogenesis of ADPKD such as intracellular dysregulation of calcium, increasing levels of cyclic adenosine monophosphate (cAMP) and induction of mitogen-activated protein (MAP) and mammalian target of rapamycin (mTOR) kinases (reviewed in Chang and Ong, 2012).

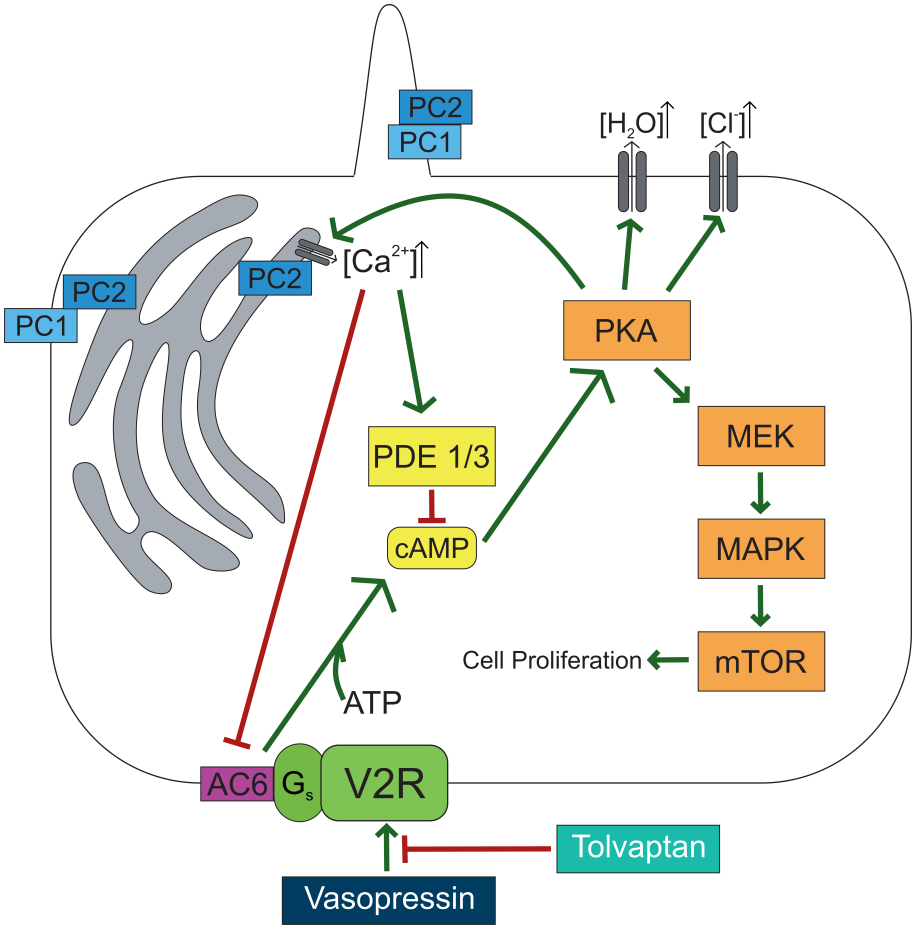

Figure 1.6: **Genetic mechanisms and signaling pathways in ADPKD.** Vasopressin binds to its basolaterally located G-protein-coupled receptor V2R with its stimulatory G protein (G_S) that is activating the adenylyl cyclase 6 (AC6). AC6 is then converting ATP to the second messenger cAMP that is further activating the phosphokinase A (PKA). This kinase induces higher water reabsorption and calcium secretion but also induction of the MAP kinase pathway leading to increased cell proliferation. Furthermore, calcium gets released from the endoplasmic reticulum (ER, gray structure) via the interaction of Polycystin-2 (PC2) with ER-localized calcium-permeable channels. High cytosolic calcium decreases the cAMP levels by inhibiting AC6 and by activating phophodiesterase type -1 and -3 (PDE 1/3), thereby exhibiting its negative regulatory effect.

The most promising drug at the moment is Tolvaptan which is interfering in a crucial step in many of those signaling pathways - the production of the second messenger cAMP (Fig. 1.6). Normally, vasopressin binds to its G-protein coupled receptor vasopressin receptor 2 (V2R), that is located on the basolateral side of the epithelium of distal tubules, connecting tubules and collecting ducts (Sharman and Low, 2008). The stimulatory G protein of V2R is interacting with the adenylyl cyclase 6 (AC6) which is then further converting ATP into

cAMP. This second messenger can then induce protein kinase A (PKA) activation that leads to incorporation of the water transport channel aquaporin-2 (AQP2) thereby increasing water reabsorption and to activation of apical chloride channels leading to chloride secretion. Furthermore, PKA also activates the MAP kinase pathway that is downstream inducing cell proliferation. PKA can also cause intracellular calcium release from the endoplasmic reticulum (ER) by the interaction of polycystin-2 with calcium-permeable channels located in the ER membrane. Higher cytosolic calcium levels then show a negative regulatory effect on cAMP conversion by inhibiting AC6 and activating phosphodiesterases type -1 and -3 (PDE1/3) that are responsible for degradation of cAMP (reviewed in Nobakht et al., 2020).

Tolvaptan is a highly selective antagonist of vasopressin at the V2 receptor and a blockade evokes free water excretion (aquaresis), reduced urine osmolality, suppression of vasopressin-induced cAMP production and decreased kidney cyst cell proliferation (Reif et al., 2011; Meijer et al., 2011). Thereby, oral treatment with tolvaptan could significantly slow the increase of TKV in ADPKD patients compared to a group of patients with placebo over a 3-year period (Torres et al., 2012). However, there are several problems in the treatment with tolvaptan, since the drug must already be given to the patient before any symptoms are shown and this can only be achieved when a pre-symptomatic diagnosis of ADPKD was determined. Other disadvantages of tolvaptan are thirst, increased drinking, increased urine volume and frequency and the need to pass urine at night. Typically patients will pass 5-6 liters of urine per day which makes life very inconvenient and since patients have to deal with these troubles before the actual symptoms appear, the acuteness of a new, other drugs is very high (Meijer and Gansevoort, 2020).

All the self-regulatory signaling pathways shown in Figure 1.6 are very sensitive to a dysbalance of calcium as it can be seen in ADPKD patients (Yamaguchi et al., 2003, 2004). This emphasizes the importance of functionality of every single component involved in calcium homeostasis.

1.3 Transient Receptor Potential (TRP)- Channels

First described in *Drosophila melanogaster* in 1989 when studies of the fruit fly's visual system were conducted, nowadays more than 100 transient receptor potential genes have been characterized in different species. According to sequence homology analyzes, TRP genes can be divided into seven subfamilies with varying number of family members across species: TRPC (canonical), TRPV (vanilloid), TRPM (melastatin), TRPP (polycystin), TRPML (mucolipin), TRPA (ankyrin) and TRPN (NOMPC-like) - with the latter only found in invertebrates and fish (see fig. 1.7). The super family of TRP genes are named after a

mutation called "transient receptor potential mutant" yielding flies with a transient response to steady light compared to a sustained electro-retinogram recorded in wild-type flies (Cosens and Manning, 1969). After further 20 years, this mutation was then assigned to the *trp* gene by Montell and Rubin (1989) and further investigation revealed the *trp* gene product as a putative six-transmembrane segment protein that allegedly functions as a Ca^{2+}-permeable cation channel (Hardie and Minke, 1992).

Among all subfamily members, the greatest homology can be found in the transmembrane segments. The TRPC subfamily ('canonical') shows high homology to *Drosophila* trp channels. TRPVs ('vanilloid') are named after the vanilloid receptor 1 (now TRPV1). The TRPM subfamily comprises homologs of melastatin-1 (now TRPM1). TRPMLs and TRPPs include mucolipins and polycystins, respectively. The members of the TRPA subfamily are nociceptive channels with characteristic 14 ankyrin repeats. The TRPN subfamily is named after the 'NO-mechano-potential C' (NOMP-C) channel of *Caenorhabditis elegans*. Up to now, the only TRPN family member being known in vertebrates is from zebrafish (reviewed in Nilius and Owsianik, 2011).

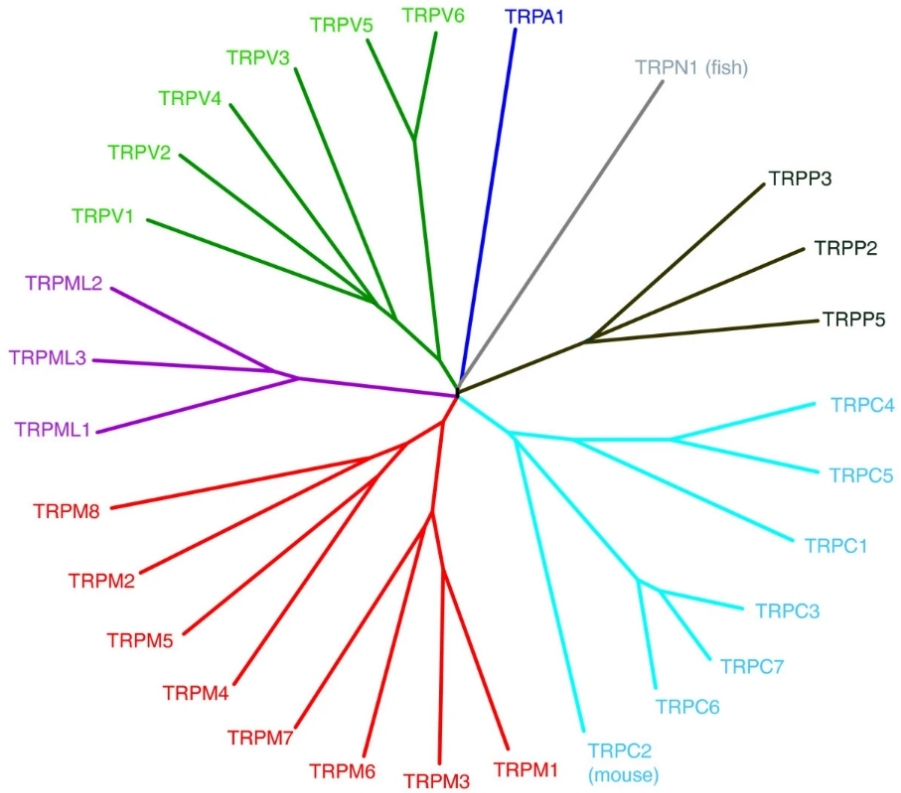

Figure 1.7: **Human transient receptor potential channels displayed in a phylogenetic tree.** Sequence homology analyzes have shown that all TRP channels can be divided into seven subfamilies (TRPVs in green, TRPA in blue, TRPN in grey, TRPPs in black, TRPCs in cyan, TRPMs in red and TRPMLs in purple) with different numbers of channels within each subfamily across species. To show relations between all subfamilies, TRPNs that do not exist in mammals and TRPC2 as being a pseudogene in human are also shown in this tree (adapted from Nilius and Owsianik, 2011).

Structural analysis of proteins by nuclear magnetic resonance (NMR) and electron microscopy (EM) can normally be obtained by the availability of highly pure and stable protein samples which in case of these proteins appears to be a problem because membrane proteins are difficult to produce in large quantities and purify in a stable native state. Furthermore, TRP channels form very large tetramers of 70-250 kDa subunits consistent of multiple domains which are inaccessible to high-resolution NMR techniques. To compensate for the lack of structural information on TRP channels, numerous studies have used modeling approaches to provide a context for their mutagenesis data. These can be very meaningful, especially when the structures of close structural homologues are known. For this purpose, the structures of potassium channels like KcsA (Doyle et al., 1998) – whose structure is expected

to be similar to the channel pore domain of TRP channels, and the Shaker channels Kv1.2 and Kv2.1 (Long et al., 2005, 2007) were helpful to solve the structures of TRP proteins. Not only by structural modeling, but also by the use of EM, NMR and X-ray crystallography of structural homologue channels, it could be shown that in general, a TRP protein contains six putative transmembrane segments (S1 to S6) with a pore-forming re-entrant loop between S5 and S6. Intracellular amino and carboxyl termini differ in length and comprise a variety of domains as shown in figure 1.8 (reviewed in Gaudet (2008) and Owsianik et al. (2006)).

TRP channels are mostly located on the plasma membrane in both excitable and non-excitable tissues, with the exception of the nuclear envelope and mitochondria. Their essential role is reported to be the transport of cations and trace metal ions for controlling their cellular entry. These contributions are important for a diversity of physiological processes, e.g. pure sensory- and/or homeostatic functions or other motile functions like muscle contraction (reviewed in Nilius and Owsianik, 2011).

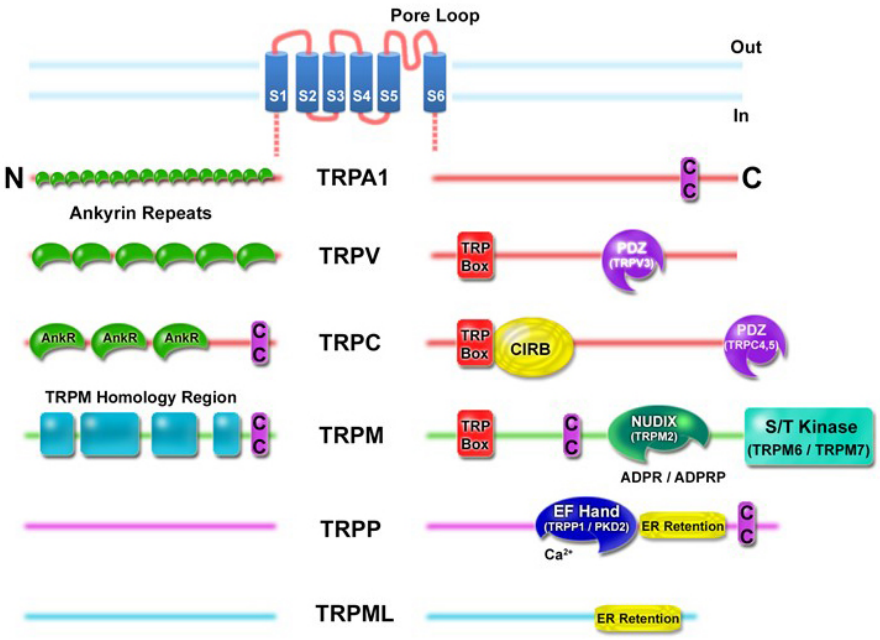

Figure 1.8: **Structural overview of the TRP subfamily channels.** All TRP members comprise a predicted 6 transmembrane topology (S1-S6) with a pore region between S5 and S6. Both N- and C-termini lie in the intracellular space showing different structural and functional elements characteristic for the respective subfamily. TRP Box; AnkR, ankyrin repeats (number differs by subfamily members); CC, coiled-coil domain (position in the cytoplasmic termini varies); S/T Kinase, serine/threonine kinase intrinsic to TRPM6 and TRPM7; CIRB, calmodulin- and inositol triphosphate receptor ($InsP_3R$)-binding site; PDZ, amino acid motif binding PDZ domains (TRPV3 contains a consensus PDZ binding motif); NUDIX, NUDT9 homology domain binding ADP ribose (ADPR) or ADPR-2'-phosphate (ADPRP); EF Hand, canonical Ca^{2+}-binding domain in TRPP1/PKD2 (EF Hand sequence motif in TRPA1 not shown); ER retention, endoplasmic reticulum retention signal. The TRPM Homology Region is of unknown function (modified from Hellmich and Gaudet, 2014).

1.3.1 The transient receptor potential polycystic- subfamily

The focus of this work was set on the gene products of the TRPP subfamily. This subfamily is named after the protein that was discovered to be disrupted in ADPKD - TRPP2 (also Polycystin-2). From a structural point of view, the polycystins can be divided into two groups: the Polycystin-1 (PC1)-like and Polycystin-2 (PC2)-like proteins. PC1-like proteins, such as PC1 and polycystin-REJ (receptor for egg jelly; PCREJ), have a large extracellular N-terminal domain, up to 11 transmembrane domains and a short intracellular carboxy tail (Hughes et al., 1995, 1999). Polycystin-2, polycystin-2L1 and polycystin-2L2 belong to the group of PC2-like proteins with six putative membrane-spanning domains, a pore region and

short intracellular N- and C-termini (Guo et al., 2000). The carboxy terminus contains a coiled-coil domain and in PC2 and PC2L1, there is also a calcium binding site which is called the EF hand (Mochizuki et al., 1996; Guo et al., 2000; Murakami et al., 2004). PC1 and PC2 are the best-known members of the polycystin family and are in the focus of this thesis.

1.3.1.1 Polycystin-1

Structure and topology

Polycystin-1 is a large protein consisting of 4302 amino acids and is encoded by the 46-exon gene *PKD1*, that is localized on chromosome 16p13.3. Since there are six pseudogenes highly homologous to the 5' part sharing a sequence identity of up to 99% and these are also positioned on chromosome 16 (Hughes et al., 1995), it is very challenging to sequence *PKD1* and direct mutation analysis becomes very complex.

Compared to the other member of the PC1-like proteins PC1REJ, PC1 contains an amino-tail that is much larger. About 3000 amino acids are protruding into the extracellular space comprising a variety of potential ligand-binding sites: a cysteine-rich domain, two leucine-rich repeats (LRR) - a motif responsible for its interaction with the extracellular matrix and cell adhesion, a cell wall integrity and stress response component (WSC) that is thought to interact with carbohydrates, 16 copies of unique immunoglobulin (Ig)-like PKD domains with a putative ligand-binding functionallity (Bycroft, 1999), a C-type lectin domain, a low density lipoprotein A (LDL-A) related motif - suggested to be important for a possible interaction between PC1 and LDL-related molecules, a region of homology with a sea urchin receptor for egg jelly (REJ) (Hughes et al., 1995) and a G protein-coupled receptor proteolytic site (Ponting et al., 1999) where the protein cleaves itself into a N-terminal fragment (NTF) and a multi transmembrane core (Wei et al., 2007). Between transmembrane domain 10 and 11, a lipoxygenase homology (LH2 or polycystin-1, Lipoxygenase, α-Toxin (PLAT)) domain is located (Ponting et al., 1999). The intracellular C-terminus contains a coiled-coil motif and several protein kinase A (PKA) phosphorylation sites (Hughes et al., 1995) (see Figure 1.9). The last six transmembrane domains of PC1 show high sequence homology with TRP channels and domains of Na^+ and Ca^{2+} channels but an expression of PC1 alone does not exhibit measurable currents, suggesting that PC1 molecules are not able to form homomeric ion channels (Hanaoka et al., 2000; Delmas et al., 2002).

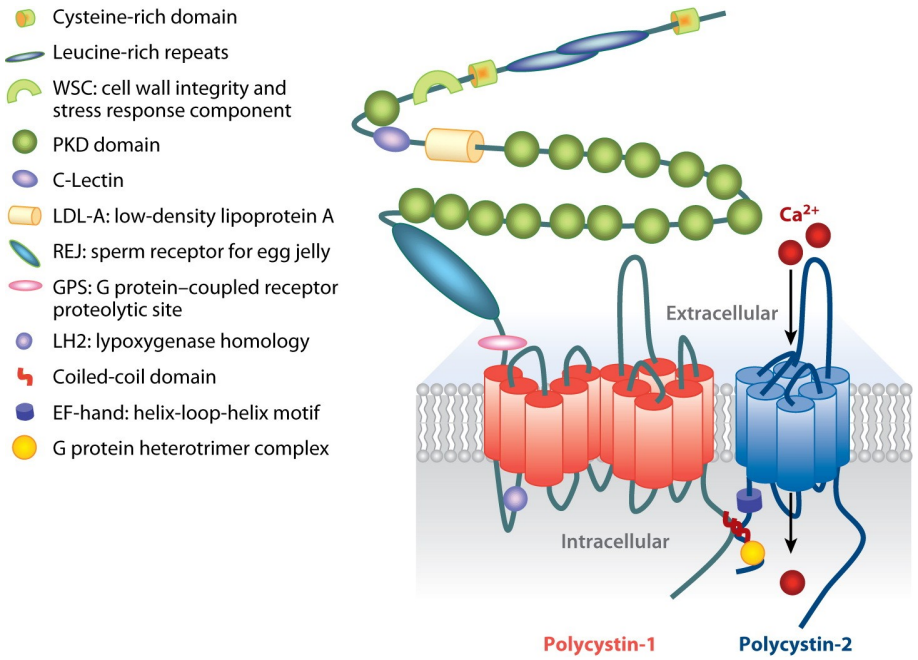

Figure 1.9: **Topology of polycystin-1 and polycystin-2.** As depicted, polycystin-1 comprise a large amino terminus with several domains whereas polycystin-2 only show few domains situated on the carboxy terminus. On the carboxy terminus of PC1 and PC2, a coiled coil domain is localized which acts as interaction site of the two proteins (adapted from Zhou, 2009).

Specific interest lies on the 16 PKD domains which protrude into the extracellular space. These domains are known in other proteins to participate in protein–protein and protein–carbohydrate interactions intimidating that polycystin-1 might undergo complex interactions with different proteins and components in the extracellular space or of the extracellular matrix. Only less is known so far about these 46 exons spanning domains located on chromosome 16p13.3 (Hughes et al., 1995).

Function

PC1 has a broad tissue expression early in development, e.g. in the kidney, brain, heart, bone and muscles (Geng et al., 1996) and is now generally accepted as a protein that is located in the plasma membrane in ductal epithelial cells. This expression pattern goes along with the suggested function as a cell surface receptor in both cell-cell and cell-matrix interactions (Kim et al., 2000; Scheffers et al., 2000). Heterologous expression of PC1 in sympathetic neurons showed that PC1 behaves similar to G protein coupled receptors (Delmas et al., 2002) although the number of transmembrane domains does not accord to typical receptors

with seven transmembrane domains which makes PC1 an atypical GPCR. Some studies propose an inhibiting function of PC1 in the heteromeric PC1/PC2 complex (Su et al., 2018) or a putative fine tuning ability of the channel's ion selectivity (Wang et al., 2019). This might be affiliated to the extracellular N-terminus and since a disruption of autoproteolytic cleavage of PC1 into a CTF and the multi-core complex leads to *PKD1* associated ADPKD (Qian et al., 2002), a biological relevance of the 3000 amino acid tail is suggested.

In 1999, Bycroft had a particular focus on the PKD domains and determined the solution structure of one of these 16 domains in order to find out more about putative ligand-binding sites and thereby further investigating the functional relevance of these repeats. By expression of ^{13}C and/or ^{15}N-labeled *PKD1* domain 1 in *E. coli,* it was shown that details of the structure comprise a novel protein family, although the topology is similar to that found in other domains in cell-surface proteins so that it is possible that PKD domains could comprise similar functions. *PKD1* PKD domain 10 is the best conserved domain among species so that the authors suggest a specific functional role (Bycroft, 1999). Nevertheless, it is still unknown what precise role these domains play in the extracellular space.

1.3.1.2 Polycystin-2

Structure and topology

PKD2 is localized on chromosome 4q21-23 and encompasses 968 amino acids encoded by 15 exons that are yielding a protein of 110 kDa. Polycystin-2 presents an intracellular carboxy terminus comprising a calcium-binding EF-hand and a coiled-coil domain for interacting with PC1 and other putative binding partners (Mochizuki et al., 1996). Contrary to polycystin-1, polycystin-2 has a small amino terminus which lies in the cytosol offering motifs which are stated to be important for the protein's localization. The RVxP motif in the first 15 amino acids of the amino terminus is suggested to be important for the localization to the cilium (Geng, 2006) and the ER retention signal that is allocated to amino acids 787-820 featuring a high number of acidic amino acids (Cai et al., 1999). A voltage-sensing domain (VSD) was reported to be formed by transmembrane helices 1-4 and between transmembrane segment 5 and 6 a pore forming domain with an interfering reentrant pore loop was found. Both domains are connected by the S4-S5 linker which is a short helix located almost parallel to the inner leaflet of the lipid bilayer where the protein is located (Long et al., 2007) (see figure 1.10).

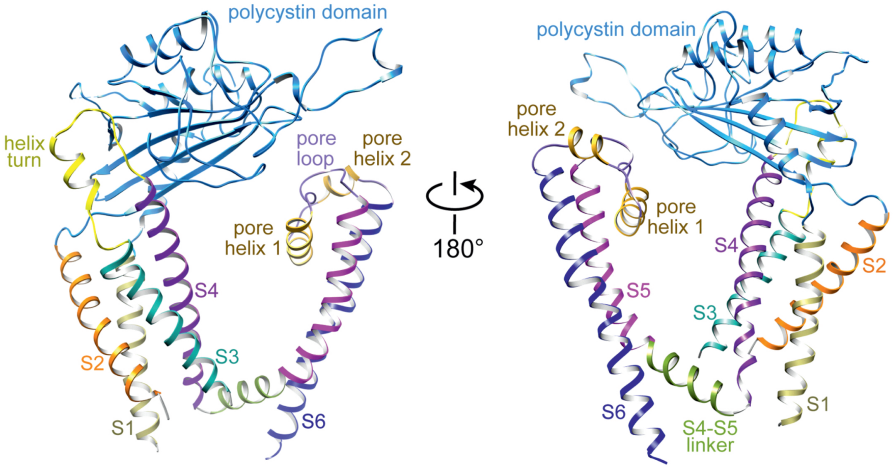

Figure 1.10: **Structure of polycystin-2.** Side view of polycystin-2 with its different structural domains (adapted from Shen et al., 2016).

Function

Regarding the function of polycystin-2, it was early speculated to be a cation channel since sequence and structure show similarity to alpha-subunits of voltage-activated calcium channels (Mochizuki et al., 1996) and since it was also described to interact with polycystin-1 (Tsiokas et al., 1999). This assumption was further supported, when researchers found the closely related polycystin-2L1 with its high sequence homology in the pore region to polycystin-2 (see fig. 1.11) to act as a non-selective cation channel (Chen et al., 1999).

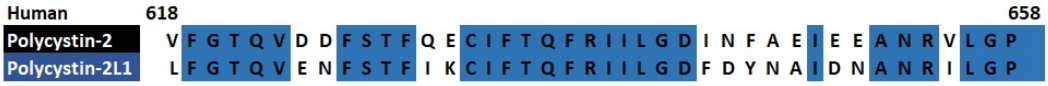

Figure 1.11: **Sequence comparison of the pore region of human polycystin-2 (PC2, black) and polycystin-2L1 (PC2L1, blue).** Identical residues between polycystin-2 and polycystin-2L1 are highlighted in petrol.

In further examination, polycystin-2 came into the focus of many scientists all agreeing that the gene product of *PKD2* represents a non-selective ion channel. By forming a tetrameric architecture an ion permeation pathway can be established, either by forming a homomeric channel, or with other proteins in a heteromeric complex thereby comprising distinct channel functions. In the past decades, it was found that polycystin-2 can not only heteromerize with polycystin-1, but also with TRPC1 (Tsiokas et al., 1999) and TRPV4 (Koettgen et al., 2008). The homomeric polycystin-2 complex is mainly localized at the

endoplasmic reticulum by its C-terminal retrieval signal, where it is stated to be a calcium release channel either by a direct calcium conductivity or by interacting with other channels situated in the ER membrane. In single channel experiments, it was postulated that PC2 is highly permeable to calcium and also other bivalent cations (Gonzalez-Perrett et al., 2001). Lately, contradicting literature regarding the calcium permeability was published that strongly cast into doubt whether polycystin-2 is indeed able to conduct calcium (Cai et al., 2004). In heterologous expression of PC2 in *Xenopus laevis*, it was shown that only a gain-of-function mutation was able to show calcium currents but not the wild-type polycystin-2 (Pavel et al., 2016). Even though it is highly disputed whether PC2 is a calcium channel, calcium is still an important ion regarding polycystin-2's channel function. Cytosolic calcium is described to be necessary for regulation of the channel's open probability. Here, a bell-shaped Ca^{2+} response was detected with low levels ($<$1µM) increasing the open probability and high levels ($>$1µM) showing inhibitory effects (Cai et al., 2004).

1.3.2 Interaction of polycystin-1 and polycystin-2

As mutations in *PKD1* and *PKD2* result in very similar clinical phenotypes, it suggests that these proteins function as a receptor–channel complex modulating calcium-based intracellular signaling, as shown in section 1.2, and mutations in one of these protein disturbs this signaling. Comparing PC1 and PC2 with their relatives, PC1L3 and PC2L1, which respond to acidic pH and may contribute to sour tasting detection of the tongue (Huang et al., 2006; Ishimaru et al., 2006; Kawaguchi et al., 2010), it is suggested that PC1 and PC2 might also show somehow similar sensory properties. The formation of this heteromeric complex enriches on primary cilia. However, understanding the interaction of PC1 and PC2 is difficult because experiments were often hampered by insufficient subcellular enrichment of the complex (Liu et al., 2018) or technical challenges in studying currents in primary cilia due to their small size so that divergent results were yielded in the past years. Recently, it was postulated that PC1 and PC2 form a 1:3 heterotetramer (Su et al., 2018; Yu et al., 2010) and latest cryo-EM structure analyses showed that the 11 TM helices of polycystin-1 can be divided into a peripheral TM1-5 complex and a core TM6-11 complex. The latter one is suggested to interlink with three polycystin-2 subunits thereby forming a typical "homomeric" TRP channel (Shen et al., 2016; Grieben et al., 2016; Wilkes et al., 2017). Notwithstanding, more explanatory work has to be conducted to elucidate the function of the homo- or heteromeric complex formations.

1.4 Aims

The aim of this work was focused on filling some yet unknown and undiscovered gaps that would help us to understand the function of both polycystin-1 and polycystin-2.

New insights about polycystin-1 were recently given by investigating its interaction with polycystin-2 thereby forming a heteromeric complex in the plasma/cilia membrane. Here, polycystin-1 might function as a sensor to transmit signals to the effector polycystin-2. However, less is known about how sensing is accomplished. The extracellular domain of polycystin-1 with its different domains might be relevant for this function, but recent research did not bring new knowledge on that question. For gaining more information on this, the focus was set on studying a putative ligand-binding function of the *PKD1* PKD domain 1 as a representative of the sixteen PKD domains. This domain lies apart from the other PKD domains which might hint to a certain relevance. By expression of ^{15}N-labeled *PKD1* PKD domain 1, more information on the physiological relevance should be gained whether components of the urine can bind to this domain which would suggest a chemical sensory function of the PKD domains while protruding in the luminal space of nephrons. This domain should first be analyzed by NMR and then again when incubated with urine from an ADPKD patient as well as with urine from a healthy person. In patients of ADPKD, mutations can occur in those domains thereby preventing a putative binding of components which can then be found remaining in the patient's urine. These compounds should be filtered out, hence not be present in the urine of a healthy person. Putative compound binding can be identified in NMR spectra by comparing the presence and/or shifting of peaks consequently comprising information on the potential chemosensoric relevance of the PKD domains.

In the literature, the lately discussed topic of polycystin-2 being a calcium channel or not speaks for the huge interest on the *de facto* ion channel function. Even though contradicting publications do not point into a clear direction, the relevance of the ion channel function suggests to be critical for calcium homeostasis thus maintaining kidney function. By establishing a mutant form of polycystin-2 by exchanging the pore region with that of the closely related protein polycystin-2L first *in vitro,* for characterization of the mutant protein polycystin-2^{poreL1} and preliminary calcium measurements, and consequently also *in vivo* for further calcium measurements should reveal a functional channel with distinct conducting properties compared to wild-type polycystin-2. In mice from this generated *Pkd2*^{poreL1} knock-in line, in wild-type polycystin-2 mice and in mice with a collecting duct-specific *Pkd2* knock-out calcium responses should be analyzed to gain more information on the calcium conductivity of polycystin-2 thereby giving a clearer direction to the currently contradicting literature.

2 Material and methods

2.1 Material

All consumables, chemicals and reagents used for this work are listed below in the following subsections.

2.1.1 Chemicals and reagents

Chemical/ Reagent	Source
β-mercaptoethanol	Merck
1 kb Plus DNA Ladder	NEB
^{15}N-Ammonium chloride ($>$ 99%)	Cambridge Isotope Laboratories
Acetic acid	Merck
Acetone	Acros
Acrylamide, 30% / Bisacrylamide, 0.8% solution	Serva
Agarose, NEEO quality	Roth
Ammonium chloride	Merck
Ammoniumpersulfat (APS)	Fluka
Adenosine triphosphate (ATP) disodium salt hydrate	Sigma
β-Mercaptoethanol	Merck
Bacto agar	Becton Dickinson
Bacto tryptone	Becton Dickinson
Bacto yeast extract	Becton Dickinson
Benzamidine	Sigma
Biotin	Sigma
Bovine serum albumin (BSA), fraction V	Sigma
Bromphenol blue	Serva
Calcium chloride	Roth

Chemical/ Reagent	Source
Carbenicillin	Roth
Cobalt chloride	Acros
Copper chloride	Honeywell
Chloramphenicol	Calbiochem
Coomassie Brilliant Blau R 250	Serva
Cycloheximide	Sigma
Desoxynukleosidtriphosphate (dNTPs)	Fermentas
Dimethyl sulfoxide ($>$ 99%)	Sigma
DNase I, grade II, from bovine pancreas	Sigma
Disodium hydrogen phosphate	Merck
Disodium hydrogen phosphate dihydrate	Merck
Dithiothreitol (DTT)	Roth
Doxycycline hyclate (DOX)	AppliChem
Dulbecco's modified Eagle's Medium (DMEM), high Glucose (4,5 g/L)	Sigma
Ethanol	Sigma
Ethidium bromide	Sigma
Ethylenediaminetetraacetic acid, disodium salt (EDTA)	Roth
Ethylene glycol-bis(2-aminoethylether)-	Sigma
N,N,N´,N´-tetraacetic acid (EGTA)	Serva
Fetal calf serum (FCS)	PAN Biotech
Fura-2,AM	Invitrogen
G-418-sulfate	Invitrogen
Glucose	Merck
Glycerol	Roth
Glycine	Roth
Hoechst 33258	Sigma
4-(2-Hydroxyethyl)piperazine-1-ethanesulfonic acid (HEPES)	Fluka
Imidazol	Merck
Immersol^{TM} 518F	Zeiss
Immersol W2010	Zeiss
Iron chloride	Merck
Isopropanol	Merck
Isopropyl β-D-1-thiogalactopyranoside (IPTG)	Fermentas

Chemical/ Reagent	Source
Kanamycin sulfate	AppliChem
Lysozyme	Biomol
Magnesium chloride	Merck
Magnesium sulfate	Merck
Mangan chlorid	Sigma
Methanol	Merck
3-(N-morpholino)propanesulfonic acid (MOPS)	Merck
Narcoren	Merial
PageRuler prestained protein ladder	Thermo Fisher
Paraformaldehyde (PFA)	Merck
PEI (Polyethylenimine)	Polysciences Inc.
Piperazine-N,N´-bis(2-ethanesulfonic acid) (PIPES)	Merck
Phenylmethylsulfonyl fluoride (PMSF)	Sigma
Pluronic F127	Invitrogen
Poly-L-ornithine solution	Sigma
Poly-L-lysine solution 0.1% (w/v) in H_2O	Sigma
Potassium chloride	Merck
Potassium dihydrogen phosphate	Merck
Probenecid	Sigma
Puromycine	PAA
Roti®Quant	Roth
Rubidium chloride	Sigma
Skim milk powder	Sucofin
Sodium chloride	Merck
Sodium dodecyl sulfate (SDS)	Serva
N,N,N',N'-Tetramethylethylenediamine (TEMED)	Serva
Tris base (Tris(hydroxymethyl)aminomethane)	Sigma
Triton X-100	Merck
Trypsin/EDTA	Sigma
Trypsin inhibitor from *Glycine max* (soybean)	Sigma
Tween 20	Serva
Urea	Merck
Vasopressin	Sigma
Xylene cyanol FF	Serva
Zinc chloride	Merck

2.1.2 Buffers and solutions

Unless otherwise stated, all buffers and solution were prepared with ultrapure water (aqua bidest).

Media and solutions for bacterial work

Buffer/ Solution	Ingredients		
10x M9	0.4 M	Na_2HPO_4 x 2 H_2O	
	0.2 M	KH_2PO_4	pH 7.4, sterile filtered,
	86 mM	NaCl	stored at RT
Ampicillin stock solution (1000x)	100 g/mL	Ampicillin	sterile filtered
Chloramphenicol stock solution (1000x)	30 g/mL	Chloramphenicol in 100% EtOH	sterile filtered
FTB	10 mM	Pipes	
	55 mM	$MnCl_2$	
	15 mM	$MgCl_2$	
	250 mM	KCl	sterile filtered
FTP	10 mM	MOPS	
	75 mM	$CaCl_2$	
	10 mM	RbCl	
	12 % (w/v)	Glycerol	sterile filtered
IPTG stock solution (1000x)	1 M	IPTG	sterile filtrated, stored at -20 °C
Kanamycin stock solution (1000x)	25 g/mL	Kanamycin	sterile filtered
LB	10 g/L	Bacto tryptone	
	5 g/L	Bacto yeast extract	
	10 g/L	NaCl	autoclaved
Minimal medium	10 %	10x M9	
	9 mM	NH_4Cl, (un-)labeled	
	22 mM	Glucose	
	0.1 %	1000x Trace elements	
	1 mM	$MgSO_4$	
	4 mM	Biotin	
	4 mM	Thiamine	

Buffer/ Solution	Ingredients		
	3 µM	$CaCl_2$	sterile filtered
SOB medium	20 g/L	Bacto tryptone	
	5 g	Bacto yeast extract	
	10 mM	NaCl	
	2.5 mM	KCl	
	Filled to a final volume of 980 ml H_2O,		autoclaved
Then add:	10 mM	$MgCl_2$	sterile filtered
	10 mM	$MgSO_4$	sterile filtered
Trace elements	170 mM	EDTA, pH 7.5	first, then adding
stock solution	30 mM	$FeCl_3$x 6 H_2O	
(1000x)	6 mM	$ZnCl_2$	
	0.76 mM	$CuCl_2$ x 2 H_2O	
	0.42 mM	$CoCl_2$x 6 H_2O	sterile filtered,
	1.6 mM	H_3BO_3	stored at RT

Buffers and solutions for protein isolation and purification

Buffer/ Solution	Ingredients		
Benzamidine stock solution (100x)	100 mM	Benzamidine	
Amylose elution buffer	10 mM	Maltose in NaP_ibuffer	
DNase I stock solution (100x)	1 mg/mL	DNase I	
	5 mM	Tris-HCl	pH 7.4
	75 mM	NaCl	
	0.5 mM	$MgCl_2$	
	50 %	Glycerol	
DTT stock solution (100x)	100 mM	DTT	
PMSF stock solution (100x)	100 mM	PMSF in isopropanol	
Lysozyme stock solution (100x)	20 mg/mL	Lysozyme	
	10 mM	Tris-HCl	pH 8.0
Ni-NTA elution buffer	300 mM	imidazole in NaP_ibuffer	
Sodium phosphate buffer (NaP_ibuffer)	100 mM	Na_2HPO_4	
	100 mM	NaH_2PO_4	
	150 mM	NaCl	pH 7.2
TEV protease reaction buffer	50 mM	Tris-HCl	pH 8.0
	0.5 mM	EDTA	
	1 mM	DTT	add before use

Buffers and solutions for SDS-PAGE

Buffer/ Solution	Ingredients		
5x SDS sample buffer	625 mM	Tris base	pH 6.7, HCl
	125 g/L	SDS	
	12.5 %	β-mercaptoethanol	
	0.5 g/L	Bromophenol blue	
	50 %	Glycerol	
10x SDS running buffer	0.25 M	Tris base	
	1.9 M	Glycin	

Buffer/ Solution	Ingredients		
	10 g/L	SDS	
10 % APS	100 g/L	APS	
10 % SDS	100 g/L	SDS	
Coomassie stainer	2.5 g/L	Coomassie Brilliant Blue R-250	
	10 %	Acetic acid	
	40 %	EtOH	
Coomassie destainer	10 %	Acetic acid	
	40 %	EtOH	
Tris-HCl for stacking gel	1.5 M	Tris base	pH 8.8, HCl
Tris-HCl for running gel	0.5 M	Tris base	pH 6.8, HCl

Buffers and solutions for western blotting

Buffer/ Solution	Ingredients		
10x TBS	0.25 M	Tris base	
	1.4 M	NaCl	pH 7.4, HCl
	26.8 mM	KCl	autoclaved
Blocking buffer	5 %	Skim milk powder	
		in TBS-T	
TBS-T	0.1 %	Tween 20	
		in 1x TBS	
Transfer buffer	50 mM	Tris base	
	384 mM	Glycine	
	0.1 g/L	SDS	
	20 %	Methanol	

Buffers and solutions for working with mammalian cells

Buffer/ Solution	Ingredients		
10x PBS	1.27 M	NaCl	
	27 mM	KCl	
	14.7 M	KH_2PO_4	
	81 mM	Na_2HPO_4 x 2 H_2O	pH 7.4
Cycloheximide stock solution (100x)	10 mg/mL	Cycloheximide	

Buffer/ Solution	Ingredients	
Doxycycline stock solution (100x)	10 µg/mL	Doxycycline
Medium for LLC-PK_1	90 %	Medium 199
	10 %	FCS
	2 mM	Glutamine
Medium for LtTA-2,22/PKD2,HA	90 %	DMEM, high glucose
and LtTA-2,22/PKD2(hPoreL1),HA	10 %	FCS
	200 µg/mL	G-418-sulfate
	1 µg/mL	Puromycine

Solutions for immunofluorescence staining

Buffer/ Solution	Ingredients		
Blocking solution	2 %	BSA in 1x PBS	
Fixation solution	40 g/L	PFA solved in water with drops of 1 mM NaOH, added under heating to 60 °C; 1x PBS added after complete dissolving	 pH 7.4, autoclaved
Permeabilization solution	2 % 0.2 %	BSA Triton X-100 in 1x PBS	

Buffer for cell lysis

Buffer/ Solution	Ingredients	
Lysis buffer	6 M	Urea
	1 %	Triton X-100
		in 1x PBS

Solutions for mouse work

Buffer/ Solution	Ingredients	
Narcoren working solution	1:50	Narcoren in physiological saline solution
Physiological saline solution	9 g/L	NaCl

Buffers for working with DNA and genotyping

Buffer/ Solution	Ingredients		
5x DNA loading buffer	0.1 M	Na_2EDTA x 2 H_20	
	2.5 g/L	Bromophenol blue	
	2.5 g/L	Xylene cyanol	
	30 %	Glycerol	
Oligo annealing buffer	10 mM	Tris	pH 7.5, HCl
	50 mM	NaCl	
	1 mM	EDTA	
Tail buffer	100 mM	Tris base	
	200 mM	NaCl	
	5 mM	Na_2EDTA x 2 H_20	pH 8.0, HCl
	2 g/L	SDS	autoclaved
TE buffer	10 mM	Tris	pH 8.0, HCl
	0.1 M	Na_2EDTA x 2 H_20	autoclaved

Buffers and solutions for collecting duct isolation

Buffer/ Solution	Ingredients		
Isolation buffer	NaCl	140 mM	
	KH2PO4	0.4 mM	
	K2HPO4 x 3 H2O	1.6 mM	
	MgSO4 x 7 H2O	1 mM	
	Na-Acetat x 3 H2O	10 mM	
	α-Ketoglutaric acid	1 mM	
	Ca-Gluconat monohydrat	1.3 mM	pH 7.4
Incubation solution	Glycine	5 mM	
	Trypsin inhibitor	500 µg/mL	

Buffer/ Solution	Ingredients		
		DNase I	250 µg/mL in isolation buffer
Sorting solution		BSA	7.5 mM in isolation buffer

Buffers and solutions for calcium measurements

Buffer/ Solution	Ingredients		
ATP stock solution (50x)	5 mM	ATP disodium salt hydrate	
Calcium buffer	150 mM	NaCl	
	5 mM	KCl	
	2.2 mM	CaCl2	or EGTA for Calcium free buffer
	5 mM	Glucose	
	10 mM	HEPES	pH 7.4
	1 mM	$MgCl_2$	
	5 mM	Probenecid	add before use, adjust pH to 7.4
Fura-2,AM stock solution (200x)	1 mM	Fura-2,AM in DMSO	
Pluronic F127 (800x)	20 %	Pluronic F127 in DMSO	
Probenecid (100x)	500 mM	Probenecid in 1 M NaOH	
Vasopressin (100x)	100 µM	Vasopressin	

2.1.3 Consumable material and kits

Consumable material

Equipment/Instrument	Source
Amylose Resin	NEB
Autoclave tape	VWR
Cell culture requirements, T75 and T25 filter bottles; P10, P6 and P3 shells; 24-hole, 6-hole and 96-hole plates	Sarstedt

Equipment/Instrument	Source
Cell scraper	Sarstedt
Centrifuge beakers for cooled centrifuge "Beckman Avanti; Rotor JA10" (20 mL)	Beckman Coulter GmbH
Centrifuge beakers for cooled centrifuge "Beckman Avanti; Rotor JA25.50" (250 mL)	Beckman Coulter GmbH
Coverslips, round 12 mm	VWR
Coverslips, round 22 mm	VWR
Nunc®CryoTubes®	Sigma
Falcon tubes, 50 mL and 15 mL	Sarstedt
Glass slide (76 x 26 cm)	R. Langenbrinck
Glass / plastic ware: bottles, culture flasks etc.	Roth
Gloves latex	Kimberley-Clark
Gloves nitril	Roth
Cannulas: 21 G x ½	Braun
Transparencies (clear)	Leitz/Durable
KimtechScience Task Wipes	Kimberley-Clark
Cuvettes 100 (plastic) (10 x 4 x 45 mm) for spectrophotometer "U- 2000"; 1 ml	Sarstedt
Neubauer counting chamber with cover glass, 0.1 mm depth/ 0.0025 mm^2	BRAND
HisPur™ Ni-NTA resin	Thermo Fisher
Petri dishes	Sarstedt
Pipette tips	Sarstedt/ Gilson
Polypropylene Columns, 10 mL	Thermo Scientific
PVDF membrane, 0.45 µm pore size, Immobilon-P	Millipore
Plastic reaction tubes, 0.2 mL / 0.5 mL/ 1.5 mL and 2 mL	Sarstedt
Serological pipettes	Sarstedt
SuperSignal™ West Pico	Thermo Fisher
Syringes (sterile)	Braun
Sterile filter (0.22 µm)	VWR

Kits

Kit	Source
GeneJET Plasmid Miniprep Kit	Thermo Scientific

iScript DNA Synthesis Kit	Bio-Rad
ISOLATE II RNA Micro Kit	Bioline
Plasmid Plus Midi Kit	Qiagen
Qiaquick Gel Extraction Kit	Qiagen
SensiFAST™ SYBR No-ROX Kit	Bioline

2.1.4 Antibodies

2.1.4.1 Primary antibodies and peptides

Name	Directed against	Host	Dilution	Source
anti-Actin	Actin	Rabbit, polyclonal	1:2500 (WB)	Sigma, A2066
anti-Arl13b	Arl13b	Rabbit, polyclonal	1:1000 (ICC)	Proteintech, 17711-1-AP
anti-HA (3F10)	Hemagglutinin protein (HA)	Rat, monoclonal	1:1000 (ICC)	Roche, 12158167001
anti-MBP	Maltose binding protein (MBP)	Mouse, monoclonal	1:10000 (WB)	NEB, E80325
anti-PC2C1	C-terminal region of human Polycystin-2	rabbit, polyclonal	1:100 (ICC) 1:2000 (WB)	Own lab
anti-PC2 (YCB9)	N-terminal region of human polycystin-2	Rabbit, polyclonal	1:200 (ICC)	Somlo, Yale University, New Haven
Hoechst 33258	cell-permeant nuclear counterstain binding to dsDNA	-	1:10'000 (ICC)	Sigma, 94403

2.1.4.2 Secondary antibodies

Immunogen	Conjugate	Host	Dilution	Source
Mouse IgG	Horseradish peroxidase (HRP)	Goat	1:10000 (WB)	Sigma, I5381
Rabbit IgG	Horseradish peroxidase (HRP)	Goat	1:15000 (WB)	Sigma, A0545

Immunogen	Conjugate	Host	Dilution	Source
Rabbit IgG	Alexa 568	Donkey	1:600 (ICC)	Thermo Fisher, A10042
Rat IgG	Alexa 488	Goat	1:600 (ICC)	Thermo Fisher, A11006

2.1.5 Desoxyribonucleotides

2.1.5.1 Oligonucleotides

Gene/Name	Primer	Sequence (5'→3')	Purpose
Dynll1	forward	GGCCCATATCAAGAAGGAGTTTG	qPCR
	reverse	GGATCACTGGGTGTTTGGCA	
FoxJ1	forward	ACCCTACTCCTATGCCACTCTCAT	qPCR
	reverse	TGCATGGCGGAAGTAGCAGAAGTT	
Lamin A/C	forward	TGACTTGGTGTGGAAGGCG	qPCR
	reverse	CAGTGGAGTTGATGAGAGCGG	
Nde1	forward	AGATCTGCGGCAGGAATTGG	qPCR
	reverse	GGAGCTGTCCAGACCACG	
Pkd2	forward	TTGAGCATGTGGCATACTGGC	qPCR
	reverse	GAAGAGGTCTTTGGCACATCG	
$Pkd2^{flox}$ (~ 450 bp)	forward	GGGTGCTGAAGAGATGGTTC	Genotyping
	reverse	TCCACAAAAGCTGCAATGAA	
$Pkd2^{poreL1}$ (~ 400 bp)	forward	CAAGCCGTGTTGAGATGTTGG	Genotyping
	reverse	TGTCTCCTAGAAGTGGAAACC	
Pkhd1-Cre (~ 400 bp)	forward	TGGACATGTTCAGGGATCGC	Genotyping
	reverse	TCAGCTACACCAGAGACGGA	
SacI-TEV-EcoRI	sense	CTGGTGGGGGAGGCTCGGAAAACCT CTATTTCCAAAGCACTAGTGGATCCG	Oligo-annealing
EcoRI-TEV-SacI	antisense	AATTCGGATCCACTAGTGCTTTGGA AATAGAGGTTTTCCGAGCCTCCCCC ACCAGAGCT	
MBP_6xHis_ Linker_Fw	forward	CTGAAAGACGCGCAGACTCATCATC ACCATCACCACAATTCGAGCTCTG	OE mutation primer
MBP_6xHis_ Linker_Rv	reverse	CAGAGCTCGAATTGTGGTGATGGTGA TGATGAGTCTGCGCGTCTTTCAG	OE mutation primer

Gene/Name	Primer	Sequence (5'→3')	Purpose
Flanking_BglII_ _Fw	forward	TATAACAAAGATCTGCTGCC	OE-Flanking Primer
Flanking_HindIII_ _Fw	reverse	CGGCCAGTGCCAAGCTTTCA	OE-Flanking Primer

2.1.5.2 Plasmids

Plasmid	Bacterial strain	Resistance	Source
pcDNA10-3/PKD2(hPoreL1), HA	DH5α	Amp	Own lab
pMAL-c2/PKD1d1	One Shot™ TOP10	Cam	Own lab
pMAL-c2/PKD1d1,TEV	BL21(DE3)pLysS	Amp/Cam	Own lab
pUHD10-3/TM4FL,HA	DH5α	Amp	Own lab
pWE3	DH5α	Amp	ATCC

2.1.6 Enzymes and markers

All appropriate 10x reaction buffers were ordered together with the respective enzymes at the companies. Other reaction buffers are listed under 2.1.2.

Enzymes

Enzyme	Source
BamH I–HF, 10 U/µL	NEB
Collagenase, Type II, *Clostridium histolyticum*	Sigma
DNase I, grade II, from bovine pancreas	Sigma
EcoR I-HF, 10 U/µL	NEB
Hind III-HF, 10 U/µL	NEB
Proteinase K	Roth
Sac I-HF, 10 U/µL	NEB
T4 DNA ligase: 400 U/µl	NEB
Taq DNA polymerase	Own lab
TEV protease	Own lab

Markers

Marker	Source
2-log DNA ladder	NEB
PageRuler prestained protein ladder	Thermo Fisher

2.1.7 Mouse lines

Name	Background	Description	Source
Pkd2^{poreL1}	129/Sv	Knock-in mouse line where 11 aa of the pore region of polycystin-2 were substituted with that of polycystin-2L1.	Own lab
Pkhd1::Cre	129/Sv	Tissue-specific regulation of the *Pkhd1* gene promoter located in the kidney papilla (described in Williams et al., 2014)	Own lab
Pkd2$^{+/lox}$	129/Sv	A *Pkd2^{flox}* allele made by inserted flanking *loxP* sites situated in intron 2 and intron 4 of *Pkd2* (described in Nishio et al., 2009)	Own lab

2.1.8 Cells

In the following, all bacterial strains and mammalian cells were listed that were used for transformation, DNA preparation or protein expression during this work.

'(DE3)' is indicating that the host is a lysogen of λDE3, and therefore exhibit a chromosomal copy of the T7 RNA polymerase gene under control of the lacUV5 promoter. Such strains are compatible for production of protein from target genes cloned in vectors that can be induced with IPTG. 'pLysS' indicates that the bacterial strain encodes the T7 lysozyme which is a natural T7 RNA polymerase inhibitor prior to induction by preventing the basal transcription of the lacUV5 promoter to produce the T7-RNA polymerase. Furthermore, the expression of toxic genes is kept low.

2.1.8.1 Bacteria

Name	Selection	Description	Source
BL21(DE3)pLysS	Cam	Allow high-efficiency protein expression of any gene that is under the control of a T7 promoter and has a ribosome binding site.	Novagen
DH5α	-	A versatile strain used for general cloning and sub-cloning applications, and is available in a wide variety of transformation efficiencies.	NEB
One Shot™ TOP10	-	Ideal for high efficiency cloning as well as plasmid preparation. It enables stable replication of plasmids with high copy numbers.	Thermo Fisher
Rosetta(DE3)pLysS	Cam	BL21 derivatives designed to enhance the expression of eukaryotic proteins that contain codons rarely used in E. coli. These strains supply tRNAs for AGG, AGA, AUA, CUA, CCC, GGA codons on a compatible chloramphenicol-resistant plasmid. Thus the Rosetta strains provide for "universal" translation which is otherwise limited by the codon usage of E. coli. The tRNA genes are driven by their native promoters.	Thermo Fisher
Rosetta2(DE3)pLysS	Cam	BL21 derivative designed to enhance the expression of eukaryotic proteins that contain codons rarely used in E. coli. These strains supply tRNAs for 7 rare codons(AGA, AGG, AUA, CUA, GGA, CCC, and CGG) on a compatible chloramphenicol-resistant plasmid. The tRNA genes are driven by their native promoters.	Thermo Fisher

2.1.8.2 Mammalian cells

Name	Selection	Description	Source
LtTA-2,22	G 418	LLC-PK_1 cells with constitutive synthesis of the tetracycline transactivator (tTA) by the CMV promoter sequence in the regulator plasmid (pUHD15- 1neo; G418 resistance)	Own lab
LtTA-2,22/ PKD2,HA Clone #3	G 418 & Puromycin	LtTA-2,22 cell line, stably transfected with pUHD10-3/PKD2fl, HA; regulated synthesis of PC2,HA via doxycycline (Tet-off)	Own lab
LtTA-2,22/ PKD2(hPoreL1),HA Clone #59	G 418 & Puromycin	LtTA-2,22 cell line, stably transfected with pUHD10-3/PKD2(hPoreL1), HA; regulated synthesis of PC2(hPoreL1),HA via doxycycline (Tet-off)	Own lab

2.1.9 Hardware and software

Hardware

Equipment/ Instrument	Source
ÄKTAmicro	GE Healthcare
Agarose gel electrophoresis chamber "Owl EasyCast B2"	Thermo Scientific
Autoklav „Systec 5050 ELV"	Tuttnauer
Blotting Chamber "Tank Blot SE 600"	Hoefer
Centrifuge "Hitachi himac CT15RE"	VWR
Centrifuge "Multifuge 3 L-R"	Hereaus
Centrifuge "Pico"	Hereaus
Chemiluminescence system "Fusion Fx7"	Vilber Lourmat
CO_2 incubator for cell culture	Binder
Fluorescence microscope camera PCO edge	PCO AG

Equipment/ Instrument	Source
Freezers -20°C	Privileg
Freezers -80°C “Herafreeze"	Heraeus
Gel Documentation System “GelDoc XR+”	BioRad
Gel electrophoresis cell “Mini Protean 3”	BioRad
Hybridization oven “HB-1000” and “OV3”	UVP; Biometra
Ice machine	Ziegra
Incubator	Heraeus
Laminar flow bench “Lamin Air HA 2448 GS”	Heraeus
LightCycler® 480	Roche Diagnostics, Ltd., Rotkreuz, Switzerland
Liquid nitrogen container “ARPEGE TP 170”	Air Liquide Medical GmbH
Magnetic Stirrer “MR3001”	Heidolph
pH electrode “SenTix60”	WTW
Photometer “NanoDrop”	ThermoScientific
Power Supply “PS608”	life technologies
Power Supply “Standard Power Pack 25”	Biometra
qPCR Cycler “LightCycler 480 II”	Roche
Refrigerators	AEG, privileg
Repetitive pipette “HandyStep electronic”	Brand
Rosette cooling cell “RZ3”	Bandelin
Shaking plate “Duomax 1030”	Heidolph
SONOPLUS ultrasound homogenizer	Bandelin
Sonotrode “KE 76”	Bandelin
Stereomicroscope “StereoDiscovery.V12”	Zeiss
Thermal cycler “T100”	Bio-Rad
VisiChrome HighSpeed Polychromator System	Visitron Systems GmbH

Epifluorescence microscope

	Name	Source
Microscope	Axiovert 200M	Zeiss
Light source	LEJ (HXP-120)	Visitron Systems GmbH
	VisiChrome High Speed Polychromator System	Visitron Systems GmbH
Objectives	10x/1.5 20x/0.75 40x/1.3	Zeiss
Camera	sCMOS-camera	PCO AG

Confocal microscope

	Name	Source
Microscope	Observer.Z1	Zeiss
Laser	405 nm, diode laser, LSM710 488 nm, Argon multiline, LDN301 561 nm, DPSS laser, LSM710	Zeiss Lasos Zeiss
Objectives	Plan-Apochromat 20x/0.8 LD C-Apochromat 40x/1.1 W C-Apochromat 63x/1.20 W	Zeiss Zeiss Zeiss
Detection module	LSM BiG	Zeiss

Software

Name	Version	Purpose	Source
Bio 1D	15.07	WB quantification	Vilber Lourmat
Excel	Office 2016	Data processing	Microsoft
Fiji (ImageJ)	1.51s	Image processing	National Institutes of Health
Fusion	15.18	WB imaging	Vilber Lourmat
ImageLab	5.2	Gel documentation	Bio-Rad
NanoDrop 2000/2000c	1.6	DNA quantification/ Photometric measurement	Thermo Fisher

Name	Version	Purpose	Source
Origin 2019	9.6.0.172	Data processing, diagrams	OriginLab
SnapGene Viewer	4.1	Gene/ plasmid handling	GSL Biotech, LLC
VisiView	4.1.0.4	Image recording	Visitron Systems GmbH
ZEN 2011 SP3 (black edition)	8.1	Image recording	Zeiss MicroImaging

Internet databases

Name	Source
BLAST	https://blast.ncbi.nlm.nih.gov/Blast.cgi
Primer 3	http://primer3.ut.ee/
PubMed	https://www.ncbi.nlm.nih.gov/pubmed/

2.2 Methods

2.2.1 Working with bacteria

In the following, working with bacteria is described. All solutions are listed under 2.1.2.

2.2.1.1 Cultivation and storage of bacteria

All procedures while working with bacteria were carried out with autoclaved or sterile-filtered material and solutions under sterile conditions. For inoculation of bacterial cultures, only fresh o/n plates (see 2.2.1.4) were used for picking colonies. For inoculating bigger cultures from smaller cultures a dilution factor of 1:100 was used. Cultures were cultivated at 37 °C and 230 rpm shaking in the appropriate medium with respective antibiotics (see 2.1.2). Stock cultures of bacteria were stored in glycerol (300 µL 100 % autoclaved glycerol with 600 µL of an o/n culture) at -80 °C.

2.2.1.2 Measurement of the optical density

For determination of the optical density (OD) of bacterial cultures 1 mL of the culture was transferred into a plastic cuvette and measured with the spectrophotometer at a wavelength of 600 nm. When absorption was higher than 1.0, cultures were diluted with the respective

medium and measured again. The dilution factor was then multiplied with the measured density. The bacterial culture medium served as blank values.

2.2.1.3 Production of competent cells

For protein expression in *E. coli*, three different strains were selected for maximizing protein levels: BL21(DE3)pLysS, Rosetta(DE3)pLysS and Rosetta2(DE3)pLysS. Therefore, competent cells of those three strains were produced as followed:

On day 1, bacteria of the respective strain were stricked out on LB plates with or without antibiotics and were incubated o/n at 37 °C. On the next day, a pre-culture of 3 mL SOB medium was inoculated with 10-20 colonies and was further cultivated at 37 °C during the day. In the evening, a culture of 250 mL SOB medium was inoculated with 1 mL of the pre-culture. This culture was cultivated in the following days at 18 °C until an OD_{600} of approx. 0.6 was reached. The cell suspension was then pelleted at 2'000 x g at 4 °C for 10 min. The pellet was gently resuspended in 1/3 of the original volume in chilled FTB buffer. After incubation on ice for 10 min, cells were again centrifuged at 2'000 x g at 4 °C for 10 min. This pellet was then again resuspended in 1/12 of the original volume in chilled FTP buffer. DMSO was added to a final volume of 7 % and cells were again incubated on ice for further 10 min. The bacteria were aliquoted in sterile reaction tubes in a volume of 100 µL and immediately frozen in liquid nitrogen to be finally stored at -80 °C.

2.2.1.4 Transformation of bacteria

5-10 µL of a ligation assay or 10-20 ng of a sequenced plasmid was used for the transformation process and was added to 100 µL of thawed competent cells and incubated on ice for 30 minutes. In order to force the bacteria to take up the plasmid, they were exposed to a heat shock (42 °C, water bath) for 30 sec. Afterwards, bacteria were kept on ice for 1.5 min and then supplemented with 250 µL of culture medium without antibiotics and incubated for 60 min at 37 °C shaking at 250 rpm for regeneration. Then, plating of 50 µL and 150 µL of the bacterial suspension on LB agar plates with the respective antibiotics followed. Plates were then incubated o/n at 37 °C.

2.2.1.5 Protein expression in *E. coli*

Test expression in LB medium

For domain expression in the pMAL-c2 vector, 2 g/L glucose were added to the medium to avoid synthesis of the enzyme amylase. This could lead to inefficient binding of the MBP tag to amylose beads later on in the purification step. For optimal induction time and temperature of the *PKD1* PKD domain 1, initial experiments were conducted. Therefore, 3 mL pre-culture was inoculated with a colony of the o/n plates for each domain. On the next day, two cultures of 20 mL LB medium with antibiotics were inoculated 1:100 from the pre-culture for each domain. When cultures of each domain reached an OD of 0.5 and 0.8, one half of the culture was shifted to 18 °C and the other half to 25 °C, where an induction with 1 mM IPTG followed for 0 h, 1 h, 2 h, 4 h, 8 h and o/n. At every time point, the OD of 1 mL per culture was determined via spectrophotometric measurements and 200 µL 1x SDS sample buffer per OD=1/ mL was added and the samples were boiled at 100 °C for 5 min for SDS polyacryleamid gel electrophoresis and a following coomassie staining.

Expression in minimal medium

Since carbenicillin is more stable than ampicillin in growth medium because its better tolerance for heat and acidity when used in large-scale culturing experiments, carbenicillin was used instead of ampicillin in minimal medium cultures. For efficient protein expression in minimal medium, a protocol was used that was established by the lab of Prof. Dr. Remco Sprangers from the department of Biophysics I from the University of Regensburg. Therefore, a single colony of the o/n plate was picked and cultivated in 3 mL of LB medium with the respective antibiotics for 6-8 h shaking at 37 °C. For an o/n culture, 25 mL LB medium with the respective antibiotics was inoculated 1:100 with the pre-culture and was then further cultivated o/n shaking at 37 °C. In the next early morning, a fresh 25 mL culture was inoculated 1:10 with the o/n culture. For cultivation of bacteria in minimal medium, 500 mL of minimal medium with the respective antibiotics were inoculated 1:40 with the fresh LB culture when it reached an OD of 0.8 while cultivating at 37 °C shaking. The minimal medium culture was then further cultivated at 37 °C until the optimal OD of either 0.5 or 0.8 for induction was obtained. After letting the culture cool down to 25 °C, 1 mM IPTG was used to induce protein synthesis. For checking induction efficiency, samples of 1 mL before and after induction were taken and pellets were resuspended in 200 µL 1x SDS sample buffer per OD=1.0. Before further purification steps followed, samples were loaded on SDS gels and protein levels were verified by a staining with coomassie as described in following sections.

2.2.2 Working with mammalian cells

In the following, working with mammalian cell lines is described. All solutions are listed under 2.1.2.

2.2.2.1 Cultivation of mammalian cells

When working with mammalian cell lines, every step was carried out in a laminar flow bench. Cells were kept at 37 °C with 5 % $CO_2$and 95 % relative humidity in a CO_2 incubator. For cultivation cell culture flasks with a filter cap at a size of 25 cm^2 or 75 cm^2 were used with 5 mL or 15 mL medium, respectively. The equipment was sterilized with 70 % ethanol and liquids were autoclaved or sterile filtered before use. Cell numbers were determined by counting cells in all four quarters of a Neubauer chamber.

2.2.2.2 Passaging of cells

When cell density showed a confluency of approximately 80 %, cells were washed twice with 1x PBS and detached with 1 mL (T25 cell culture flask) or 2 mL (T75 cell culture flask) trypsin/EDTA solution for 6 – 10 min. After complete detachment, cells were split 1:5 - 1:20 in culture medium with FCS depending on cell growth rate and density.

2.2.2.3 Freezing and thawing of cells

For freezing, cells were grown to 80 % confluency in a T75 cell culture flask and were then trypsinized for detachment. After transferring to an appropriate reaction tube, cells were centrifuged at 100 x g for 5 min at 4 °C. The supernatant was removed and the cells were resuspended in 4.5 mL of 90 % FCS supplemented with 10 % DMSO. One T75 flask was split into three 1.8 mL cryovials with 1.5 mL of cell suspension each. For ensuring slow freezing at approx. 1 °C/min, cryovials were transferred into polycstyrene containers at -80 °C, where they were kept for short-term storage. For long-term storage, cells were transferred to the gas phase of liquid nitrogen.

For thawing, the cryovial with cells was kept on ice until cells were partially thawed by hand warmth. Culture medium was pipetted to the cells and the resulting cell suspension was transferred to a reaction tube, where it was further diluted to 10 mL. After centrifugation for 5 min at 100 x g and 4 °C, the supernatant was removed and the cell pellet was resuspended in 5 mL growth medium and transferred into a T25 cell culture flask.

2.2.2.4 Stable transfection with poly-L-ornithine

For establishing the cell line LtTA-2,22/PKD2(hPoreL1),HA LtTA-2,22 cells were used. tTA is a fusion protein of the tetracycline repressor (tetR) binding to the tetracycline operator and the VP16 protein; Tetracycline can bind tTA and thereby changes the protein's conformation, which inhibits the binding of the fusion protein to the tetracycline operator. This prevents the induction of transcribing a target DNA sequence that is under control of a tetracycline operator and a downstream following minimal CMV promoters. After removing tetracycline, the fusion protein is again capable of binding to the operator sequence to re-activate transcription (= tet-off system). In this work, doxycycline, a derivative of tetracycline that shows a higher affinity to tetR, was used. Hence, lower concentration could be used which is beneficial for cell physiology.

The following descriptions are provided for cultivation in T25 flasks. LtTA-2,22 cells were split in T25 on the day before to reach 70-80 % confluency on the following day. 3 mL of culture medium supplemented with 3 µL of poly-L-ornithine solution was mixed thoroughly with 8 µg of plasmid-DNA (7 µg of the target protein coding vector pUHD10-3 and 1 µg of puromycin plasmid pWE3). After removing the medium, cells were incubated with the transfection solution for 6 h at 37 °C in the CO_2 incubator. Afterwards, the transfection solution was removed and the cells were incubated for 3.5 min with a DMSO solution (30 % DMSO in culture medium). After removing the DMSO solution, the cells were washed twice with 1x PBS and the cells were then cultured in the appropriate medium.

On the next day, cells were trypsinized with 3 mL culture medium and 1 mL trypsin/EDTA (see 2.2.2.2). Afterwards, 3 mL and 1 mL of the cell suspension were transferred into two separate P10 dishes and were further cultivated for two days. To start selection, 0.5 µg/mL puromycin was added to the medium. Approximately 14 days after transfection, clones could be harvested. Picked clones (in a volume of 150 µL) were transferred into 2 mL culture medium supplemented with doxycycline in a 24 well plate, where they were further cultivated up to a confluency of 70-80 %. To identify positive clones, clones were trypsinized in 2 mL (500 µl trypsin/EDTA, 1.5 ml medium) after reaching the required confluency. One third of the suspension was transferred back into one well of a 24 well plate for cultivation. The rest was separated into two P6 dishes and further cultivated until 70 % confluency was reached. Then, cells were induced or not induced for 4 days by medium with or without doxycycline in P6 dishes without coverslips for producing cell lysates to test protein expression in western blots and in P6 dishes with coverslips to identify the protein localization by immunofluorescence.

2.2.2.5 Induction of protein synthesis in stable transfected cells

In all stable transfected cell lines during this work, the so called 'Tet-off system' was used. By adding 100 ng/mL doxycycline to the cultivation medium, protein synthesis was repressed whereas removing doxycycline from the cultivation medium induced protein synthesis. To remove all doxycycline from the cells, two additional washing steps with 1x PBS followed before cultivation medium without DOX was then again added to the cells.

Protein induction time was optimized by conducting an induction series to identify appropriate protein amounts for further analysis. Therefore, cells from the lines LtTA-2,22/PKD2(hPoreL1), HA and LtTA-2,22/PKD2, HA were induced for 3 to 7 days before cells were lysed for quantifying protein amounts via western blot with an antibody against HA. As a negative control, uninduced cells were lysed.

2.2.2.6 Production of mammalian cell lysates

For producing mammalian cell lysates, P10 dishes of (un-)induced cells were harvested at 100 % confluency to ensure ciliogenesis. All solutions (see 2.1.2) were pre-cooled and cells were kept on ice during the whole procedure. After removing the medium, the cells were cautiously washed twice with 5 mL of 1x PBS. 1 mL ice cold 1x PBS was added to the cells and the cells were scraped off with a cell scraper. This cell suspension was then transferred into a reaction tube for centrifugation at 4'000 rpm for 5 min at 4 °C. The supernatant was discarded and the cell pellet was resuspended in 100-150 µL lysis buffer and incubated for 15 min on ice. The suspension was then again centrifuged for 30 min at 14'000 rpm at 4 °C and the pellet was removed with a pipette tip. Lysates were stored at -80 °C until further analysis.

2.2.2.7 Immunocytochemistry

Coverslips are washed cautiously three times with 1x PBS to remove medium from the cells. Cells were fixed for 20 min with fixation solution and again washed three times with 1x PBS afterwards. For permeabilization, cells were incubated in permeabilization solution for 45 min at RT and then again washed with 1x PBS for 5 min. Primary antibodies were diluted as described in 2.1.4 in blocking solution and were added to the cells for 1 h at RT or 4 °C o/n. Then, the primary antibody was removed and the cells were washed twice with 1x PBS for 5 min. Secondary antibodies were diluted as described in 2.1.4 in blocking solution and were added to the cells in the dark for 1 h at RT. Cells were again washed three times with 1x PBS afterwards. If a nucleic staining was required, cells were counter-stained with Hoechst

33258 diluted in 1x PBS in the dark for 1 min at RT and again washed three times with 1x PBS. Coverslips were then inversely mounted with mowiol on a glass slide for recording fluorescence images on the following day.

2.2.3 Working with rodent tissue

2.2.3.1 Handling and genotyping of *Mus musculus*

General handling

The mice are bred in euro standard type II and III cages in a conventional animal laboratory of the University of Regensburg. Offspring was marked by footpad tattoos and tail biopsied 4 – 21 days after birth and separated from the mother at 19 – 28 days of age. Animals had unlimited access to drinking water and complete food in a 12 h day/night cycle.

Genotyping

For DNA isolation, mouse biopsies were treated with 0.2 g/L proteinase K in 700 µL tail buffer in a rotating hybridization oven at 50 °C o/n. On the next day, samples were centrifuged (10'000 x g, 30 min) to remove undigested material. The supernatant was transferred into new reaction tube and 700 µL isopropanol was added. After inverting the samples thourougly, the precipitaded DNA was collected by centrifugation at 10'000 x g for 15 min. The pellet was then washed with 500 µL 70 % EtOH and again centrifuged (10'000 x g, 15 min). The ethanol was then removed and the pellets were dried at 40 °C for 20-30 min and finally resolved o/n in a hybridization oven (50 °C, rotating) in 50-100 µL TE buffer.

By a following PCR, genotypes of the mice were identified. As a positive control, a sample with known genotype showing the expected bands was used and as a negative control, water instead of DNA was used in the reactions. All reactions were performed with the following ingredients and cycler program:

Reagents	Volume
DNA	1 µL
10 mM dNTPs	0.5 µL
10 µM Primer forward	0.5 µL
10 µM Primer reverse	0.5 µL
Taq Polymerase	0.25 µL
10x Thermopol buffer	2.5 µL
Aqua bidest	19.75 µL

Temperature	Time	
94 °C	3 min	
94 °C	30 sec	35 x
58 °C	1 min	
68 °C	1 min	
68 °C	5 min	
12 °C	hold	

After PCR, an agarose gel electrophoresis (2 % agarose gel, see 2.2.5.3) with 12.5 µL of PCR product supplemented with DNA loading dye followed to visualize and document the amplified and separated DNA fragments. In samples of mice with the $Pkd2^{poreL1}$ genotype, wild-type bands were expected at 307 bp and the band of the allel with substituted pore region was expected at 400 bp.

2.2.3.2 Perfusion and enzymatic digestion of mouse kidneys

Male mice were anesthetized with 0.12 – 0.15 mg Narcoren/kg body weight. Both kidneys were rapidly removed and transferred into cold isolation buffer. After perfusion through the renal artery with 3 mL of pre-warmed 50 µg/mL collagenase II- containing incubation solution, the papilla and the rest of the kidney were separately reduced to small pieces and digested with 500 µg/mL collagenase II in incubation solution at 37 °C for 10 minutes. Subsequently, the released tubules were collected (fraction 1) and washed three times with ice-cold sorting solution after letting them sink down to the bottom of the reaction tube .Thus, four additional fractions were collected, each digested for 5 minutes at 37 °C in decreasing concentrations of collagenase II (dilution factor 1:2).

2.2.3.3 Sorting of kidney tubules

Tubules were sorted in ice-cold sorting solution under 60-100x magnification of a stereo microscope (ZEISS SteREO Discovery.V12) with continuous cooling (4 °C) of the tubules for a maximum of two hours. Sorted collecting ducts for RNA isolation were centrifuged at 500 x g at 4 °C and subsequently kept at -80 °C until further preparation.

2.2.3.4 Labeling of collecting ducts with a ratiometric calcuim indicator

The isolated collecting ducts were incubated with 5 µM Fura-2,AM and 0,025 % pluronic F127 in calcium buffer or calcium free buffer supplemented with 5 mM probenecid on poly-L-lysine coated coverslips for 30 minutes at room temperature. Afterwards, the collecting ducts were washed twice with calcium (free) buffer/probenecid and incubated in this buffer until the start of the experiment.

2.2.3.5 Recording of intracellular calcium levels in collecting ducts

Pictures were taken every second over a period of 610 seconds with the excitation wavelength alternating between 340 nm and 380 nm by using a grating monochromator. Vasopressin or ATP was added after the 10^{th} image (= 10 seconds after start). Images were taken with the Zeiss AxioVert 200mot fluorescence microscope using either a x10/0.75 or x20/0.75 fluor objective and recorded with the VisiView software package and a PCO edge camera. The central 50 % of intact collecting ducts were used as regions of interest (ROIs), and the basal fluorescence (F_0) was defined as the mean fluorescence of the first ten frames without stimulation. Two cortical and two papillary collecting ducts isolated from one animal were separately analyzed after addition of ATP or vasopressin in consecutive measurements. All papillary and all cortical collecting ducts were taken together as n=1 by forming the mean value, respectively. By choosing a ROI where no fluorescence signal was detected, the background fluorescence was subtracted from every recorded image (F/F_0). In order to determine a relative calcium level in the intracellular space, the ratio of fluorescence intensity at the two wavelengths was calculated. For imaging without extracellular calcium, a calcium free imaging buffer was used during the experiment and the experiment was started within 1 minute to avoid physiological damage. All graphs are averaged responses from animals of the respective genotype and are illustrated as means ± SD. Statistical significance between calcium levels of wild-type and Polycystin-2^{poreL1}mice was accepted by Student's t test at $p < 0.05$.

2.2.4 Working with RNA

2.2.4.1 RNA isolation and synthesis of cDNA from mouse collecting ducts

Total RNA was prepared using the Isolate II RNA micro kit (BIOLINE). In the final step, RNA was eluted with 15 µL of ddH_2O for further generating cDNA with the iScript cDNA synthesis kit (Bio-Rad) by adding 1 µL of iScript Reverse Transcriptase and 4 µL of 5x iScript Reaction Mix according to the manufacturers' reaction protocol.

2.2.4.2 Quantitative real time PCR

Quantification of gene expression was performed in duplicates using SensiFAST™ SYBR® No-ROX Kit and the Roche LightCycler® 480. In every replicate, 2 µL of the previously diluted cDNA (1:2) was used in a total volume of 20 µL. Primers were used in a final concentration of 400 nM each. After the cDNA was denatured for 7 minutes at 95 °C, 35

PCR cycles (20 seconds at 90 °C, 20 seconds at 64 °C and 10 seconds at 72 °C) followed. Data normalization was based on the efficiency (E) corrected comparative threshold cycle (CT) method (see equation 2.1) after (Pfaffl, 2001) with normalization of the raw data to the included housekeeping gene Lamin A/C. Differences between wild-type and Polycystin-2^{poreL1} samples were expressed as means ± SD and tested by one-sided Student's t test at $p < 0.05$.

$$Ratio = \frac{(E_{Target})^{\Delta Ct_{Target}(Control-Mutant)}}{(E_{Reference})^{\Delta Ct_{Referenc}(Control-Mutant)}} \tag{2.1}$$

2.2.5 Working with DNA

2.2.5.1 Preparation of plasmid DNA from *E. coli*

Miniprep

In this work, plasmids were isolated from *E. coli* cells by using the GeneJET Plasmid Miniprep Kit (Thermo Scientific). Cells of a 5 mL o/n culture were collected by centrifugation (16'000 x g, 1 min) and were resuspended in 250 µL of resuspension solution. Then, 250 µL lysis solution and 350 µL neutralization solution were added and the suspension was again centrifuged (16'000 x g, 1 min). The supernatant was transferred to a GeneJet column and after another centrifugation step at 16'000 x g for 1 min, the column was washed twice with washing solution and two following centrifugation steps (16'000 x g, 1 min). The column was then spin dried (16'000 x g, 1 min) and the DNA was eluted in 50 µL H_2O.

Midiprep

For larger amounts of plasmids, the Plasmid plus Midiprep Kit (Qiagen) was used. Therefore, bacterial cells of a 50 mL o/n culture were collected by centrifugation (4'000 x g, 15 min, 4 °C) and the pellet was then resuspended in 2 mL P1 buffer. Afterwards, 2 mL of P2 buffer was added and the solution was then incubated for 3 min. Subsequently, 2 mL of S3 buffer was added and the lysate was put in a filter cartridge and incubation for 10 min followed. After filtering through the cartridge, the lysat was mixed with 2 mL of BB buffer and the solution was then passed through the midi spin column by vacuum. The spin column was then successively washed with 700 µL ETR buffer and 700 µL PE buffer by centrifugation at 10'000 x g for 1 min. Afterwards, the column was spin dried (10'000 x g, 1 min) and the DNA was eluted with 200 µL H_2O.

2.2.5.2 Concentration determination of DNA

The concentration of DNA solutions was either measured with a NanoDrop photometer or a 1 % agarose gel by comparison the sample bands with bands of an adequate DNA ladder. In this work, the 1 kb plus ladder (NEB) was used for concentration determination.

2.2.5.3 Gel electrophoresis with agarose gels

For size and concentration determination of DNA fragments, agarose gel electrophoresis with 1 % - 3 % (w/v) agarose according to the required separation was conducted. Therefore, agarose was boiled in 1x TAE buffer until it was completely dissolved. After the solution cooled down briefly, ethidium bromide was added to an end concentration of 0.4 µg/mL and the solution was mixed thoroughly before being poured into the gel tray without air bubbles. Before letting the gel polymerize completely at RT, a gel comb with the required amount of pockets was inserted. DNA samples were loaded into the gel with a DNA loading dye. As a size reference, a DNA ladder was additionally loaded (see 2.1.2) and the gel was run at 150 V. Preparative gels for concentration determination were run at 100 V for a better separation of bands. Nucleic acids were thereby stained by ethidium bromide and visualized and documented by UV light with the GelDoc system.

2.2.5.4 Elution of DNA from agarose gels

When bands of the expected size were detectable in the agarose gel, a scalpel was used for excising the bands and the DNA containing gel pieces were subsequently prepared with the E.Z.N.A. Gel Extraction Kit. Therefore, bands were eluted in 1 volume (=1 mL per g) XP2 buffer and incubated at 60 °C until the gel has completely melted. After transferring the solution into a HiBind DNA mini column, the column was spun at 10'000 x g for 1 min. Then, 300 µL XP2 was added and the column was again spun at 14'000 x g for 1 min. Subsequently, a washing step followed by adding 700 µL SPW wash buffer and centrifuging at 14'000 x g, 1 min. Then, the column was dry spun for 2 min at 14'000 x g and the DNA was eluted with 30 µL H_2O.

2.2.5.5 Cleavage of DNA via restriction enzymes

For a digestion of DNA, 10 units per restriction enzyme were used to cleave 1 µg DNA in an assay supplemented with a 10 x reaction buffer suitable for the respective enzymes. This overdigestion is recommended to overcome variability in DNA source, quantity and purity.

The total amount of enzymes was kept below 10 % of the reaction volume to avoid star activity caused by the glycerol that is contained in the restriction enzymes.

When a plasmid was used as a vector in a subsequent ligation, 10 µg of DNA was digested. Double digestions were conducted sequentially when both enzymes required the same reaction buffer. First, one enzyme was added to 10 µg of vector supplemented with the required enzyme reaction buffer in 100 µL volume and the approach was then incubated o/n at 37 °C. In a test digestion, 100-200 ng of DNA was then loaded on a gel to check for the expected DNA fragments. Then, the second enzyme was added with the respective reaction buffer in additional 100 µL of volume. This approach with a total volume of 200 mL was then further incubated for 4 h at 37 °C.

Digested DNA fragments were then eluted from appropriate agarose gels as described in 2.2.5.4.

2.2.5.6 Oligoannealing

For the insertion of a double-stranded oligo into a vector, complementary single strands with sticky ends were designed and ordered dissolved in 100 µM at metabion international AG. 3 µg per strand were then incubated with oligo annealing buffer (see 2.1.2) in a total volume of 50 µL for 4 min at 90 °C and 70 °C at 10 min followed by a slow cool down to 10 °C (-1 °C/min). Double-stranded oligos were then stored at -20 °C until needed.

2.2.5.7 Ligation

Ligation after oligoannealing

Ligation of 200 ng vector with an annealed oligo was conducted in a molar ration of 1:100 and was calculated as shown in 2.2.

$$Amount\,of\,vector - DNA\,[ng]\,x\,\frac{Size\,of\,insert - DNA\,[bp]}{Size\,of\,vector - DNA\,[bp]}\,x\,100 \qquad (2.2)$$

The reaction with a total volume of 10 µL was performed in a water bath at 60 °C for 15 min and after letting the approach cool down to RT, 1 µL T4 ligase and 10x ligation buffer (NEB) was added and it was incubated in a water bath at 15-17 °C, o/n. As a negative control, the approach was conducted in parallel without insert. Here, no colonies should be seen on a later o/n-plate after transformation.

Standard ligation

Ligation of 150 ng digested vector with a digested insert was conducted in a molar ration of 1:3 and was calculated as shown in 2.3.

$$Amount\,of\,vector - DNA\,[ng]\,x\,\frac{Size\,of\,insert - DNA\,[bp]}{Size\,of\,vector - DNA\,[bp]}\,x\,3 \tag{2.3}$$

The reaction with a total volume of 10 µL was performed by adding 1 µL T4 ligase and 10x ligation buffer (NEB) in a water bath at 15-17 °C, o/n. As a negative control, the approach was conducted in parallel without insert. Here, no colonies should be seen on a later o/n-plate after transformation.

2.2.5.8 Sequence analysis

Cloned plasmids were checked with appropriate primers premixed in a concentration of 4 µM by sequencing at Microsynth Seqlab. Therefore, plasmids were diluted to a concentration of 40-100 ng/µL.

2.2.5.9 Site-directed mutagenesis by overlap extension PCR

The technique of an overlap extension PCR is a useful method for inserting a required mutation into a specific site of a given vector. Therefore, four primers are designed to synthesize two overlapping strands in separately conducted PCR reactions (see fig. 2.1).

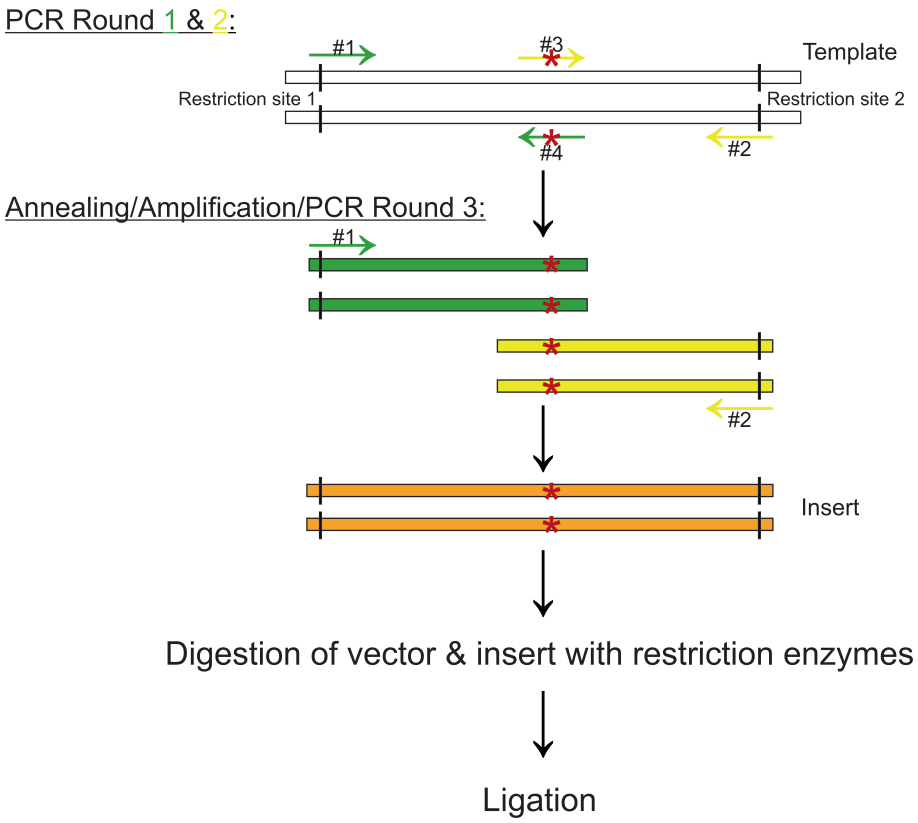

Figure 2.1: **Schematic overview of an overlap extension PCR to introduce mutations.** First, in two separate PCR reactions (green and yellow), flanking primers (#1 & #2) with restriction sites (black bars) and two complement primers (#3 & #4) carrying a desired mutation (red asterics) were used to amplify partially overlapping strands. Next, the overlapping strands were annealed and amplified with both flanking primers (#1 & #2) to produce longer strands carrying the desired mutation. These strands and the target vector are then digested with the restriction enzymes existing in both vector and insert for a following ligation and plasmid preparation.

Primer #1 and #2 are flanking primers showing restriction sites that are also present in the target vector. Primer #3 and #4 are complementary towards each other carrying the desired mutation. Since the Taq polymerase is not able to proof-read its synthesized strands, Pfu polymerase with its 3'->5' exonuclease activity was used to ensure a more accurate synthesis. The first two PCR reactions were conducted with the primers #1 + #5 and #3 + #2 as listed below:

Reagents	Volume
Vector template [10 ng]	X µL
10 mM dNTPs	0.5 µL
10 µM Primer forward	0.5 µL
10 µM Primer reverse	0.5 µL
Pfu Polymerase [3 U/µL]	1 µL
10x Pfu buffer	2 µL
Aqua bidest	add to 25 µL

Temperature	Time	
95 °C	2 min	
95 °C	30 sec	35 x
55 °C	30 sec	
68 °C	30 sec	
68 °C	10 min	
14 °C	hold	

PCR products were then loaded on an agarose gel for gel extraction when the expected band was present (see subsections 2.2.5.3 and 2.2.5.4). Eluted bands were then annealed in a 1:1 molar ratio [50 ng] in a total volume of 20.5 µL for 2 min at 98 °C followed by 10 min at 98 °C for denaturation and a subsequent gradient of -1 °C/min (45x). Afterwards, 1 µL Pfu polymerase [3 U/µL], 1 µL 10 mM dNTPs and 2.5 µL 10 x Pfu buffer were added for a further amplification of the annealed strands at 72 °C for 15 min. For a final amplification, 1 µL of Primer #1 + #2 each were added with 0.5 µL 10x Pfu buffer and 2.5 µL aqua bidest in a total volume of 30 µL and the reaction was conducted with the following reaction program:

95 °C	5 min	
95 °C	30 sec	35 x
50 °C	1 min	
72 °C	2 min	
72 °C	10 min	
14 °C	hold	

The final PCR product carrying the mutation was then loaded on an agarose gel and bands of the expected size were extracted out of the gel. Then, restriction digestion with enzymes that can cleave both vector and insert was conducted and ligation followed as described in subsections 2.2.5.5 and 2.2.5.7. In next steps, transformation into competent E. coli (see 2.2.1.4) and preparation of plasmid DNA (see 2.2.5.1) followed.

2.2.6 Working with proteins

All approaches with proteins were conducted on ice and extracted proteins were stored at -80 °C unless otherwise stated.

2.2.6.1 Lysis of expressed protein in mammalian cells

For protein lysis, medium was removed from the culture plates and the cells were washed twice with 1x PBS. After adding 1 mL ice-cold 1x PBS, cells were scraped off with a cell scraper and were transferred into a reaction tube. For harvesting, cells were centrifuged at 4'000 rpm for 5 min, 4 °C and the pellet was resuspended in 200 µL lysis buffer (see 2.1.2). After a following incubation for 15 min on ice, lysates were again centrifuged for 30 min at 14'000 rpm, 4 °C and the supernatant was transferred into a new reaction tube.

2.2.6.2 Lysis of expressed protein in *E. coli*

During the following procedures, pellets were resuspended according to equotion 2.4.

$$2\,x\,OD_{600}\,x\,culture\,volume\,[mL])\,/\,100 \tag{2.4}$$

Bacteria were harvested at 4'000 rpm, 15 min at 4 °C. The pellet was then resuspended in the recommended buffer for the following purification steps. To visualize the solubility of the protein, 20 µL of sample was taken in every step of this experiment and was supplemented with 5x SDS sample buffer. For lysis, lysozyme and DNase I was added 1:100 from the stock solutions and an incubation for 15 min on ice followed. Immediately before sonation, PMSF and benzamidin was added 1:100 from the stock solutions and sonication in 8 cycles for 30 sec with a pause of 1 min between each cycle followed (power intensity ~ 40 %). During this procedure, lysates were kept in an ice-bath to prevent foaming. The lysate was then centrifuged (3'700 x g, 15 min, 4 °C) and the pellet was resuspended for visualization of putative insoluble proteins. The resulting supernatant was then again centrifuged (50'000 x g, 30 min, 4 °C). This supernatant containing the soluble fusion protein was then given to chromatography columns with amylose beads for affinity purification (see 2.2.6.7) and the pellet was again resuspended for visualization of putative insoluble proteins.

2.2.6.3 Determination of protein concentration

For colorimetric determination of whole protein concentrations after Bradford (1976) the Roti®Quant solution was used according to the manufactor's protocol. Extinction wave length were measured with 450 nm and 595 nm filters in plastic cuvettes and as a reference BSA stock solutions of 0.0 (=water) / 0.1/ 0.25/ 0.5/ 1.5/ 5.0/ 10.0 µg/µL were prepared. 10 µL of the prepared BSA solutions were vigurously mixed with 1 mL of Roti®Quant solution for establishing a standard series. Afterwards, 10 µL of the protein of interest was added to

1 mL of Roti®Quant solution . After incubation for 5-10 min of the prepared samples, the cuvettes were measured at the photospectrometer. As a blank, aqua bidest was used.

2.2.6.4 SDS polyacrylamide gel electrophoresis after Laemmli

By SDS-PAGE, proteins were separated according to their molecular weight and during this work, 15 % polyacrylamide gels were used to optimally display bands with protein sizes of approx. 10-70 kDa. Mini and maxi gels were casted according to the following tables (Tab. 2.21 and Tab. 2.22). After preparing the running gel solution, the mixture was immediately poured between two glas plates clipped into the casting apparatus and covered with a 1 cm layer of isopropanol to define a clear edge. The running gel was allowed to polymerize for at least 45 min before isopropanol was removed and the prepared stacking gel was added on top with a comb comprising the required amount of gel pockets. After further 30 min, the gel was either used for gel electrophoresis on the same day or wrapped into wet paper towels and aluminium foil for storage at 4 °C.

Table 2.21: Amounts for the casting of mini gels. 7.2 mL were used for running gels and 2.5 mL for stacking gels.

Gel	Ingredients		
4 % stacking gel	1.53 mL	H_2O	
	325 µL	Acrylamide, 30 %/ Bisacrylamide, 0.8 % solution	
	625 µL	0.5 M Tris	pH 6.8, HCl
	25 µL	10 % SDS	
	2.5 µL	TEMED	added at last
	25 µL	10 % APS	
15 % running gel	2.3 mL	H_2O	
	5.0 mL	Acrylamide, 30 %/ Bisacrylamide, 0.8 % solution	
	2.5 mL	Tris	pH 8.8, HCl
	100 µL	10 % SDS	
	10 µL	TEMED	added at last
	100 µL	10 % APS	

Table 2.22: Amounts for the casting of maxi gels. 25 mL were used for running gels and 10 mL for stacking gels.

Gel	Ingredients		
4 % stacking gel	6.1 mL	H_2O	
	1.3 mL	Acrylamide, 30 %/ Bisacrylamide, 0.8 % solution	
	2.5 mL	0.5 M Tris	pH 6.8, HCl
	100 µL	10 % SDS	
	10 µL	TEMED	added at last
	100 µL	10 % APS	
15 % running gel	5.7 mL	H_2O	
	12.5 mL	Acrylamide, 30 %/ Bisacrylamide, 0.8 % solution	
	6.3 mL	Tris	pH 8.8, HCl
	250 µL	10 % SDS	
	25 µL	TEMED	added at last
	250 µL	10 % APS	

The polymerized gels were clamped into separation chambers and 1x SDS running buffer was added. Samples were supplemented with 5x SDS sample buffer and after boiling for 5 min at 100 °C, the samples were centrifuged and a maximum of 30 µL for mini gels and 50 µL for maxi gels were loaded into the gel pockets. Commonly, 40 µg of total protein determined by Bradford assay were loaded in a volume of 50 µL. When one sample was set as a protein level reference, the volume covering 40 µg total protein was identified and from all other samples this volume was then also loaded into the gel to ensure a comparison of equal numbers of cells. As a reference for protein sizes, 2-4 µL of pre-stained protein ladder was used. Empty pockets were filled with 1x SDS sample buffer to guarantee a precise running front. Gel electrophoresis was conducted by first applying 80 V until the running front has reached the running gel and then for either further 150 V for mini gels (8 cm x 4 cm x 1.5 mm) or further 500 V for maxi gels (14 cm x 12 cm x 1.5 mm) while stirring. Maxi gels were continuously cooled to 10 °C. After the run was completed, the stacking gel was removed and the running gel was either used for staining with coomassie (see 2.2.6.5) or for western blotting (see 2.2.6.6).

2.2.6.5 Coomassie Brilliant Blue staining of polyacrylamide gels

For staining polyacrylamide gels, a staining solution containing Coomassie Brilliand Blue R 250/50 was prepared according to subsection 'Buffers and solutions for SDS-PAGE' of section 2.1.2. The gel was incubated shaking for 40 min and after several washing steps

with aqua bidest the gel was incubated in destainer solution or aqua bidest over night until unspecific staining was completely removed. The gels were then scanned with a conventional scanner.

2.2.6.6 Immunodetection of proteins by western blotting

For specific detection of proteins or determination of protein amounts, tank western blots with SDS polyacrylamide maxi gels were conducted. These gels were run in 1 x SDS running buffer (see 2.1.2) at 500 V under continuous cooling (details see 2.2.6.4). Afterwards, the separated proteins in the gel were transferred to a PVDF membrane (0.45 µm pore size) by tank blotting. Therefor, three layers of Whatman paper were soaked in transfer buffer and placed on a foam also soaked with buffer. Then, the gel was placed onto the layers of Whatman papers. Before placing the PVDF membrane on the gel, it was incubated for 10 min in methanol to activate and increase the protein binding capacity and for few minutes in transfer buffer to equilibrate the membrane. Finally, three more layers of Whatman paper soaked in buffer were placed on the membrane and a foam also soaked in buffer completed the western blot arrangement. Air bubbles were removed from this layer arrangement and it was then placed between the anode and cathode so that the negatively charged proteins were transferred from the gel to the PVDF membrane in the direction of the cathode. The tank blot apparatus was filled with transfer buffer and the transfer was conducted with 1 Ampère under continuous cooling (10 °C) for 2 h.

After the transfer, the bands of the protein ladder were marked with a pen for easier recognition of the protein sizes in the later detection. Then the PVDF membrane was incubated in blocking buffer (see 2.1.2) shaking for 30 min. In the mean time, the primary antibodies were diluted in blocking buffer according to the appropriate dilution (see 2.1.4.1) and were added to the membrane after blocking. When two proteins should be detected simultaneously, the membrane was cut into two pieces that the expected protein bands could be incubated separately. Membranes were incubated with the primary antibody at 4 °C o/n or at RT for 2 h. Then, three washing steps (10 min) with 1x TBS-T followed and the secondary antibody diluted in blocking buffer was added for 1 h (RT) to the membrane shaking. Three further washing steps followed before one final washing step with TBS was conducted. For detection of the HRP conjugated secondary antibodies, the membrane was incubated for 1 min with the enhanced chemiluminescence (ECL) reagent (SuperSignal™ West Pico, Thermo Fisher) at RT. The membranes were then placed into transparencies and protein bands were recorded with the chemiluminescence system "Fusion Fx7" (Vilber Lourmat) and were analyzed with the software Bio 1D (Vilber Lourmat).

2.2.6.7 Purification of expressed proteins by amylose columns

For purification of MBP-tagged proteins, plastic chromatography columns were used in which amylose resin (NEB) was placed. 1 mL of amylose beads exhibit a binding capacity of >4 mg and depending on the expected amount of protein the corresponding amount of beads were used (= 1 column volume, CV). Before coupling, beads were washed with sodium phosphate buffer (3x 10 mL, 2'000 rpm, 3 min) and were afterwards incubated with the supernatant containing the soluble fusion protein from section 2.2.6.2 via gravity flow by consecutive loading of the plastic columns. After binding, beads were washed with a minimum of 10 CVs of NaP_i buffer for further preparation.

For estimating the concentration of the expressed fusion protein, fractions were eluted and collected after coupling the fusion protein to amylose beads. Therefor, 1/2 CV of column buffer supplemented with 10 mM maltose was given to the loaded column. To guarantee an optimal distribution of maltose containing sodium phosphate (NaP_i) buffer, the column was flicked on and incubated for 1 min. Then, the fraction was collected. Usually up to 10 fractions were collected and the elution profile of the collected fractions was documented by Bradford assay (see 2.2.6.3) and by SDS PAGE (see 2.2.6.4). The protein containing fractions were then pooled for further preparation.

For regenerating the amylose beads, the column was washed with 10 CVs NaP_ibuffer + 10 mM maltose to elute the bound MBP protein, followed by 3 CVs of aqua, 3 CVs 0.1 % SDS solution, 3 CVs aqua bidest and 3 CVs NaP_i buffer containing 20% EtOH, in which the column was then stored at 4 °C. For purification of ^{15}N-labeled *PKD1* PKD domain 1 only new beads were used.

2.2.6.8 Cleavage of fusion proteins with TEV protease

TEV protease cleavage was conducted in sodium phosphate buffer. For cleavage of fusion proteins on column, the fusion protein coupled to amylose beads were loaded onto the column and the appropriate amount of TEV protease and 5 mM β-mercaptoethanol serving as a reducing agent were added. The reaction was conducted at room temperature for different time spans while rotating constantly side-to-side to assess the optimal cleavage time. Afterwards, the domain could be collected in the flow-through whereas most of the MBP-tag was bound to amylose.

2.2.6.9 Purification of cleaved protein by size exclusion chromatography

The size exclusion chromatography was conducted by the lab group of Prof. Dr. Christine Ziegler from the department of structural biology of the University of Regensburg by using a Superose 6 Increase 5/150 GL column coupled to a Micro Äkta. Therefore, the reaction volume was concentrated to 500 µL with a 3 MWCO column and subsequently centrifuged for 2 min at 21'300 x g to pellet particles that would disturb the gel filtration. The column was loaded with the supernatant containing the fusion protein fragments in a total volume of 4 mL of sodium phosphate buffer. The thereby separated proteins were then collected in fractions of 75 µL after separation by size. By ultraviolet absorbance measurements at 280 nm, proteins released from the column could be recorded and assigned to the collected fractions. Additionally, the fractions were loaded on a SDS-PAGE to check protein sizes of the respective fractions.

2.2.6.10 Purification of cleaved protein by Ni-NTA beads

Ni-NTA beads with a binding capacity of <30 mg per mL were used for purification and the required amount of beads for the domain expression was washed with NaP_i buffer (3x 10 mL, 700 x g, 3 min). After a first round of incubation with Ni-NTA beads for 1h at room temperature rotating side-to-side, beads were washed with 4 CV NaP_ibuffer and the collected flow-through was used for another round of incubation with new beads followed to ensure that all His-tagged compounds were removed from the domain containing flow-through. Again, beads were washed with 4 CV NaP_i buffer and the flow-through was collected for further preparation.

For eluting and washing the Ni-NTA beads, 10 CVs NaP_ibuffer + 300 mM imidazole were used to elute the bound His-tagged proteins, followed by 10 CVs of aqua bidest and 3 CVs NaP_i buffer. The beads were then stored in NaP_i buffer containing 20 % EtOH at 4 °C. For purification of ^{15}N-labeled *PKD1* PKD domain 1 only new beads were used.

2.2.6.11 Concentration of protein domains

The purified and isolated domains were concentrated with centrifugal filter units with a molecular weight cut-off of 3 kDa. By centrifuging at 4000 x g for ~20 min at room temperature the volume was consecutively narrowed down to 500 µL. Afterwards, the column was again washed by filling with NaP_i buffer and another following centrifugation to remove putative residing glycerol that are present in the concentrators for the following NMR analysis.

2.2.6.12 Preparation of urine and incubation with *PKD1* PKD domain 1

Prof. Dr. Banas from the University hospital Regensburg kindly provided spot urine from a patient with ADPKD. As a control, spot urine from a healthy person was taken. Both samples were centrifuged at 6'000 x g for 15 min at 4 °C to remove macromolecules and cell compartments. Urine samples were then stored at -80 °C until further use. Right before a NMR measurement was conducted, 12 mL urine was incubated with 600 µg *PKD1* PKD domain 1 (equal to 20 µL urine per µg domain) was incubated for 30 min rotating at room temperature. For avoiding different buffer conditions after urine incubation, the sample was washed twice with 4 mL of NaP_ibuffer and subsequently concentrated to 500 µL.

2.2.6.13 NMR measurements

Nuclear magnetic resonance (NMR) spectroscopy is a technique used in research for determination of the content and purity of a sample as well as its molecular structure. This technique is based on the fact that every nuclei has a characteristic property known as 'spin'. In this method a sample is set under a constant magnetic field and via applying a radio frequency pulse an energy transfer is accomplished that rises the nucleic energy from the base level to a higher energy level. A spinning nucleus in a higher energy level generates a magnetic field in the opposite direction to the external magnetic field and when this spin then returns to its base level the emerging energy is emitted at the same radio frequency. This signal is measured in many ways to yield an NMR spectrum for the nucleus concerned. The effective magnetic field at this nucleus is dependent on the environment of the nucleus since neighboring electrons can have a shielding effect and the more electronegative the nucleus, the higher the resonant frequency. This resonant frequency of the energy transition is called the chemical shift (Keeler, 2010).

A one dimensional (1D) NMR spectra can comprise information about the investigated sample along two dimensions. The x-axis displays the chemical shift in parts per million (ppm) whereas the y-axis corresponds to the shift intensity. Unfortunately, shifts lying closely to each other can make the spectra hard to analyze so that the shifts cannot be matched properly. This is when researchers take advantage of a two dimensional (2D) NMR. 2D experiments are conducted by a sequence of radio frequency pulses with delay periods in between. They normally consist of four stages: a preparation period where a set of radio frequency pulses create a magnetization coherence; an evolution period where no pulses are delivered and the nuclear spins can freely process; a mixing period where another set of pulses is manipulating the coherence and will give a detectable signal and a last detection period where the free induction decay signal is recorded as a function of time. Since two sets

of radio frequency pulses are applied to a sample the output of such an experiment is a plot of two frequency axes each representing a chemical shift thereby showing an intensity value for each pair of frequency variables which is often presented in contour plots using a third dimension (Keeler, 2010) comparable to a geographical height map.

NMR measurements were conducted at 298 K with a Bruker 500 MHz spectrometer equipped with an NEO AVANCE console and a nitrogen cooled cryogenically cooled probehead by Prof. Dr. Remco Sprangers. To all samples 5 % D_2O was added for the lock. The signal of the solvent is used to stabilize the magnetic field because the measurement of an NMR spectrum requires a high level of stability. Modern NMR devices constantly monitor the resonance frequency of the solvent and when this frequency is in constant relation to the magnetic field, deviations in frequency show that the field has changed which then entails that the device can initiate a correction of the field. Thereby, the field stays "locked" to the frequency, also called a "deuterium-lock".

^{1}H-^{1}H COSY

In the homonuclear correlation spectroscopy (COSY) spins are identified which are occurring between nuclei of the same type. COSY experiments consist of a single pulse followed by an evolution time followed by a second pulse and the measurement period. It displays the frequencies for a single isotope, most commonly hydrogen ^{1}H, along both axes. Diagonal peaks in such a spectra correspond to peaks in a 1D-NMR while cross-peaks occur when there is a correlation between the signals along each of the two axes indicating couplings between pairs of nuclei. The coupling pairs can be identified by finding the corresponding diagonal peaks directly above or below and left or right of the cross peak. The nuclei represented by those diagonal peaks are coupled (Keeler, 2010).

^{1}H-^{15}N HSQC

Heteronuclear single-quantum correlation spectroscopy (HSQC) detects correlations between nuclei of different types that are separated by one bond. By this, one peak per pair of coupled nuclei is displayed in the spectra comprising less peaks with a better resolution. In a ^{1}H-^{15}N HSQC, one peak can then be matched to an amino group present in the protein backbone or in side chains of some amino acids. This is why this method is also called the "protein fingerprint". In a subsequent assignment the peaks can be allocated to the residues existing in the protein (Keeler, 2010).

2.2.7 Statistical analysis

When the data followed a normal distribution, statistical significance was calculated according to Student's t-test. Otherwise the Mann-Whitney U test was employed.

2.2.8 Ethics statement

All experiments were conducted in accordance with the German Animal Protection Law and were approved by the local government.

3 Results

3.1 Structural analysis of the PKD domain 1 in *PKD1*

In recent years, new information about polycystin-1 became known such as N-terminal autoproteolytic cleavage events with a subsequent translocation to the plasma membrane of the resulting fragments (Wei et al., 2007) or the heteromerization with polycystin-2 (Qian et al., 1997), the other protein involved in ADPKD development. However, only less is known about the variety of domains located on the large N-terminus of the *PKD1* gene product except for its putative general relevance in interacting with other proteins or carbohydrates supporting the suggestion that PC1 may participate in cell-cell or cell-matrix associations (Sandford et al., 1997). It is also assumed that this extracellular tail might be important for chemical sensing of substances (Barr and Sternberg, 1999; Delmas et al., 2004; Koettgen et al., 2011). For this hypothesis, the repetitive sixteen PKD domains might be promising candidates for gradual sensing of chemical compounds. However, the function of the PKD domains is poorly investigated so that the focus of the following experiments was set on examining the role of the PKD domain 1 as a representative of the repeats in ligand-binding, especially in ligands present in the human urine. A potential binding of components in the urine might lead to downstream events, e.g. in regard to a polycystin-2 interaction (Babich et al., 2004). This assumption should be investigated in the following by a nuclear magnetic resonance measurement of the domain without and with incubation of urine donated from an ADPKD patient or a healthy person. Recorded NMR spectra of these conditions should be compared afterwards to detect presumptive shifts suggesting a ligand-binding function of the domain.

3.1.1 Establishment of the expression vector 'pMAL-c2/MBP-His-TEV-PKD1d1'

For the upcoming experiments, an efficient expression vector had to be established that yield an appropriate amount of protein that is well-folded and easy to purify. Therefore, the expression vector 'pMAL-c2/PKD1d1' cloned by the former colleague Markus Dietz had to

be edited for a more efficient expression and purification. The thereby established vector 'pMAL-c2/MBP-His-TEV-PKD1d1' comprising the maltose binding protein-tag (MBP, 42 kDa) followed by a 6x His sequence, a TEV cleavage site (ENLYVQ|S), a glycine and serine-linker and the human *PKD1* PKD domain 1 (~10 kDa) was then used for the subsequent experiments (see supplemental fig. 5.1). The protein that is synthesized by this vector will result in a size of ~52 kDa.

Figure 3.1: **Schematic overview of the fusion protein.** For optimal expression and purification, *PKD1* PKD domain 1 was cloned downstream of a MBP tag (~42 kDa), followed by a 6x His tag, a glycine and serine-linker and a TEV cleavage site resulting in a fusion protein with a total size of ~52 kDa.

3.1.2 Expression and purification of unlabeled *PKD1* PKD domain 1-fusion protein

First, three different *E. coli* strains BL21(DE3) pLysS, Rosetta(DE3) pLysS and Rosetta2(DE3) pLysS were cultivated in LB medium and were induced with 1 mM IPTG when the optical density has reached 0.5-0.6. Induction of protein expression was conducted for 0 h, 1 h, 2 h, 4 h, 8 h and o/n at 37 °C. By that, not only the general expression was tested but also the best bacterial strain and induction time could be identified. Thus, the strongest expression based on SDS-PAGE band intensity after staining with coomassie was achieved with Rosetta2(DE3) pLysS when induced for 8 h (see fig. 3.2).

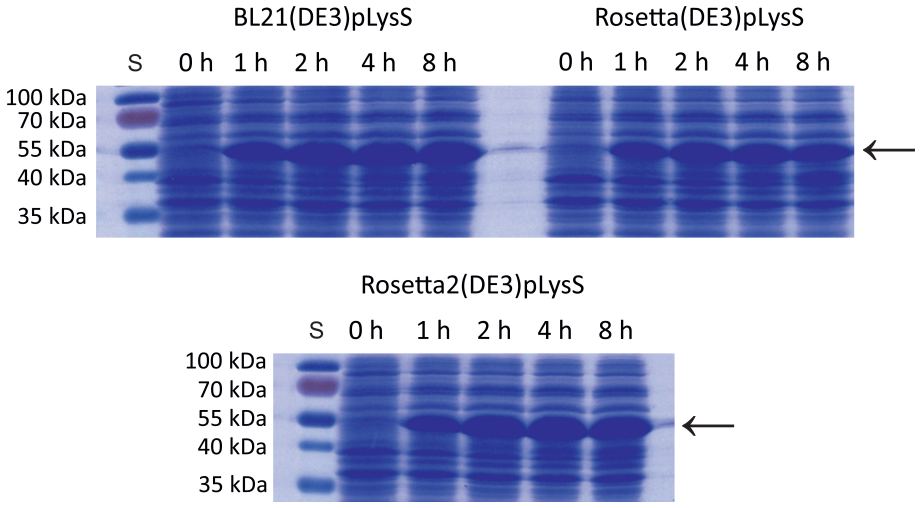

Figure 3.2: **Test expression in LB medium.** Expression was induced with 1 mM IPTG at an OD of 0.5-0.6 for different induction time spans at 37 °C. The resulting fusion protein with a size of ~52 kDa (arrow) was enriched over time in all three *E. coli* strains with the strongest expression detectable in Rosetta2(DE3) pLysS. Protein detection was accomplished by coomassie staining. S, molecular weight standard.

Since an expression in minimal medium for NMR analysis has to be defined carefully to ensure a soluble and correctly folded protein, more parameters were tested to optimize *PKD1* PKD domain 1 expression. Hence, two different induction starting points (OD= 0.5 or 0.8) and two different temperatures were tested (25 °C and 37 °C) while expression was conducted in minimal medium.

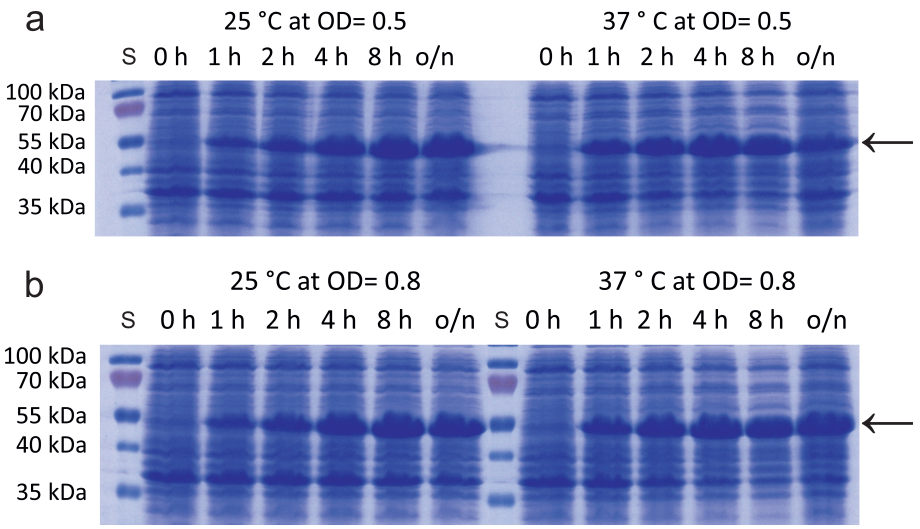

Figure 3.3: **Test expression in minimal medium.** In Rosetta2(DE3) pLysS, no obvious differences in expression intensity could be observed at the expected size of ~52 kDa (arrow) when induction with 1 mM IPTG was started at an OD of 0.5 (a) or 0.8 (b). Higher temperature (37 °C) did also not result in a better expression of *PKD1* PKD domain 1 compared to when a lower expression temperature was chosen (25 °C). Hence, the expression parameters that were used further on were defined as an induction starting point at an OD of 0.8 for 8 h at 25 °C. Protein detection was accomplished by coomassie staining. S, molecular weight standard.

By the fact that expression strength did not differ much among the different parameters (fig. 3.3), it was decided to conduct expression at a lower temperature (25 °C) when the OD reached ~0.8 to enable protein solubility and folding. To avoid inclusion of synthesized protein in inclusion bodies, expression was conducted for 8 h even though o/n samples showed slightly stronger bands in the gel.

Under those conditions, the PKD domain 1 of *PKD1* was expressed in 1 L (2x 500 mL cultures) of unlabeled minimal medium and subsequently purified with amylose beads as described in subsections 2.2.6.2 ff. After lysing the bacterial cells by ultrasound, cell compartments of greater size were centrifuged down to the pellet by a centrifugation step at 3'700 x g for 15 min at 4°C and in a following centrifugation at 50'000 x g for 30 min at 4°C smaller cell compounds like inclusion bodies were separated into the pellet. Soluble proteins should remain in the supernatant. Since the main portion of the fusion protein with a size of ~52 kDa was present in the supernatant it could be assumed that the expressed fusion protein is soluble under the determined conditions (see fig. 3.4).

For an impression of how much protein is expressed at a scale of 1 L, the 50'000 x g supernatant was incubated with amylose beads and 10 fractions of the amylose-bound fusion

protein were eluted with 10 mM maltose in NaP_i buffer. The collected fractions were then analyzed by SDS-PAGE and a following coomassie staining additionally to a Bradford assay of the protein-containing fractions to determine the concentration. According the SDS gel shown in fig. 3.4, fractions 1-4 comprised the main portion of the fusion protein so that those four fractions were pooled and measured for concentration determination.

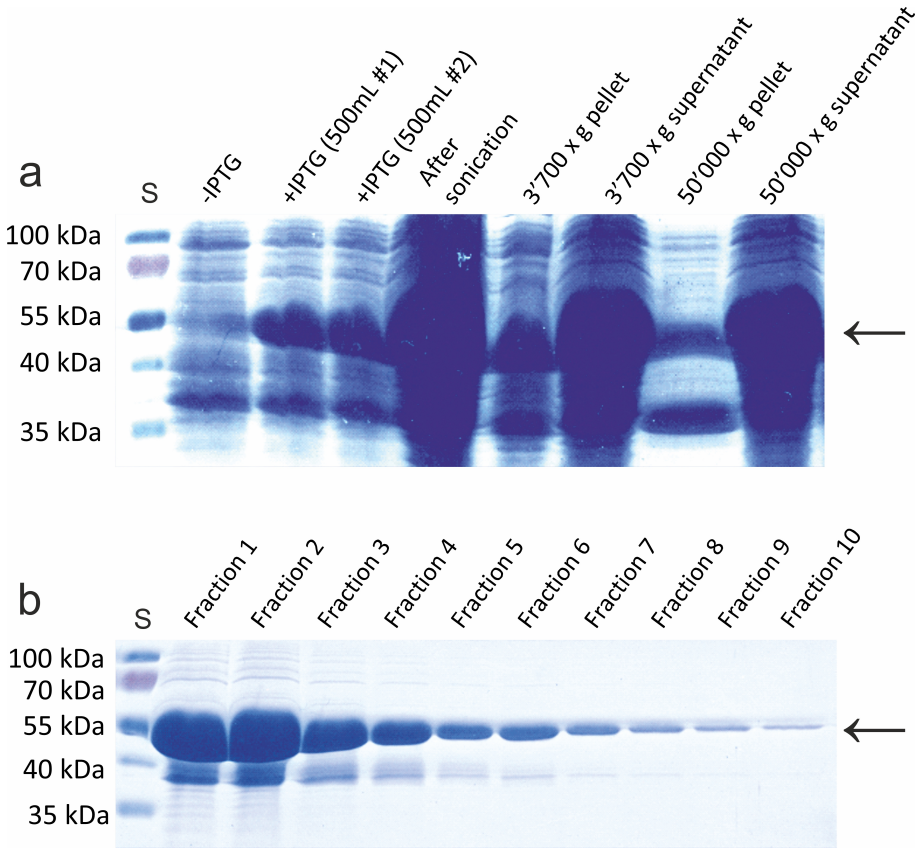

Figure 3.4: **Solubility test and purification of *PKD1* PKD domain 1-fusion protein.** 2x 500 mL minimal medium cultures of expressed 'pMAL-c2/MBP-His-TEV-PKD1d1' in *E. coli* were lysed by ultrasound and subsequently centrifuged by a centrifugation at 3'700 x g for 15 min at 4 °C and a further centrifugation at 50'000 x g for 30 min at 4 °C. After both centrifugation steps, the main portion of fusion protein (~52 kDa, arrow) was detectable in the supernatant (a). This fusion protein was then purified with amylose beads. After several washing steps, 10 fractions were collected with 1/2 CV 10 mM maltose containing NaP_i buffer showing the fractions 1-4 as those comprising the main portion of the 52 kDa-fusion protein (arrow) (b). Protein detection was accomplished by coomassie staining. S, molecular weight standard.

The following Bradford assay determined a concentration of 4.2 µg/µL in ~5 mL pooled fractions which results in ~21 mg of fusion protein per 1 L expressed culture. This calculation

was important for the following upscaled expressions to estimate required volumes of amylose beads as well as volumes of TEV protease for fusion protein cleavage and Ni-NTA beads for a second purification step.

Preceding experiments for optimizing TEV protease cleavage of the fusion protein showed that an amount of $1/50^{th}$ of protease from the protein-to-cleave is necessary to successfully cleave all the fusion protein in at least 2-4 h when the experiment was conducted at 25 °C (data not shown). To remove protease and putative residuals of MBP from the pure *PKD1* PKD domain 1, two purification steps with Ni-NTA followed (see subsection 2.2.6.10). As represented in figure 3.6, an o/n reaction at 25 °C was conducted with 420 µg of TEV protease that corresponds to $1/50^{th}$ of 21 mg fusion protein. Cleaving the fusion protein resulted in a complete cleavage into the MBP-tag and the *PKD1* PKD domain 1.

First, it was tried to separate the resulting fragments after TEV protease cleavage by size exclusion chromatography. Prof. Dr. Christine Ziegler kindly offered to conduct the chromatography in her lab. Hence, a Superose 6 Increase 5/150 GL column coupled to a Micro Äkta was used for fragment separation.

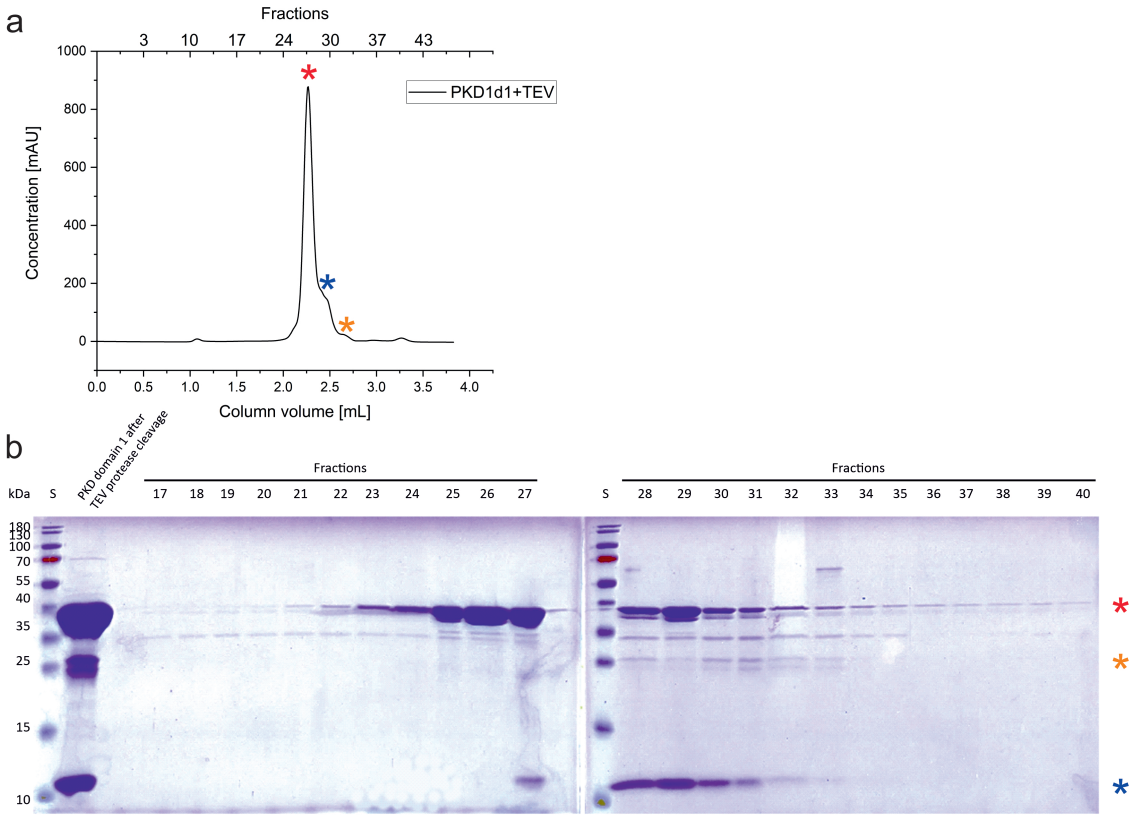

Figure 3.5: **Size exclusion chromatography to separate the MBP-tag and *PKD1* PKD domain 1.** By using a Superose 6 Increase 5/150 GL combined with a Micro Äkta, proteins in a total column volume of 4 mL were collected in fractions of 75 µL after separation by size. As shown in the spectra, a high peak occurred between fraction 24-33 expected to be the large MBP-tag (red asterisk). This peak fused into a shoulder at fraction 28-30 (blue asterisk). At fractions 31-33, another small peak appeared in the spectrum (orange asterisk) (a). The peaks could then be assigned to the proteins after running a SDS gel of the relevant fractions. As expected, the high peak matched with the MBP-tag (~42 kDa, red asterisk) whereas the shoulder turned out to be the PKD domain 1 (~10 kDa, blue asterisk). The following small peak could be assigned to the TEV protease that was applied for cleavage of the fusion protein (~23 kDa, orange asterisk). Protein detection was accomplished by coomassie staining. mAU, milli absorbance units. S, molecular weight standard.

Here, a high peak in the absorbance was detectable between fraction 24-33. This could be assigned to the large MBP tag by SDS-PAGE. At fractions 28-30, the graph fused into a shoulder and at fractions 31-33 another small peak appeared in the spectrum. The shoulder could be identified as PKD domain 1 and the small peak as the TEV protease, as seen in the SDS gel. This overlay of the proteins in the fractions 27-33 suggested that the huge MBP tag could not be separated from the PKD domain 1 of *PKD1*. Hence, a purification

with Ni-NTA after the initial purification with amylose and the subsequent TEV protease cleavage should solve this problem.

By purifying twice with Ni-NTA, the TEV protease could be removed successfully as well as most of the MBP-tag, both visualized in the SDS gel by the ensuing elution with NaP_i buffer containing 300 mM imidazole.

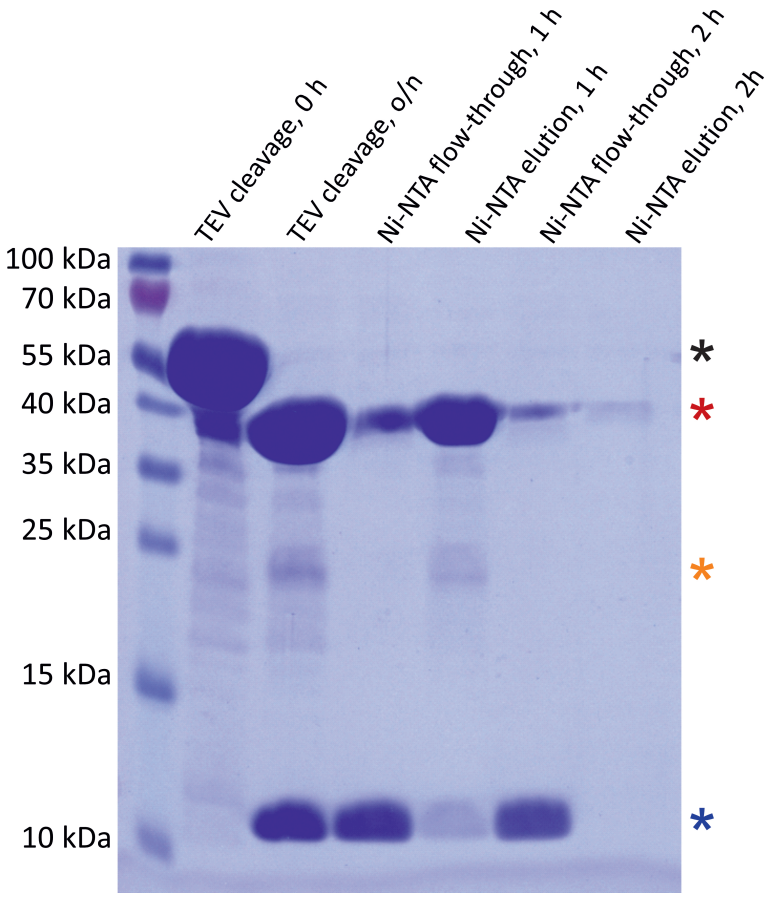

Figure 3.6: **Cleavage of expressed fusion protein with TEV protease and an additional purification step with Ni-NTA beads.** After cleaving the fusion protein with its size of 52 kDa (black asterisk) at 25 °C o/n with $1/50^{th}$ of protease, two fragments with sizes of ~42 kDa (MBP, red asterisk) and ~10 kDa (*PKD1* PKD domain 1, blue asterisk) resulted. To remove the His-tagged proteins MBP and TEV protease (~23 kDa, orange asterisk) from the pure domain, two ensuing Ni-NTA purification steps followed by incubating 2x for 1 h at RT. The beads were washed afterwards with 4 CV and the collected flow-through contained pure PKD domain 1 and marginal remains of cleaved MBP. In the eluate, the TEV protease and most of the MBP-tag could be isolated. Protein detection was accomplished by coomassie staining. S, molecular weight standard.

A following determination of concentration by Bradford assay and by SDS-PAGE revealed

a concentration of ~2 µg/µL that corresponds to 1 mg in 500 µL or ~0.2 mM (see fig. 3.7).

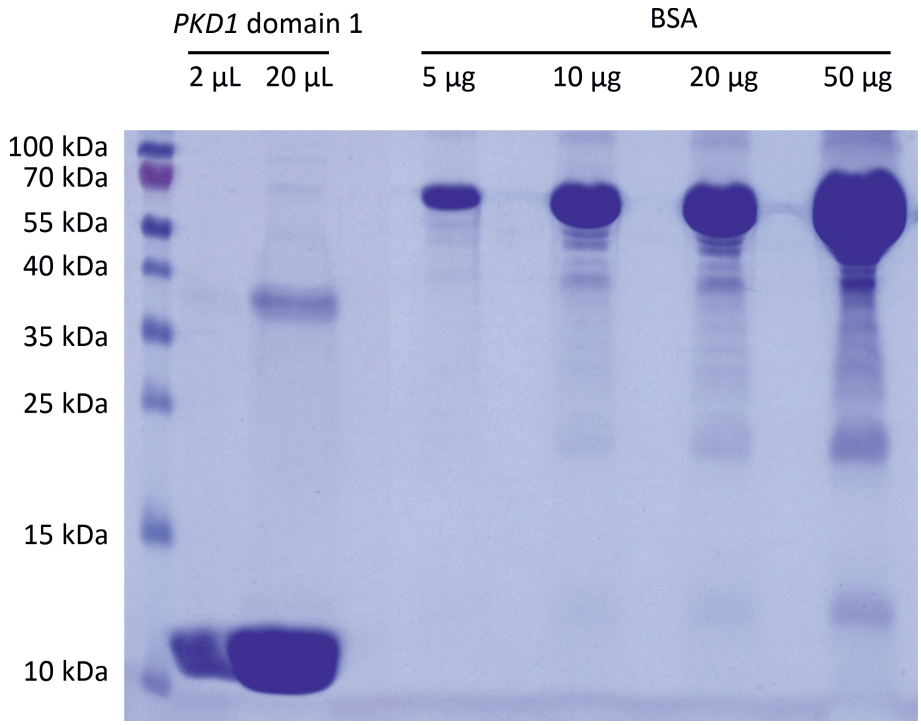

Figure 3.7: **Determination of unlabeled PKD domain 1 protein concentration by SDS-PAGE.** 1 L of unlabeled PKD domain 1 resulted in >90 % pure protein (~10 kDa) with minor remains of MBP (~42 kDa) visible when higher amounts of protein were loaded into the gel. For concentration estimation, BSA was loaded in different amounts to compare band intensity. This suggests a sample concentration of ~2 µg/µL. Protein detection was accomplished by coomassie staining. S, molecular weight standard.

3.1.3 NMR measurements of unlabeled PKD domain 1 of polycystin-1

For analyzing the PKD domain 1 protein structure regarding a putative ligand-binding of components present in patient *versus* control urine, ^{1}H-^{15}N heteronuclear single-quantum correlation spectroscopy (HSQC) was conducted that is used to detect correlations between protons and ^{15}N-labeled amino groups separated by one bond. By this, the so called “protein fingerprint" can be examined that can show interactions of the protein with a presumed ligand existing in the urine which would be implied by peak shifts in the NMR spectrum.

The cooperating Prof. Dr. Remco Sprangers from the department of Biophysics I from the University of Regensburg suggested to have a protein purity of 90 % and a concentration of 0.1 mM in a 500 µL sample to ensure clear NMR spectra with distinguishable peaks. In a first 2D measurement of unlabeled PKD domain 1, the spectra suggested the presence of a

~10 kDa protein that is properly folded (data not shown).

3.1.4 Expression and purification of ^{15}N-labeled PKD domain 1 of polycystin-1

For expression and purification of ^{15}N-labeled protein, customary ammonium chloride was replaced in the minimal medium by ^{15}N-labeled ammonium chloride as the only source of nitrogen so that a following recorded NMR spectrum would be based on these incorporated ^{15}N atoms. The required amount of fusion protein was expressed and purified with amylose from 10x 500 mL cultures. After TEV protease cleavage, Ni-NTA purification was conducted to remove remaining MBP and the TEV protease (see fig. 3.8).

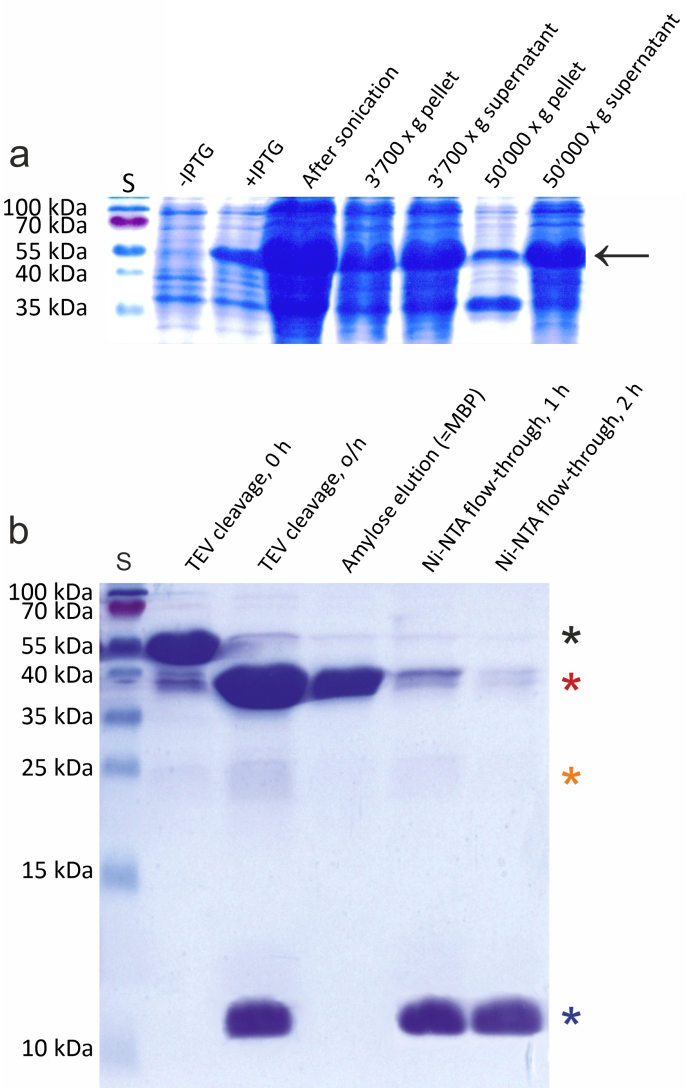

Figure 3.8: **Purification and cleavage of ^{15}N-labeled PKD domain 1 of polycystin-1.** 10x 500 mL minimal medium cultures of expressed 'MBP-His-TEV-PKD1d1' in *E. coli* were lysed by ultrasound and subsequently centrifuged by a centrifugation at 3'700 x g and a further centrifugation at 50'000 x g. After both centrifugation steps, the main portion of fusion protein (~52 kDa, arrow) was detectable in the supernatant (a). After purification with amylose and cleaving the fusion protein with its size of 52 kDa (black asterisk), two fragments with sizes of ~42 kDa (MBP, red asterisk) and ~10 kDa (*PKD1* PKD domain 1, blue asterisk) resulted. To remove the His-tagged proteins MBP and TEV protease (~23 kDa, orange asterisk) from the pure domain, two ensuing Ni-NTA purification steps followed (2x 1 h). The collected flow-through contained pure PKD domain 1 and marginal remains of cleaved MBP (b). Protein detection was accomplished by coomassie staining. S, molecular weight standard.

The *PKD1* PKD domain 1-containing flow-through was than concentrated and analyzed by SDS-PAGE suggesting a sample concentration of ~5 µg/µL (see fig. 3.9).

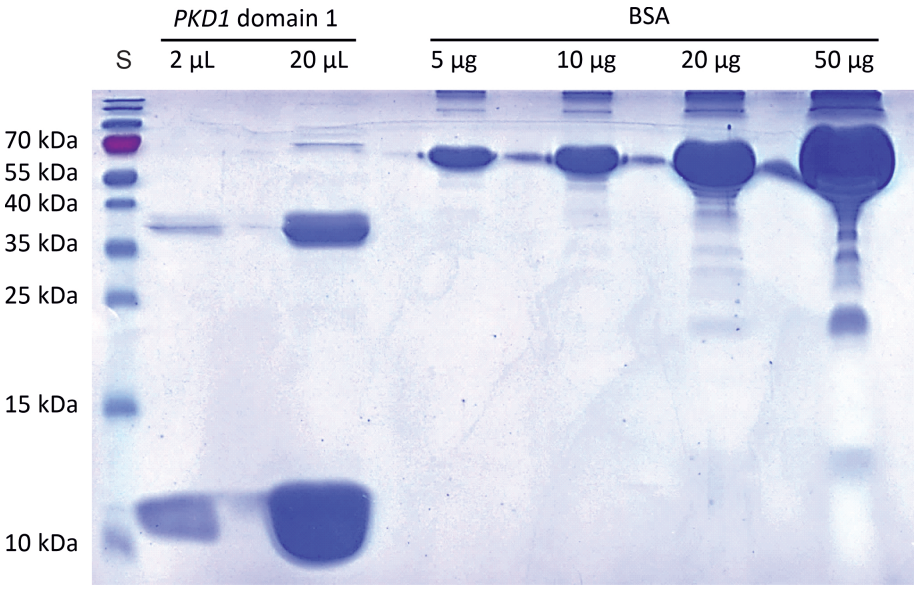

Figure 3.9: **Determination of ^{15}N-labeled PKD domain 1 protein concentration by SDS gel.** 5 L of ^{15}N-labeled *PKD1* PKD domain 1 resulted in >90 % pure protein (~10 kDa) with minor remains of MBP (~42 kDa) visible when higher amounts of protein were loaded into the gel. For concentration estimation, BSA was loaded in different amounts to compare band intensity. This suggests a sample concentration of ~5 µg/µL. Protein detection was accomplished by coomassie staining. S, molecular weight standard.

A Bradford assay determined a marginally higher concentration of ~6 µg/µL in 500 µL. The determined mean concentration corresponds to ~3 mg or 0.6 mM. This final sample was then split in aliquots of 500 µL with 0.1 mM to ensure a comparability of the NMR spectra of samples that were either incubated or not incubated with urine. Afterwards, the aliquots were plunge frozen in liquid nitrogen and subsequently stored at -80 °C until NMR measurements.

3.1.5 2D-HSQC NMR analysis of ^{15}N-labeled PKD domain 1 of polycystin-1

A first measurement of ^{15}N-labeled *PKD1* PKD domain 1 by 2D-HSQC NMR that was not incubated with urine showed a spectra of very high quality. The proton frequency is shown on the x-axis and the nitrogen frequency is displayed on the y-axis. Protons which are separated by one bond from ^{15}N-labeled amino groups are then displayed in a cross-peak of

both x- and y-axis.

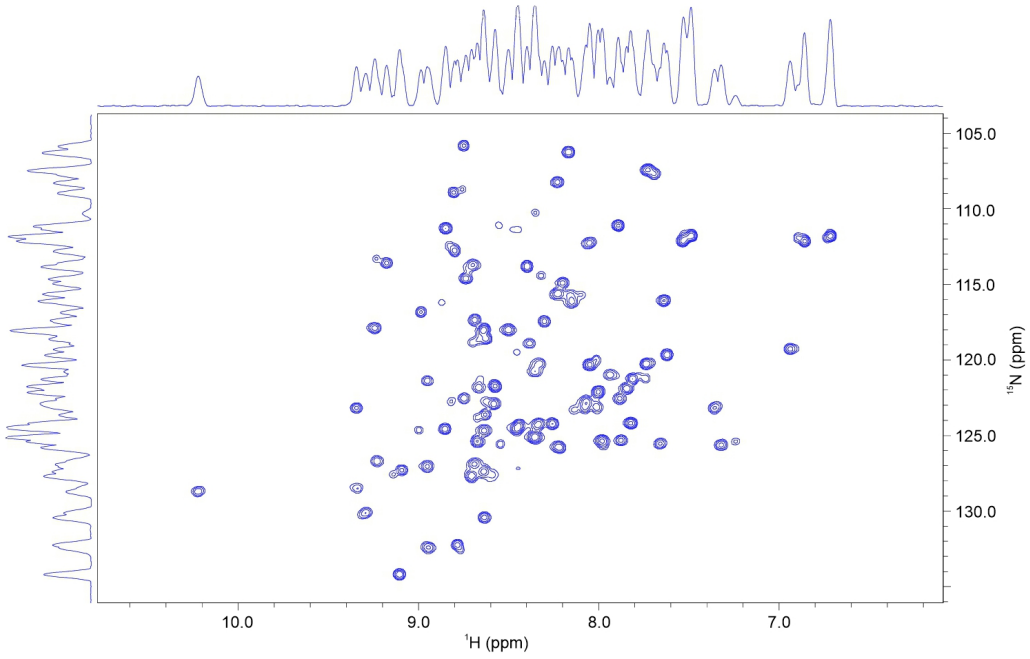

Figure 3.10: **Two dimensional-HSQC spectroscopy of ^{15}N-labeled PKD domain 1 of polycystin-1.**The proton frequency is shown on the x-axis and the nitrogen frequency is displayed on the y-axis. The upper axis shows the recorded 1D-spectrum of the ^{1}H measurement and the left axis shows the recorded 1D-spectrum of the ^{15}N measurements . The dot plot shows interaction of protons with labeled amino groups that are separated by one bond. The chemical shift is displayed in parts per million (ppm).

Next, PKD domain 1 samples that were incubated with patient or control urine were measured by two dimensional HSQC and compared to the spectrum of the sample that was not incubated with urine.

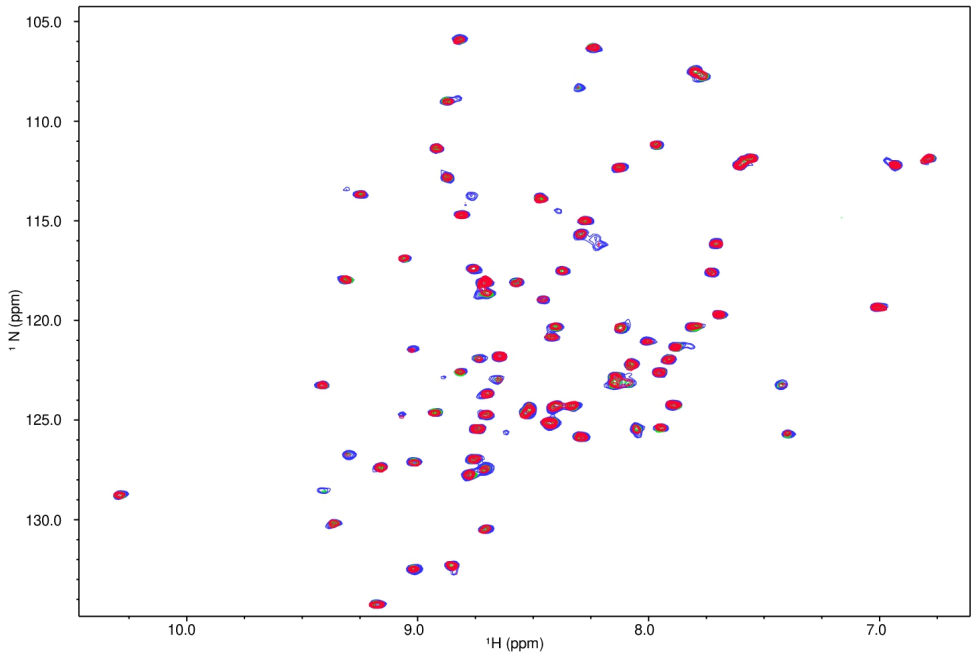

Figure 3.11: **2D-HSQC spectra of *PKD1* PKD domain 1 not incubated or incubated with urine.** The dot plot shows interaction of protons with labeled amino groups that are separated by one bond. Peaks detected when PKD domain 1 was not incubated with urine (blue) did not show shifts when compared to peaks detected after the domain was incubated with urine of an ADPKD patient (red) or with urine of a healthy person (green). The proton frequency is shown on the x-axis and the nitrogen frequency is displayed on the y-axis. The chemical shift is displayed in parts per million (ppm).

Here, spectra did not show clear differences among samples that were either incubated or not incubated with urine (fig. 3.11) suggesting that this domain is not involved in ligand-binding.

These data suggest that the PKD domain 1 might not be involved in a ligand-binding function of the extracellular domain of polycystin-1 to transduce chemical signals. However, more experiments have to be conducted in the future to corroborate this finding.

3.2 Analysis of the channel conductivity of polycystin-2

Since the pore forming region that extends from amino acids 618 to 658 is conserved among species (Fig. 1.11) and often shows missense mutations in patients of polycystic kidney disease (Shen et al., 2016), it is assumed that the pore properties for ion conduction are crucial for channel functionality. By setting the focus on this pore forming region, more information about the importance of this region should be gained. The basic idea was here to exchange the pore-forming loop of polycystin-2 with that of the closely related polycystin-2L1, thereby creating a mutant protein - polycystin-2^{poreL1}. In a *vice versa* assay, this was carried out previously by another working group to study the channel properties of polycystin-2L1 by exchanging its pore region with that of polycystin-2 (Shen et al., 2016).

3.2.1 Establishment and characterization of a polycystin-2^{poreL1} mutant protein *in vitro*

For channel conductivity experiments *in vitro,* an inducible porcine kidney cell line was used to establish the cell line LtTA-2,22/PKD2(hPoreL1),HA comprising a pore-modified polycystin-2. This cell line should be afterwards compared regarding the respective calcium conductivity with the cell line LtTA-2,22/PKD2,HA that already existed in the lab which comprises wild-type polycystin-2.

After transfection and selection with antibiotics, positive clones were selected by western blot analysis and immunofluorescence to quantify overall protein amount and protein localization in the primary cilia and the endoplasmic reticulum. After analyzing 60 clones, ten positive clones could be identified with clone #59 turning out to be adequate for further experiments. In western blot analysis when using the antibody 3F10 against the HA-tag clone #59 showed a clear band at the expected molecular size (~110 kDa) which could be detected after induction for three days by removing doxycycline from the culture medium. In immunofluorescence stainings using an antibody against polycystin-2 for detecting the mutant protein in the endoplasmic reticulum and in the cilia by costaining with the primary cilia marker acetylated tubulin, the expected localization pattern could be verified (see fig. 3.12). This clone #59 was then used in all following *in vitro* analyses.

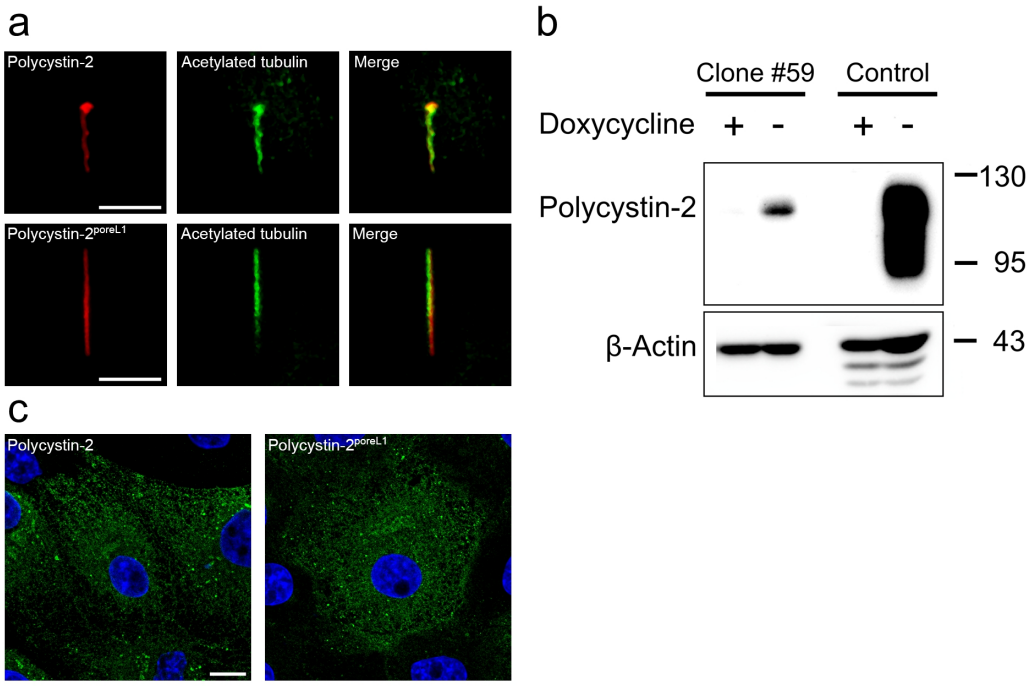

Figure 3.12: **Characterization of a positive clone inducible for the mutant protein polycystin-2^{poreL1}.** A costaining with the ciliary marker acetylated tubulin demonstated the localization of the wild-type protein as well as the mutant protein in the primary cilium (a) and the reticular pattern in the cytoplasm was representative for the endoplasmic reticulum (c). In western blot analysis with an antibody against the HA epitope, clone #59 showed an expression of polycystin-2 via a band with the expected molecular size (110 kDa) after induction by removing doxycycline (-). No band appeared when cells were treated with doxycycline (+). As control, cells of the pre-existing stable transfected LLC-PK$_1$ cell line expressing HA-tagged wild-type polycystin-2 with identical induction conditions were used. 40 µg of cell lysates were loaded per lane and as a loading control, an antibody against β-actin was applied (expected band at 42 kDa) (b). Bar, 10 µm. The numbers on the right of the blots give the size of the molecular weight standard in kDa.

3.2.2 Investigation of the protein half life of mutant polycystin-2^{poreL1}compared to wild-type polycystin-2 *in vitro*

Since the protein level of the clone #59 showed a weak expression in the conducted western blot compared to the control it should be tested whether this could be due to a lower protein stability of the mutant protein polycystin-2^{poreL1}. Thus, in a next assay, protein stability of the mutant polycystin-2^{poreL1} protein should be determined and compared to wild-type polycystin-2 by inhibiting ribosomal translation with cycloheximide. To do so, first it had to be determined after how many days of induction both cell lines produce an equivalent

amount of polycystin-2 that protein degradation could be better monitored and compared. Previous work showed that three days of doxycycline removal was enough for cells of the line LtTA-2,22/PKD2,HA to produce a sufficient amount of protein that a band could be detected in a following western blot with an antibody against the C-terminus of polycystin-2. Hence, cells producing the wild-type protein were induced for three days before they were harvested and lysed at 100 % confluency. LtTA-2,22/PKD2(hPoreL1),HA cells were induced for 3 d, 4 d, 5 d, 6 d and 7 d before they were harvested and lysed with a cell confluency of 100 %. Lysates were then analyzed via western blot. From the reference sample (= 3d -DOX, wild-type polycystin-2) 40 µg were calculated by Bradford assay and loaded on the gel. This amount of volume was also used for all other conditions to load equal amounts of cells on the gel. After blotting the gel to a PVDF membrane, bands were detected with a primary antibody that is directed against the C-terminus of polycystin-2. As an internal loading control, the antibody β-actin was used. The protein level was quantified and normalized to wild-type. As depicted in figure 3.13, six days of induction revealed an equivalent amount of mutant polycystin-2^{poreL1} to wild-type polycystin-2.

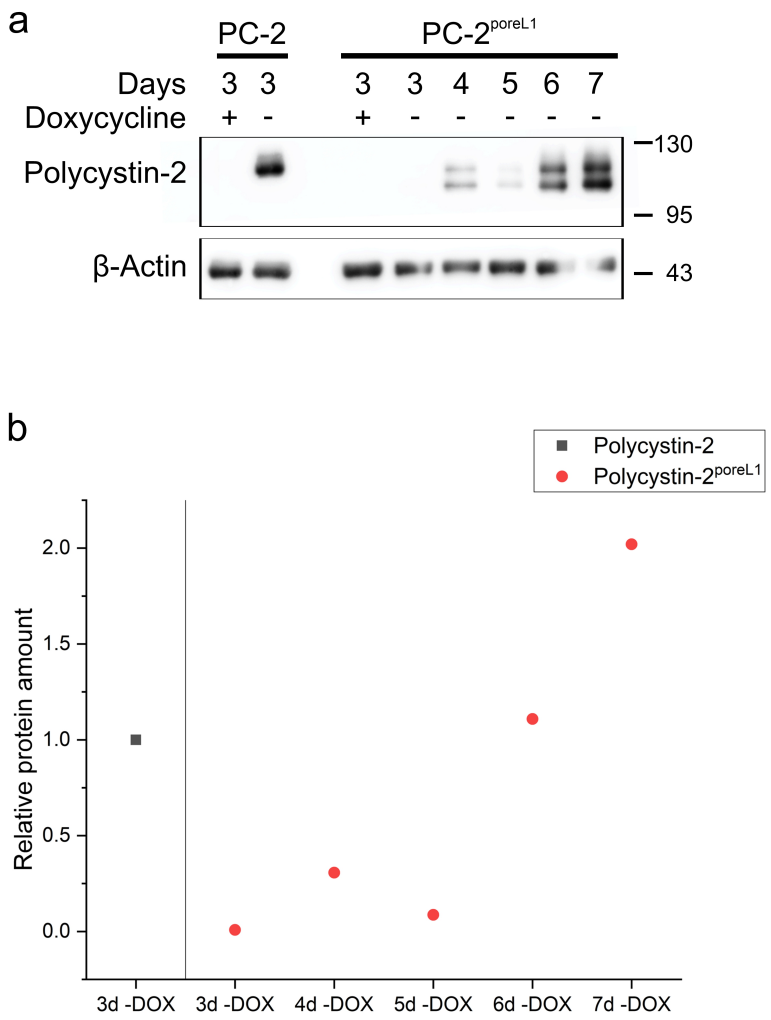

Figure 3.13: **Adjustment of protein levels of mutant polycystin-2^{poreL1} and wild-type polycystin-2.** For establishing equal protein amounts, LtTA-2,22/PKD2,HA cells were induced for 3d before harvested and lysed. Cells producing the mutant polycystin-2^{poreL1} were induced for 3 to 7 d before they were harvested and lysed. All seeded P6 plates showed a ~100 % confluency on the day of the experiment. As a negative control, one P6 per cell line was concomitantly incubated with doxycycline to repress protein synthesis. Equal amounts of cells representing 40 µg of the reference lysat (3d -DOX, PC-2) were loaded and analyzed in the following by western blot with the antibody PC2C1 to detect both polycystin-2 variants and with an antibody against β-actin as an internal loading control (a). For quantification, the detected signal for wild-type polycystin-2 at three days without doxycycline was used as a reference. By this, an induction time of six days for LtTA-2,22/PKD2(hPoreL1),HA cells appeared adequate to produce an equal amount of mutant polycystin-2^{poreL1}protein compared to wild-type polycystin-2 levels after three days of induction (b). The numbers on the right of the blots give the size of the molecular weight standard in kDa.

Furthermore, a reasonable amount of the ribosomal inhibitor cycloheximide had to be defined. Therefore, both cell lines expressing wild-type polycystin-2 (clone #3) or mutant polycystin-2^{poreL1}(clone #59) were induced for 3 d (#3) or 6 d (#59), respectively. On the day of the experiment, cells were incubated with either 100 µg, 200 µg or 300 µg of cycloheximide for 0 h, 4 h and 24 h before they were lysed with 200 µL of 6 M Urea/ 1 % Triton/ PBS. Overall protein amount of the 0 h samples was determined by Bradford assay for each cell line to ascertain the volume needed to load 40 µg. Same volumes were then loaded in all other lanes representing the different treatment conditions of both cell lines. Bands were then detected and analyzed by western blot with the primary antibody against PC2C1. Signal strength of the bands were quantified with the software Bio-1D and the value at 0 h was set as reference (=1.0) for each cycloheximide concentration.

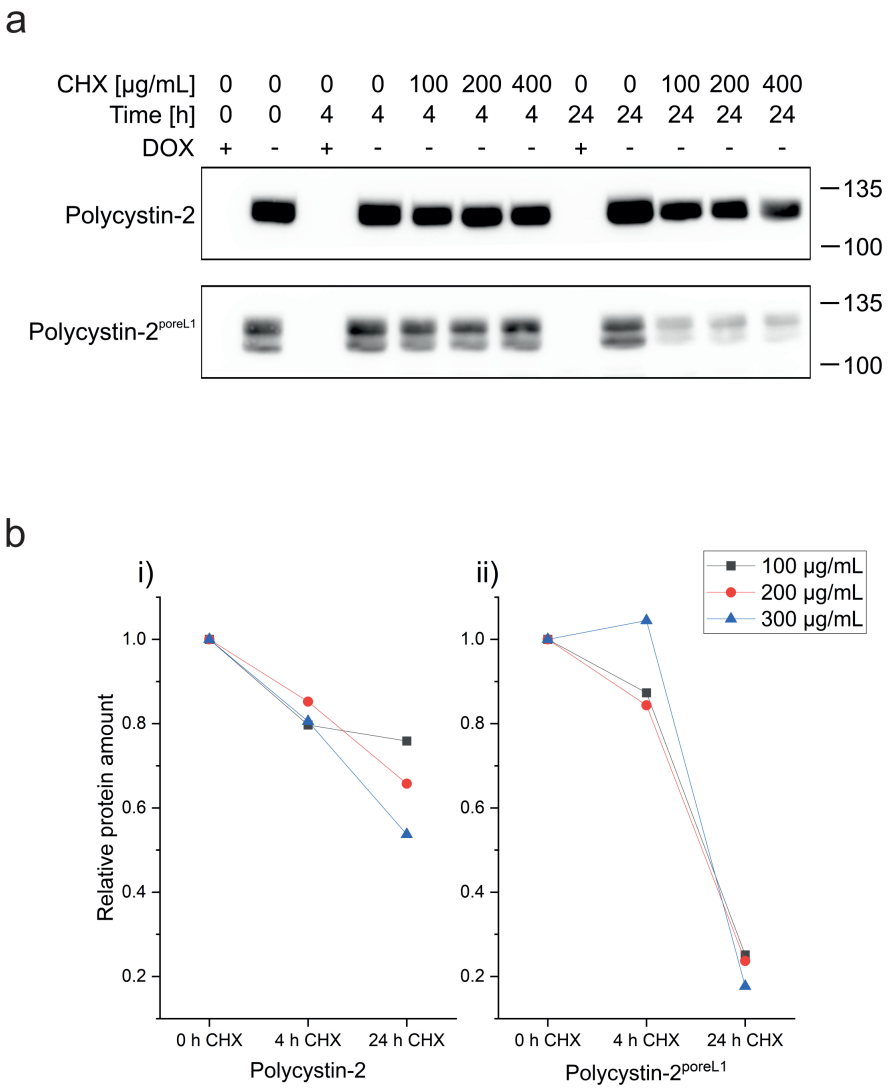

Figure 3.14: **Relative protein amount of wild-type polycystin-2 or mutant polycystin-2^{poreL1} after addition of 100, 200 or 300 µg/mL of cycloheximide (CHX) *in vitro*.** Western blots of 3 d or 7 d induced LtTA-2,22/PKD2,HA and LtTA-2,22/PKD2(hPoreL1),HA were conducted with the antibody PC2C1 for protein detection (a). As quantification shows, polycystin-2 displayed a reduction of about 20 % after 4 h and a further reduction to 50-75 % of protein left after 24 h (i). Polycystin-2^{poreL1}showed controversial results after 4 h with a 15 % decrease when treated with 100 or 200 µg/mL and an increase of 5 % when treated with 300 µg/mL. Protein levels were stronger reduced after 24 h to ~20 % of mutant protein left (ii) (b).

As figure 3.14 shows, polycystin-2 showed a decrease of ~20 % after 4 h when treated with all three concentrations of cycloheximide whereas polycystin-2^{poreL1}appeared a decrease of 15 % when treated with 100 and 200 µg/mL but also displayed an increase of 5 % in

protein levels when treated with 300 µg/mL. After further 20 h, wild-type polycystin-2 showed an overall reduction of protein levels of 25-50 % and polycystin-2^{poreL1}levels were even more reduced to ~20 % of protein left. Since cycloheximide is a general ribosomal inhibitor and cells treated with 300 µg/mL started to detach from culture plates, lower concentrations appeared more appropriate to ensure cell viability. Hence, following experiments were conducted with 100 µg/ml of cycloheximide.

For the determination of protein stability, LtTA-2,22/PKD2,HA cells were induced for three days and LtTA-2,22/PKD2(hPoreL1),HA cells for six days by removing doxycycline. As control, one cell plate was cultured with doxycycline per cell line. An equal amount of cells per time point and treatment (0 h +DOX; 0 h -DOX, 1 h, 2 h, 4 h, 6 h, 8 h, 10 h, 24 h +CHX; 24 h -CHX) were seeded in P6 plates by trypsinizing and resuspending three T75 cell flasks in 10 mL medium and 500 µL of LtTA-2,22/PKD2,HA or 1 mL of LtTA-2,22/PKD2(hPoreL1),HA cell suspension were then transferred to each P6 one day before the experiment. On the day of the experiment, P6 plates without cycloheximide treatment were harvested and lysed in 200 µL lysis buffer. All other P6 plates were incubated with 100 µg/mL CHX for the respective time span before they were harvested and lysed in 200 µL lysis buffer. As a negative control, one P6 was cultivated for further 24 h without CHX treatment to check for general cell viability (data not shown in the graph). For detection of protein levels, rabbit-anti PC2C1 was used as primary antibody which should result in a ~110 kDa band. For both cell lines, volumes representing 40 µg of total protein from the 0 h lysates (=untreated control) were calculated and loaded into the gel. The same volume from lysates of the following time points was then loaded into the SDS gel to compare equal numbers of cells during one experiment. Every experiment comprising a time span of 24 h was conducted five times per cell line. As seen in fig. 3.15, protein signals in wild-type polycystin-2 were generally stronger than in polycystin-2^{poreL1} and resulted in a double band. This might hint to posttranslational modifications of this mutant protein. Negative controls with doxycycline showed no bands at the expected height of ~110 kDa on the blots (0 h, + Doxycycline, - Cycloheximide). Regarding protein stability, wild-type polycystin-2 showed a stronger decrease in protein level in the course of 10 h of cycloheximide treatment whereas mutant polycystin-2^{poreL1} levels indicated a milder decrease over time. After 24 h, a strong reduction in both protein variants could be seen. Lysates of further induced cells without cycloheximide treatment showed an overall healthy state of both cell lines (24 h, - Cycloheximide, - Doxycycline).

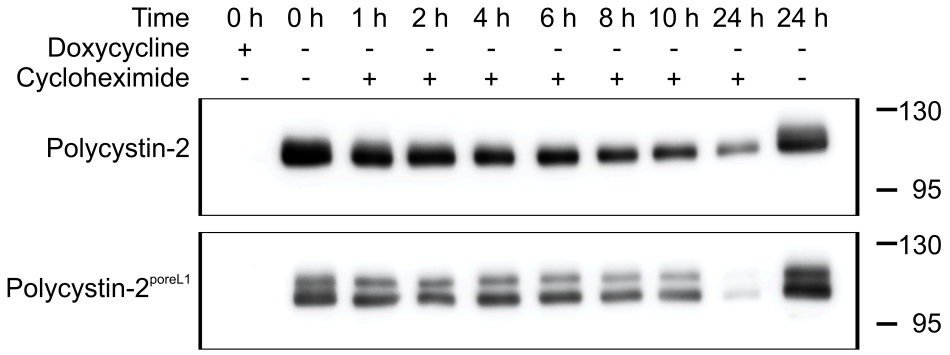

Figure 3.15: **Visualization of wild-type polycystin-2 and mutant polycystin-2^{poreL1} protein stability by western blot analysis after cycloheximide treatment.** LtTA-2,22/PKD2,HA cells were induced for 3 d and LtTA-2,22/PKD2(hPoreL1),HA cells for 6 d by removing doxycycline from the culture medium. As a negative control, one P6 plate per cell line was cultivated with doxycycline (0 h, + Doxycycline, - Cycloheximide) and for a viability check, one P6 was further cultivated for 24 h without cycloheximide (24 h, - Doxycycline, - Cycloheximide). For comparability, equal volumes of cell lysates were loaded representing 40 µg of total protein from the starting point (0 h, - Cycloheximide, - Doxycycline). Band detection via the antibody PC2C1 showed a stronger signal reduction over time in the wild-type protein whereas the mutant polycystin-2^{poreL1} seemed to display a milder decrease up to 10 h of cycloheximide treatment. One representative blot is shown. The numbers on the right of the blots give the size of the molecular weight standard in kDa.

Signal strength of the untreated control condition was set as reference (1.0) and other data points were then normalized to this. By using the software Origin, a fitting curve displaying an exponential decay was calculated by approximation to the data points resembling the mean $\pm$ standard deviation of five repetitions.

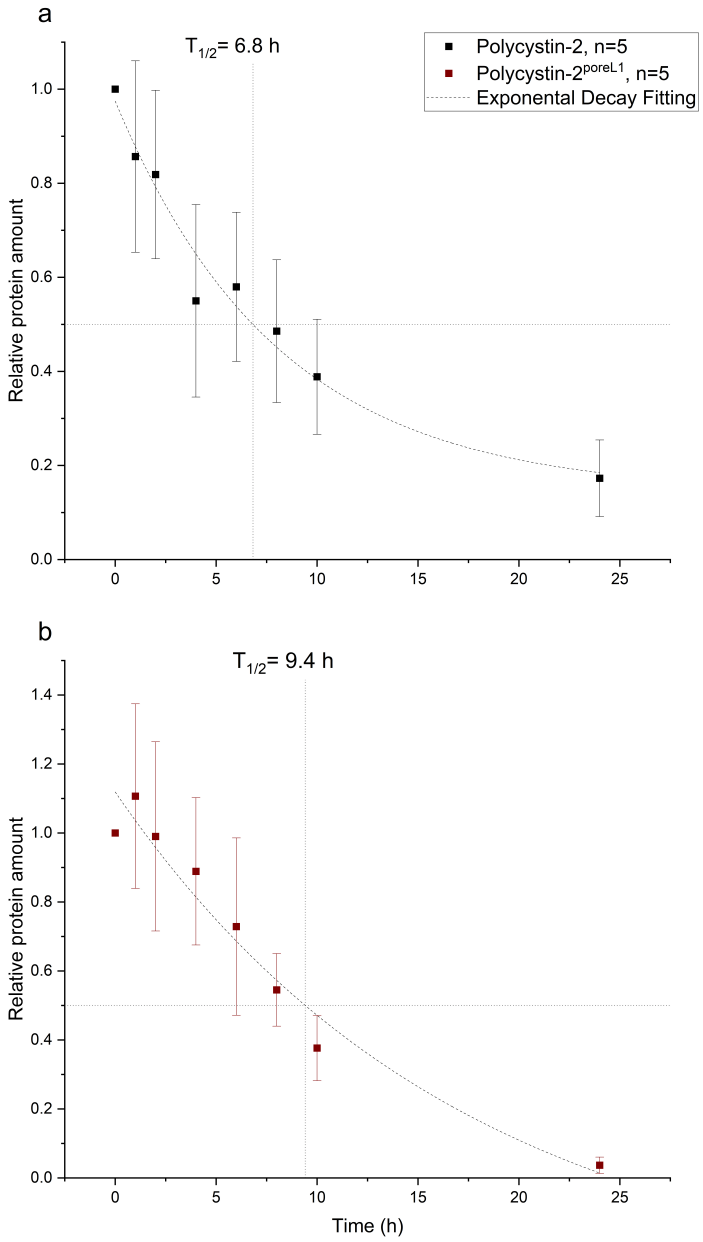

Figure 3.16: **Quantification of protein half life of wild-type polycystin-2 and mutant polycystin-2^{poreL1}.** LtTA-2,22/PKD2,HA cells were induced for 3 d and LtTA-2,22/PKD2(hPoreL1),HA cells were induced for 6 d before they were treated with cycloheximide for either 0 h, 1 h, 2 h, 4 h, 6 h, 8 h, 10 h or 24 h to analyze protein stability. Signal strength of resulting bands detected with the antibody PC2C1 were then relativized to the untreated control for each cell line. Polycystin-2 showed a half life ($T_{1/2}$) of 6.8 h (a) whereas mutant polycystin-2^{poreL1} displayed a longer half life of 9.4 h (b). Dashed curve indicates a computational exponential decay fitting curve approaching to the data points. Horizontal pointed line indicates 50 % of protein level (y=0.5) and vertical pointed line comprises where y=0.5 hits the fitted curve for identification of protein half life. Error bars resemble the standard deviation of each data point of five biological replicates; CHX, cycloheximide; DOX, doxycycline.

By computational fitting of the data points, polycystin-2 exhibited a half life of 6.8 h whereas polycystin-2^{poreL1} showed a longer half life of about 9.4 h after five biological replicates (see fig. 3.16). This might hint to a more stable mutant protein after exchanging the pore region *in vitro*.

3.2.3 Measurements of cilia with or without mutant polycystin-2^{poreL1} to detect putative differences in length *in vitro*

Recent studies described that a change in length of the primary cilium triggers different pathological processes in ADPKD. Abnormal cilia length is dependent on the tissue where the cilia are present, e.g. stages of interstitial fibrosis and end-stage renal disease are associated with cilia elongation (Saito et al., 2015; Han et al., 2016). Due to this, a closer look on the ciliary length should illustrate whether an altered ciliary length could be identified when the pore region was substituted in the mutant polycystin-2^{poreL1}compared to wild-type polycystin-2.

For measurements, pioneer experiments were conducted to find best conditions for growing many primary cilia showing a positive wild-type or mutant polycystin-2 signal with an adequate length for measurement. Hence, different induction times were tested in LtTA-2,22/PKD2,HA and LtTA-2,22/PKD2(hPoreL1),HA cells. Cells of the respective cell lines were pre-induced for either 4 days or 7 days before they were split and were then further cultivated and induced for either 3, 5 or 7 days. For detection by fluorescence microscopy, cells were fixed and stained with an antibody against the HA-epitope to identify wild-type or mutant polycystin-2. As a primary cilia marker, acetylated tubulin was used to recognize polycystin-2 or polycystin-2^{poreL1} positive primary cilia. For each induction condition, cilia with a co-localization of strong or weak polycystin-2 signals were counted. Furthermore, all cilia were counted that were not HA-positive but only showed a signal for acetylated tubulin. For unbiased analysis, one cover slip was divided into facial fields along the equatorial plane and all cilia showing the expected signals were counted. As illustrated in fig. 3.17, LtTA-2,22/PKD2,HA cells with 4 days of pre-induction showed an increase in acetylated tubulin-marked cilia during the induction time of 7 days to a total number of 143. Only ~1.5 % of cilia exhibited a strong HA signal (2) and in ~25 % cilia with a weak signal could be identified (35). After 7 days of pre-induction, overall numbers of cilia were lower (71) with ~7 % of polycystin-2 positive cilia showing a strong HA signal (5) and in ~17 % cilia exhibited a weak signal (12).

In LtTA-2,22/PKD2(hPoreL1),HA cells with 4 days pre-induction, the highest number of total cilia was reached after 5 days of post-splitting-induction with 118 cilia, with ~14

% of cilia showing a strong polycystin-2 signal (17) and with ~35 % of cilia exhibiting a weak signal (41). Cells pre-induced for 7 days indicated the maximum number of cilia when induced further on for 7 days. Here, 173 acetylated tubulin-marked cilia could be detected with ~31 % of polycystin-2-positive cilia showing a strong HA-signal (54) and 47 % of cilia showing a weak signal (82).

For the following experiments, a strong wild-type or mutant polycystin-2 signal in a maximum number of primary cilia was desirable so that this experiment suggested to induce cells of both cell lines for 7 days before splitting and cultivate and induce them further on for 7 days.

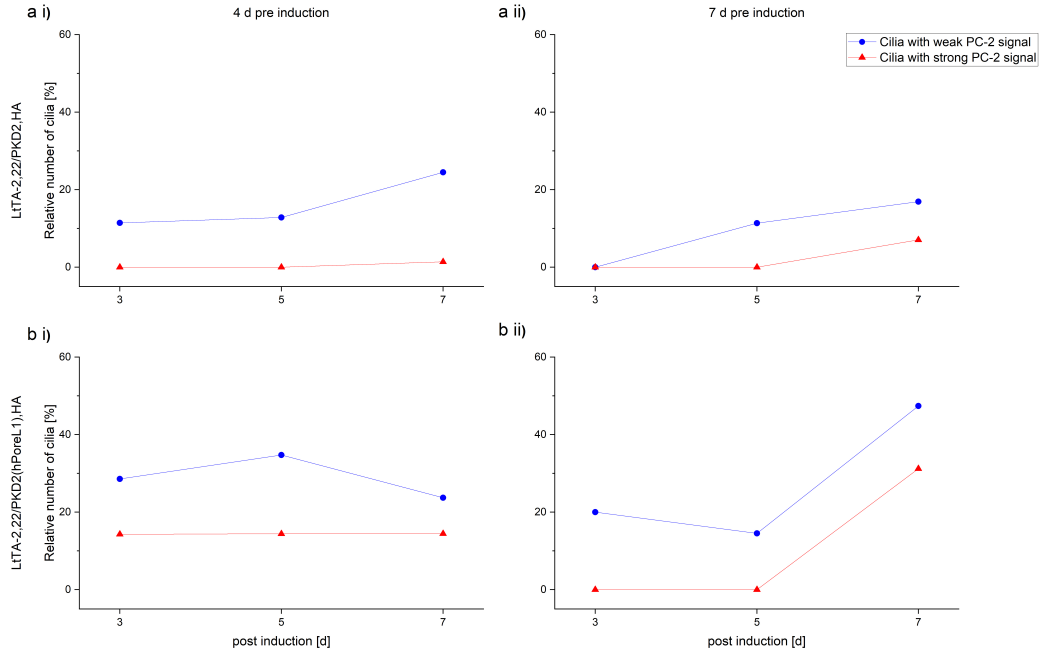

Figure 3.17: **Optimization of induction conditions to measure ciliary length *in vitro*.** To test the best induction period before splitting (pre induction) and a further induction until the day of the experiment, cells were either pre-induced for 4 or 7 days and were then further on cultivated and induced for either 3, 5 or 7 days. Cells showing either a strong (red data points) or a weak polycystin-2 signal (blue data points), indicated by a staining against the HA-epitope colocalizing to acetylated tubulin-marked primary cilia, were counted and normalized to the total amount of grown cilia. In LtTA-2,22/PKD2,HA cells pre-induced for 4 days, almost no strong polycystin-2 signal was detectable in cilia after 7 days whereas only 24 % of cilia showed a weak signal after this induction period (a i)). Wild type cells pre-induced for 7 days showed a maximum of 7 % of positive cilia with a strong and 17 % of cilia with a weak polycystin-2 signal on day 7 of post induction (a ii)). LtTA-2,22/PKD2(hPoreL1),HA cells after 4 days of pre-induction revealed a maximum of 14 % of cilia with a strong and 35 % of cilia a weak polycystin-2^{poreL1} signal on day 5 of post induction (b i)). After 7 days of pre and 7 days of post induction, the maximum percentage of signal-positive cilia was reached with 31 % of cilia showing a strong and 47 % of cilia exhibiting a weak polycystin-2^{poreL1} signal (b ii)).

Not only a signal that is easily detectable was of importance, but also that cilia have an adequate length ($\geqq$5 µm) since very short cilia would exacerbate the upcoming measurements. From the experiment before, 7 days of pre induction seemed to be appropriate to result in enough polycystin-2-positive cilia to count. For identifying the maximum in ciliary length, wild-type cells were then used for a further induction for 3, 5 and 7 days before they were fixed and stained with acetylated tubulin. To again ensure an unbiased analysis, one cover slip was divided into facial fields along the equatorial plane and all cilia recognizable by

acetylated tubulin were measured.

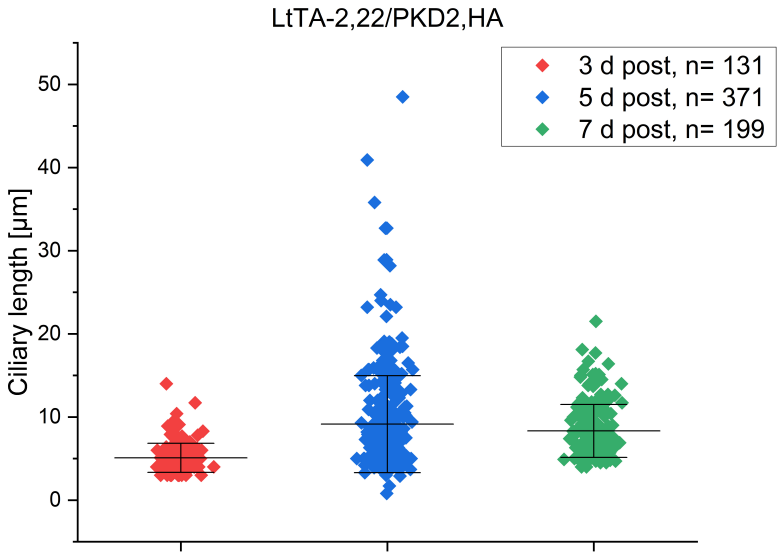

Figure 3.18: **Optimizing ciliary length *in vitro* by testing different induction periods.** For having primary cilia with an adequate length to measure, LtTA-2,22/PKD2,HA were induced for 7 days before splitting and were then further induced for either 3, 5 and 7 days. Cells were then fixed and stained with an antibody directed against acetylated tubulin to identify primary cilia for measuring their length. On day three post-splitting, 131 cilia were identified showing a length of ~5 µm (red). After 5 days of further induction, most cilia were detectable (371) displaying a broad range in length with an average of ~9 µm (blue). On day 7 after further induction, 199 cilia could be measured with an average length of ~8 µm (green). Since 5 days of further induction not only showed the longest, but also very short cilia, 7 days of further induction appeared to be the most appropriate condition for further experiments.

As figure 3.18 displays, average cilia length was ~5 µm in 131 cilia after 3 days of further induction. The highest number of cilia (371) were detected after 5 days with an average length of ~9 µm. Here cilia showed the highest variability in length, so that a further induction of 7 days displaying an average length of ~8 µm in 199 cilia turned out to be the best condition. In agreement with the previous experiment when optimizing cilia number and polycystin-2-positive ciliary signal, an induction time of 7 days pre-splitting with a continuous induction for 7 further days appeared to be most appropriate for the following measurement.

After establishing the right conditions for having a high number of polycystin-2-

positive cilia with an adequate length, the main experiment was conducted with LtTA-2,22/PKD2(hPoreL1),HA by cultivation for 7 days before splitting and 7 days further on with doxycycline for repressing the production of mutant polycystin-2^{poreL1} or without doxycycline for inducing the production of mutant polycystin-2^{poreL1}. This should indicate if the presence of pore-substituted polycystin-2^{poreL1} by removing doxycycline results in alterations in ciliary length as it can be seen in patients of ADPKD. On the day of the experiment, cells were fixed and stained with acetylated tubulin as a primary cilia marker. Again, for an unbiased analysis, one cover slip was divided into facial fields along the equatorial plane and all cilia showing the expected signal were counted and measured. Cells that were cultured with doxycycline thereby resembling a wild-type state showed an average length of 7.9 µm in 162 counted cilia whereas induced cells where doxycycline was removed from the medium displayed an average of 6.4 µm in 103 counted cells (fig. 3.19).

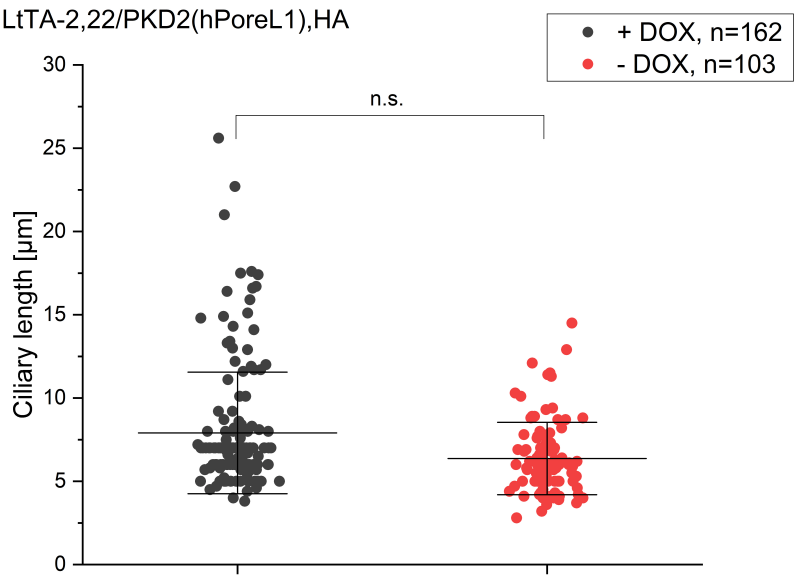

Figure 3.19: **Comparison of ciliary length when expression of polycystin-2^{poreL1} was induced compared to repressed conditions *in vitro*.** After cultivating induced and not-induced LtTA-2,22/PKD2(hPoreL1),HA cells for 7 days before splitting and 7 days further on, cells were fixed and stained with acetylated tubulin to identify primary cilia which were then measured in length. Cells without induction resembling a wild-type polycystin-2 state showed cilia with an average length of 7.9 µm in 162 cilia and induced cells with polycystin-2^{poreL1}had an average length of 6.4 µm in 103 cilia. From that, it could be concluded that no significant difference in length could be detected between non-induced cells and cells synthesizing a pore exchanged version of polycystin-2. Shown are the mean values ± standard deviations; n.s., not significant; DOX, doxycycline.

A Shapiro-Wilk test for normal distribution exhibited that data points were not normally distributed. Hence, a Mann-Whitney-U-test was conducted which revealed that no difference in mean cilia length could be identified between induced and not-induced LtTA-2,22/PKD2(hPoreL1),HA cells (n.s., p=0.99).

3.2.4 Characterization of mutant polycystin-2^{poreL1} *in vivo*

All experiments were conducted with male mice from the respective mouse line. Calcium measurements were examined in imaging buffer containing calcium unless otherwise stated.

Recently, a polycystin-2^{poreL1}knock-in mouse line was established in our lab that resulted in a strain-dependent cyst phenotype focally in the kidneys. By transfecting embryonic

stem cells with a plasmid comprising the pore-substituted mutant protein polycystin-2^{poreL1} which was generated by site-directed mutagenesis between exon 8 and 9, all the endogenous polycystin-2 was replaced by the mutant protein. Kidney cysts could be observed in mice first at the age of 4 weeks which are severely progressing up to 12 months of age in a 129/Sv background. Here, particularly collecting ducts showed wider luminal diameters (data not shown, described in Grosch *et al.*, 2021; under revision) and all following experiments were then conducted with mice in this background. To exclude that those cysts appear because of lower levels of the mutant polycystin-2^{poreL1}, collecting ducts were isolated from both wild-type (+/+) and homozygous polycystin-2^{poreL1}(p/p) mice to detect mRNA levels of the transcribed *Pkd2* gene in the respective genotypes. Primers for qPCR were selected that oligos spanned exons of both Pkd2 gene variants (see subsection 2.1.5.1). Quantitative PCR analysis of total RNA from collecting ducts from five mice per genotype showed a significant increase in mRNA levels in p/p animals (see fig. 3.20). Regrettably, a western blot of kidney lysates from mice of wild-type and mutant polycystin-2^{poreL1}animals for quantification of protein levels could not be conducted since the tested antibodies did not work in our hands.

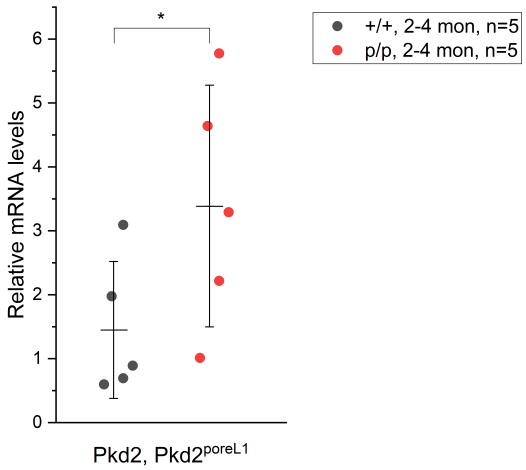

Figure 3.20: **Investigation of mRNA levels of Pkd2 in wild-type (+/+) and polycystin-2^{poreL1} (p/p) mice.** Quantitative PCR analysis of total RNA isolated from collecting ducts demonstrated higher mRNA levels for *Pkd2^{poreL1}* than for *Pkd2*. Approximately 150 to 200 collecting ducts each were harvested from 5 mice at an age of 2 to 4 months. Shown are the mean values ± standard deviations; *, p=0.04.

Not only focal cysts, but also elongated cilia could be identified by electron microscopy of homozygous *Pkd2^{poreL1}* mice earlier in our lab (data not shown, described in Grosch *et*

al., 2021; under revision) so that it was of interest to focus on the underlying mechanisms of this phenotype. As a pioneer experiment, collecting ducts of wild-type and knock-in mice were isolated and cultivated for 4 days before they were fixed and stained with an antibody against acetylated tubulin, a ciliary marker, and with YCB9, an antibody directed against polycystin-2.

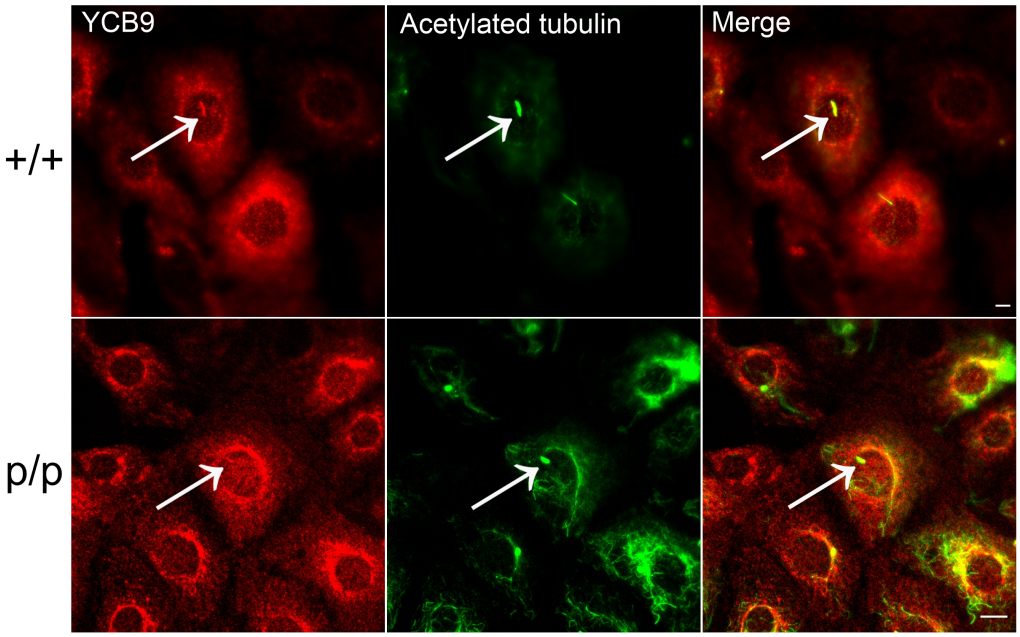

Figure 3.21: **Visualization of the ciliary localization of mutant polycystin-2^{poreL1} *in vivo*.** Primary collecting duct cells from wild-type and polycystin-2^{poreL1} knock-in mice that were cultivated for four days before fixing and staining showed a co-localization of the ciliary marker acetylated tubulin (green) and the antibody against polycystin-2 (YCB9, red) thereby corroborating a partially weak but correct ciliary localization of both wild-type and mutant polycystin-2 (merge). Bar 10 µm.

In fluorescence microscope recordings, it could be shown that the signal corresponding to polycystin-2 marginally colocalizes with the ciliary marker acetylated tubulin in primary cultures of isolated collecting ducts from both mouse lines, confirming a weak but correct localization of mutant polycystin-2^{poreL1} *in vivo* (fig. 3.21).

3.2.5 Foxj1 and Nde1 as putative contributors to ciliary elongation in homozygous *Pkd2^{poreL1}* knock-in mice

To further investigate the cellular mechanisms behind the ciliary elongation in homozygous *Pkd2^{poreL1}* knock-in mice, three putative candidates that were recently discussed to be

involved in ciliary length control were tested in quantitative PCR assays of collecting ducts isolated from homozygous *Pkd2*^{poreL1} knock-in and wild-type mice. Thus, the focus was set on the genes Foxj1, Nde1 and Dynll1. Foxj1 is a transcription factor that was described to positively regulate ciliary length (Cruz et al., 2010; Lu et al., 2015) whereas the microtubule-associated protein Nde1 was identified to have a negative regulatory effect on the length of primary cilia (Inaba et al., 2016; Wu et al., 2000). In 2011, Kim et al. suggested that Nde1 may function antagonistically to the dynein complex in the suppression of cilium length and by testing one component of this complex, they found that Nde1 may mediate its effect partially through its interaction with the dynein light chain Dynll1 (also known as LC8).

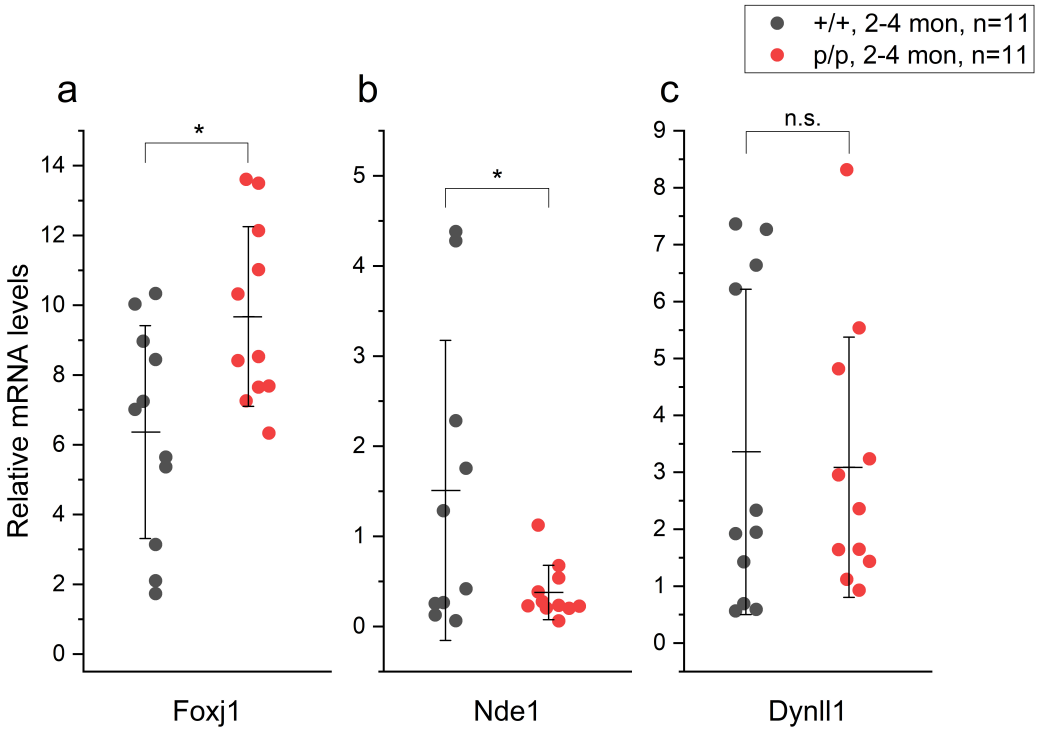

Figure 3.22: **Analysis of putative candidate genes involved in ciliary length control in *Pkd2*^{poreL1} knock-in mice.** Quantitative PCR analysis of total RNA isolated from collecting ducts revealed higher Foxj1 (a) and lower Nde1 (b) mRNA levels in homozygous *Pkd2*^{poreL1}(p/p) than in wild-type mice (+/+). The mRNA levels of Dynll1 (c) did not show alterations (p=0.4). Approximately 150-200 collecting ducts each were harvested from 11 mice at an age of 2-4 months. Shown are the mean values ± standard deviations; *, p=0.01 ; n.s., not significant.

As shown in figure 3.22, we indeed found significantly increased mRNA levels of Foxj1 (p=0.01) and significantly decreased levels of Nde1 (p=0.01) in homozygous *Pkd2*^{poreL1} mice showing elongated cilia which is consistent with the fact that Foxj1 has a positive effect

and Nde1 a negative effect on ciliary length. Although mRNA levels of Dynll1 showed marginally decreased levels of mRNA in homozygous knock-in mice, the difference did not reach statistical significance (p=0.4). This outcome suggests that the upregulation of Foxj1 and the downregulation of Nde1 could contribute to the increased length of primary cilia in *Pkd2*^{poreL1} knock-in mice.

3.2.6 Measurements of intracellular calcium levels in homozygous *Pkd2*^{poreL1} knock-in mice compared to wild-type *Pkd2* mice

For calcium measurements, preceding experiments were conducted on primary collecting duct cells that were cultured for 4 days to determine adequate concentrations of stimulants. The cell patch was then incubated with Fura-2 to visualize intracellular calcium levels (see subsection 2.2.3.4). For each condition, two technical replicates with a cell patch of around 50 cells each were measured all originating from one male homozygous *Pkd2*^{poreL1} knock-in mouse. Two different stimuli were used to investigate separate signal transduction pathways. Vasopressin has been used before to investigate the contribution of polycystin-2 to the release of calcium from intracellular stores (Koulen et al., 2002). Furthermore, ATP was used as another stimulus. The following experiment was conducted in imaging buffer containing calcium. Three different concentrations were tested for stimulating the endoplasmatic reticulum to release its intracellular calcium: 100 nM, 1 µM and 10 µM vasopressin (AVP) and 1 µM, 10 µM and 100 µM ATP. Each stimulant was applied 10 seconds after starting the record and every reaction was recorded for further 10 minutes. After dividing the recorded wavelengths and subtracting background levels as described in subsection 2.2.3.5, calcium release was illustrated in graphs to identify the optimal stimulus concentration revealing a distinct reaction.

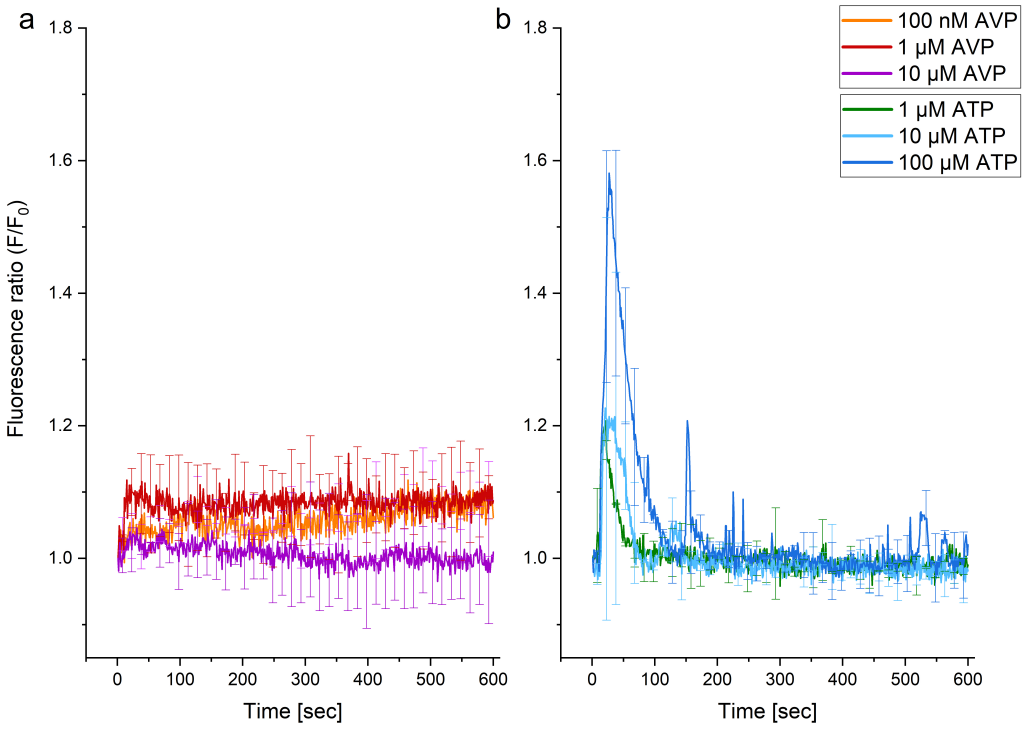

Figure 3.23: **Calcium response after stimulation with different concentrations of ATP or vasopressin in primary collecting duct cells of a homozygous *Pkd2*^{poreL1} knock-in mouse.** Collecting ducts were isolated and cultivated for 4 days and the resulting cell patch was then incubated with Fura-2 for recording calcium levels in the intracellular space. After applying different concentrations of vasopressin no clear reaction could be detected (a) whereas ATP addition revealed a high distinct peak at 100 µM (blue) and lower peaks could be detected with concentrations of 10 µM (light blue) and 1 µM (green) all decreasing in a comparable manner. Curves of 10 µM and 100 µM even showed a second smaller peak of roughly 1/3 of the peak height after approximately 100-150 seconds after ATP addition (b). Experiments were conducted in imaging buffer containing calcium. Shown are the mean values ± standard deviations. F_0, fluorescence before stimulation; F, fluorescence after stimulation at a given time point.

As figure 3.23 shows clearly, vasopressin did not result in a distinct response after application of the different concentrations, whereas ATP already displayed a response at the lowest concentration of 1 µM. With 10 µM of ATP, the peak was slightly higher and the strongest response occurred with a concentration of 100 µM. A second smaller peak with a height of approximately 1/3 of the main peak could be seen at 10 µM and 100 µM after ~100-150 seconds after ATP addition. Intracellular calcium levels decreased with all concentrations in a comparable manner and all curves reached a similar plateau phase. Since a distinct response was desirable for the following experiments 100 µM ATP was used further

on. Eventhough vasopressin did not show a response in primary collecting duct cultures, it was decided to continue with 1 µM vasopressin in other tissues in the following experiments.

The main experiment was then conducted with isolated collecting ducts from either *Pkd2*$^{+/+}$ (+/+) or *Pkd2*$^{poreL1/poreL1}$(p/p) mice that were also further cultivated for four days so that a cell patch could grow that was easily detectable under the microscope. The cell patch was then incubated with Fura-2 (see subsection 2.2.3.4) in imaging buffer containing calcium to visualize intracellular calcium levels. Since the preliminary experiment showed a distinct response with 100 µM of ATP, this concentration was used for stimulation which was applied 10 seconds after starting the record and the measurement was further recorded for 10 minutes. Again, for each condition, two technical replicates with a cell patch of approximately 50 cells each were measured.

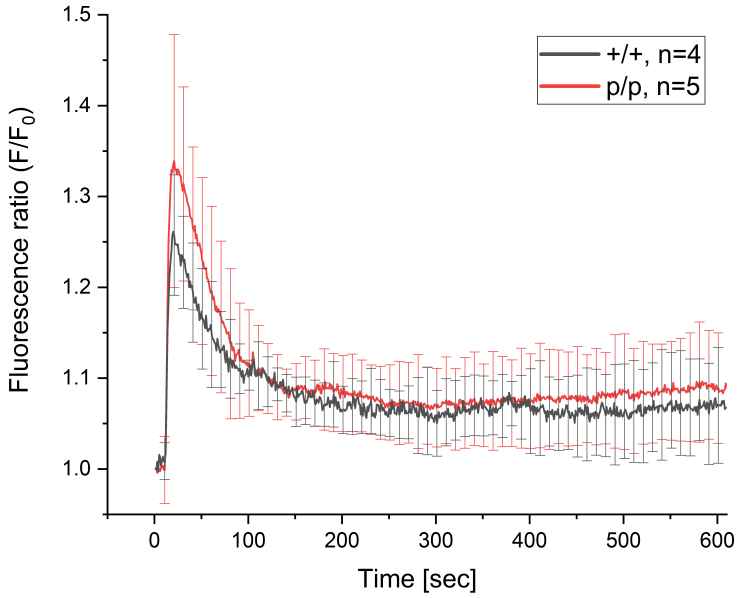

Figure 3.24: **Calcium measurements after stimulation of primary collecting duct cultures from homozygous *Pkd2*^{poreL1} and wild-type *Pkd2* mice with ATP.** After application of 100 µM ATP on isolated and 4 days cultivated primary collecting duct cells, a higher calcium response was detectable in collecting duct cell patches from homozygous *Pkd2*^{poreL1} knock-in mice (p/p) compared to those isolated from wild-type mice (+/+), although statistical significance was not reached. Experiments were conducted in imaging buffer containing calcium. Shown are the mean values ± standard deviations. F_0, fluorescence before stimulation; F, fluorescence after stimulation at a given time point.

It turned out that after addition of 100 µM ATP, the calcium response was higher in

primary collecting duct cells isolated from *Pkd2*^{poreL1} knock-in mice compared to those of wild-type mice. Regrettably the difference did not reach statistical significance (one-sided t-test, p=0.1). Both curves reached a comparable plateau phase after approximately 200 seconds.

After intensive practicing and optimizing of recording intracellular calcium levels in small structures, we were able to even measure freshly isolated collecting ducts directly after preparation. Here, collecting ducts from an enzymatic digestion of a whole kidney per mouse were used that exhibited the typical surface pattern comparable to cobblestones and/or were also branched. First test measurement demonstrated, that those collecting ducts showed responses to application of 1 µM vasopressin but no consistent responses to ATP could be detected (data not shown). Hence, the following data were collected by adding 1 µM vasopressin after 10 seconds from the start and the response was recorded for further 10 minutes. To identify whether the calcium response is only due to influx of extracellular calcium from the imaging buffer, two experimental set ups were conducted. Thus, not only imaging buffer comprising calcium was used but also imaging buffer without calcium.

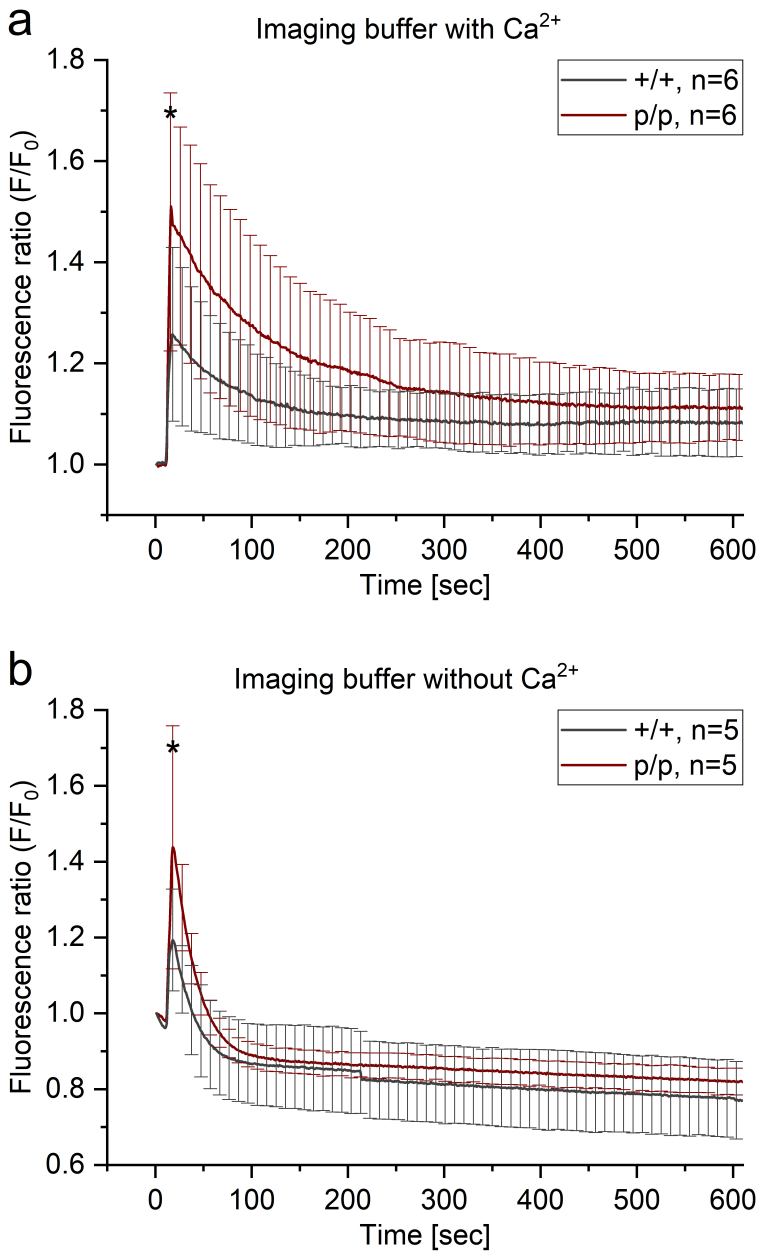

Figure 3.25: **Measurements of calcium responses in collecting ducts of *Pkd2*^{poreL1} knock-in mice and *Pkd2* wild-type mice in presence or absence of extracellular calcium.** Collecting ducts were isolated from whole kidneys of 2- to 4-month old mice of the indicated genotype. The intracellular calcium concentration in freshly isolated collecting ducts was determined with Fura-2 after stimulation with 1 µM of vasopressin. Collecting ducts isolated from homozygous *Pkd2*^{poreL1} knock-in mice (p/p) showed a stronger calcium peak than those isolated from wild-type mice (+/+) (a). In the absence of extracellular Ca^{2+} the peak response was shorter but the stronger response in homozygous knock-in mice could also be manifested under those conditions (b). Shown are the mean values ± standard deviations. F_0, fluorescence before stimulation with vasopressin; F, fluorescence after stimulation with vasopressin. *, $p < 0.05$.

Addition of vasopressin resulted in a stronger cytoplasmic Ca^{2+} response in freshly isolated collecting ducts from homozygous *Pkd2*^{poreL1} knock-in mice than in collecting ducts from wild-type mice. When collecting ducts were stimulated with vasopressin in the absence of extracellular calcium the difference in the peak response was still observed, although at reduced peak heights. Since we were interested in finding out whether higher or lower calcium responses could be seen in *Pkd2*^{poreL1} knock-in mice compared to wild-type mice, one-sided t-tests were conducted that comprised statistical significant differences in the intracellular calcium peaks when experiments were either conducted with buffer containing calcium (one-sided t-test, $p=0.04$) or buffer without calcium (one-sided t-test, $p=0.04$).

In the next approach, only collecting ducts isolated from the papilla were used to guarantee that all tubules measured are indeed collecting ducts. The region of interests (ROIs) of those collecting ducts were then set to the central 50 % of the tubules to exclude unpredictable effects arising at the ends of the fragments where the epithelial sheath may be harmed by the preparation and only tubuli with $>$100 µm were included in the calculation. Moreover, preliminary experiments showed that those collecting ducts were excitable with vasopressin as well as with ATP (data not shown).

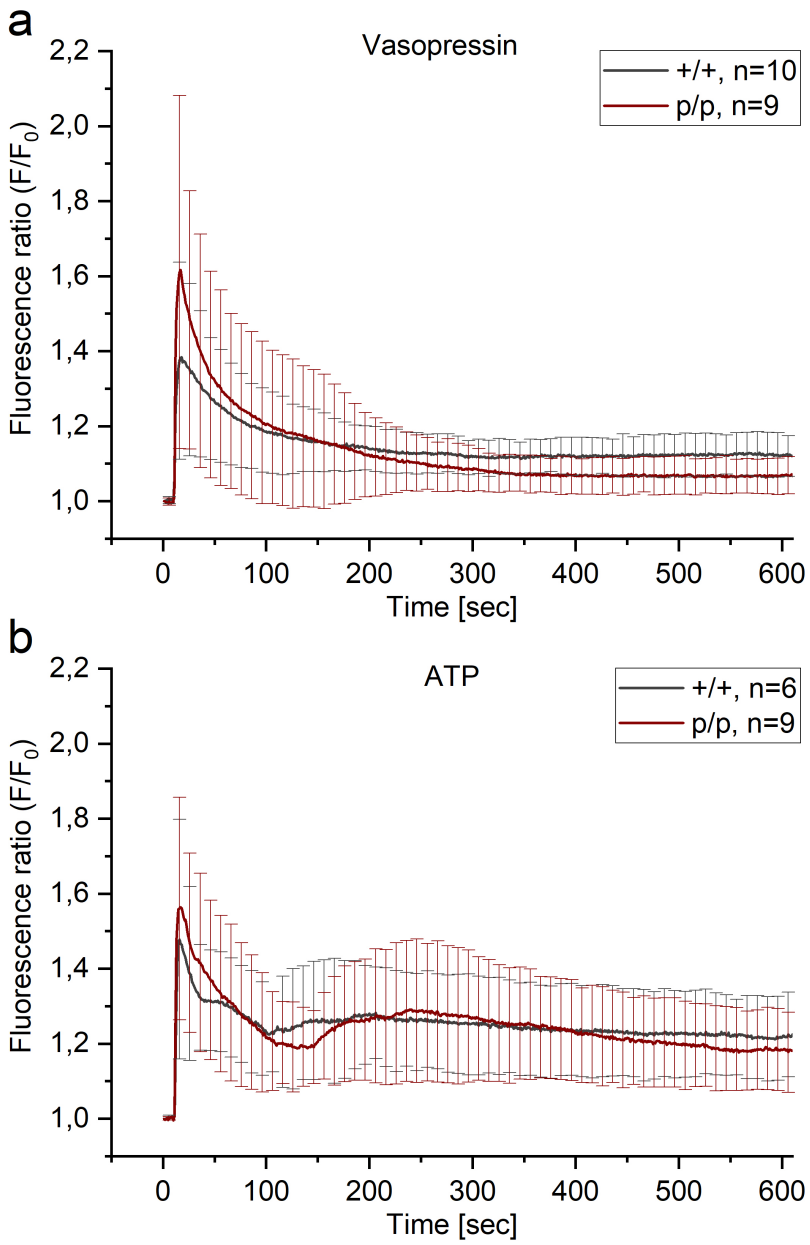

Figure 3.26: **Calcium response in papillary collecting ducts of *Pkd2*^{poreL1} knock-in mice and *Pkd2* wild-type mice.** Papillary collecting ducts were isolated from 15- to 34-weeks old mice of the indicated genotype. The intracellular calcium concentration in freshly isolated collecting ducts was visualized by Fura-2 after stimulation with 1 µM of vasopressin and 100 µM of ATP. Albeit collecting ducts isolated from homozygous *Pkd2*^{poreL1} knock-in mice (p/p) showed a stronger calcium response than those isolated from wild-type mice (+/+) for both vasopressin and ATP, statistical significance was not reached in either case. Shown are the mean values ± standard deviations. F_0, fluorescence before stimulation; F, fluorescence after stimulation.

Application of vasopressin showed a stronger intracellular calcium response in freshly isolated papillary collecting ducts from homozygous *Pkd2*^{poreL1} knock-in mice than in collecting ducts from wild-type mice (see fig. 3.26). Unfortunately, the difference did not reach statistical significance (one-sided t-test, p=0.12). After stimulation with ATP, collecting ducts isolated from homozygous *Pkd2*^{poreL1} mice also showed a stronger calcium response that those from *Pkd2* wild-type mice but again, no statistical significant differences could be reached (one-sided t-test, p=0.26).

3.2.7 Calcium measurements of collecting duct-specific *Pkd2* floxed mice to investigate a general role of polycystin-2 in calcium conduction

The data presented above suggest that the polycystin-2$^{\text{poreL1}}$ protein conducts calcium ions whereas the wild-type polycystin-2 protein either does not or does but to a lower extend - eventually by interaction with other calcium channels. In order to test whether polycystin-2 is able to conduct calcium at all, a mouse line was used where *Pkd2* was specifically knocked-out in the collecting ducts. In those *Pkhd1*::Cre;*Pkd2*$^{lox/lox}$ mice, the promoter of the *Pkhd1* drives gene expression in differentiated collecting ducts (Williams et al., 2014) and therefore allows inactivation of a floxed *Pkd2* allele by the Cre recombinase specifically therein. When polycystin-2 is not a calcium channel there should not be a difference in intracellular calcium levels after stimulation between *Pkhd1::*Cre;*Pkd2*$^{lox/lox}$ (= collecting duct-specific knock-out) and *Pkd2*$^{lox/lox}$ (= polycystin-2 present in collecting ducts, wild-type situation). Again vasopressin was used as stimulant.

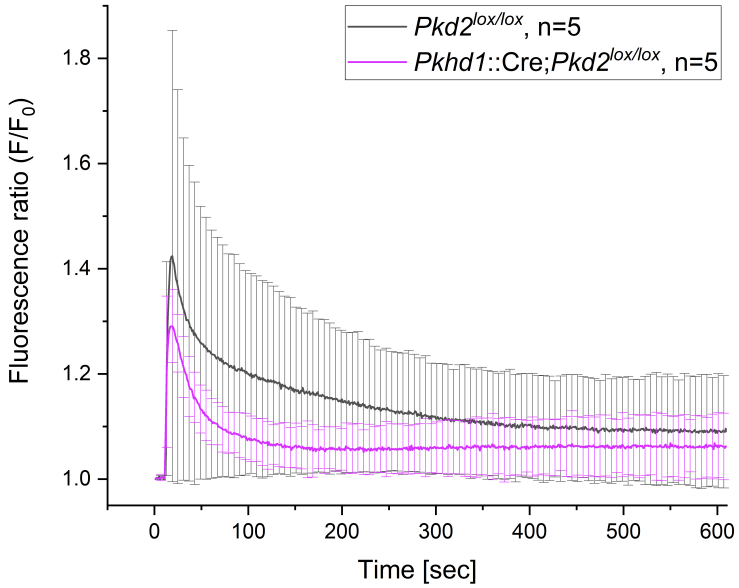

Figure 3.27: **Calcium measurements of a collecting duct specific *Pkd2* knock-out mouse line compared to mice resembling a wild-type *Pkd2* situation.** Collecting ducts were isolated from whole kidneys of 2- to 4-month old mice of the indicated genotype. The intracellular calcium concentration in freshly isolated collecting ducts was visualized by Fura-2 after stimulation with 1 µM of vasopressin. Here, no statistical significant difference could be detected. Nevertheless, in mice where *Pkd2* was floxed in collecting ducts (*Pkhd1::*Cre;*Pkd2*$^{lox/lox}$), a marginally weaker calcium response was detectable compared to mice where *Pkd2* was present in collecting ducts (*Pkd2*$^{lox/lox}$).

The application of vasopressin did not result in significant differences in the calcium response of *Pkhd1::*Cre;*Pkd2*$^{lox/lox}$ mice, where no *Pkd2* should be present and *Pkd2*$^{lox/lox}$ mice what is to be equated with the wild-type situation (one-sided t-test, p=0.13). However, marginally higher responses in *Pkd2* mice are indicated by the graph. This would in turn suggest that polycystin-2 is somehow involved in intracellular calcium conduction.

As a resume, the *in vitro* and *in vivo* calcium measurements where wild-type polycystin-2 was compared to polycystin-2^{poreL1} suggest that polycystin-2 might have a marginally lower conductivity of calcium compared to the established mutant polycystin-2^{poreL1}. However, calcium measurements of mice with a collecting duct-specific *Pkd2* knock-out hint to a general relevance of polcystin-2 in calcium homeostasis - either in a direct or indirect way.

4 Discussion

This present study examined two subprojects both concerning the proteins known to be involved in the most common monogenic kidney disease ADPKD with a prevalence of 1:400-1:1000 (Collins et al., 2012). Patients of this disease carry either mutations in the gene *PKD1* (~85 %) or *PKD2* (~15 %) coding for the proteins polycystin-1 or polycystin-2, respectively. The clinical spectrum of the disease does not only include renal but also extrarenal manifestations (Gabow, 1993). The main phenotype is described in the kidney were multiple fluid-filled cysts arise along the whole nephron with most cysts located in the collecting ducts progressing in size and number until kidney function is completely disturbed resulting in an end-stage renal disease (Verani and Silva, 1988; Niemczyk et al., 2009). Although publications from recent years continuously revealed new insights in function and putative contribution to the rise of ADPKD, a lot of information on the cellular level of both proteins is still lacking that would help to understand the diverse processes of how ADPKD can arise. By the two subprojects investigated during this study, more information should be gained on a structural and functional level of polycystin-1 and polycystin-2, respectively, for giving new insights into the cellular processes involved in ADPKD.

4.1 Structural investigation of the PKD domain 1 of polycystin-1

Structural analyses of the *PKD* domain 1 regarding its putative binding of molecules present in the urine were conducted to investigate the function of the repetitive pattern of the domain in the extracellular amino terminus of polycystin-1. This was performed by a comparison of nuclear magnetic resonance spectra when purified *PKD1* PKD domain 1 before and after incubation with patient urine or control urine.

4.1.1 Establishment of optimal expression and purification conditions

The large extracellular N-terminus of *PKD1* with its ~3000 amino acids was investigated intensively for its diversity of domains. By this, it became known that a cysteine-rich domain,

two leucine-rich repeats (LRR) - a motif responsible for its interaction with the extracellular matrix and cell adhesion, a cell wall integrity and stress response component (WSC) that is thought to interact with carbohydrates, 16 copies of unique immunoglobulin (Ig)-like PKD domains with a putative ligand-binding functionallity (Bycroft, 1999), a C-type lectin domain, a low density lipoprotein A (LDL-A) related motif - suggested to be important for a possible interaction between PC1 and LDL-related molecules, a region of homology with a sea urchin receptor for egg jelly (REJ) (Hughes et al., 1995) and a G protein-coupled receptor proteolytic site (Ponting et al., 1999) where the protein cleaves itself into a N-terminal fragment (NTF) and a multi transmembrane core (Wei et al., 2007) are present in this terminus. Interestingly, only few is known about the 16 repeats of the PKD domains. Pioneer structural investigations were conducted by Bycroft (1999) that revealed structural information of *PKD1* PKD domain 1 suggesting a putative ligand-binding function similar to those found in other cell-surface proteins but unfortunately, nothing more is known yet, e.g. about what ligands can bind at those domains or what might be the downstream effects on a cellular level of a putative ligand-binding. This fact motivated us to further investigate the PKD domain 1 of polycystin-1.

By establishing an expression vector that contains two tags for purification *PKD1* PKD domain 1 should be expressed in an adequate purity and concentration for a later measurement by nuclear magnetic resonance. After testing for the best bacterial strain in different temperatures and induction conditions to express this vector, we were able to define cultivation circumstances to produce an adequate amount of fusion protein in LB medium. Those conditions were then adopted to express the fusion protein in minimal medium to ensure an accurate folding of the protein by limiting nutrients in the medium which results in longer doubling rates. The only marginal difference in protein levels between the tested expression temperatures allowed to choose a growth under lower temperatures to additionally ensure slower protein production and thereby proper folding. Even though cultivation for longer than 8 h resulted in more protein in most tested conditions it was decided to stop protein synthesis after 8 h since longer protein induction can also lead to losing proteins in insoluble inclusion bodies. By this, soluble protein could be detected in the supernatant after fractional centrifugation suggesting that the conditions chosen successfully avoided the inclusion of the protein in inclusion bodies. Marginal remains of the fusion protein in the 50'000 x g pellet could speak for an incomplete lysis by ultrasound. Here, alternative methods could be considered for a more efficient lysis, e.g. by the use of a french press. Nevertheless, resulting amounts of fusion protein could easily be increased by upscaling culture volumes so that the loss of protein seen in the 50'000 x g pellet could thereby be compensated.

A preliminary expression of 1 L showed that purification with amylose and a subsequent

collection of eluted fractions resulted in ~21 mg of fusion protein. This information was crucial to achieve a total cleavage of the fusion protein with the TEV protease. Previous experiments with an own synthesized TEV protease (Bachelor thesis Nguyen, 2020) which yielded a necessity of 1/50th of TEV protease proportionally to the fusion protein could be confirmed and the fusion protein was completely cleaved into the larger MBP-tag and the PKD domain 1. After cleavage of the fusion protein when still bound to amylose, the subsequently collected flow-through should only contain purified *PKD1* PKD domain 1 and the TEV protease. Surprisingly, MBP was still found to be present (see section 3.1.2). The possible explanation that not enough amylose beads were used for purification could be neglected since more amylose beads did also result in remaining MBP in the flow-through (data not shown). Another reason could be that bound MBP started to uncouple during the cleavage process so that it could pass the column into the flow-through. Molecular processes like ligand-binding are known to be reversible processes. This depends on the equilibrium dissociation constant (K_d) describing the binding affinity of a single biomolecule (e.g. protein or DNA) to its ligand/binding partner (e.g. drug or inhibitor). The smaller the K_d value, the greater the binding affinity of the ligand for its target. Approximate limit values for high or low affinity are determined as follows (Bisswanger, 2017):

$K_d < 100$ nM $\triangleq$ high affinity
100 nM $< K_d <$ 10 µM $\triangleq$ medium affinity
$K_d >$ 10 µM $\triangleq$ low affinity

This can be transferred to the binding of amylose to MBP. Regrettably, the K_d of amylose to MBP is not published. However, the K_d of maltodextrins to MBP is reported to be ~3.5 µM which is a rather medium affinity (Pattenden and Thomas, 2008). Since elution of MBP from amylose beads is conducted with maltose, the K_d of MBP to amylose has to be higher than the K_d of MBP to maltose, hence K_d(MBP-amylose) $>$ 3.5 µM. This leads to the assumption that the rather high K_d of MBP to amylose could indeed lead to a dissociation during the TEV cleavage reaction.

Another purification with amylose afterwards is not possible because maltose is binding at the ligand-binding site of MBP so that the molecule is saturated after one round of purification. A dialysis process of 2x 2h and 1x o/n each 1:400 in NaP_ibuffer without maltose could not dissociate maltose from MBP so that this method was not valuable (data not shown).

When trying to separate remaining MBP from the pure PKD domain 1 by gel filtration to exclude the proteins by their size, both proteins came at similar fractions so that this method was also not suitable. As depicted in fig. 3.5, a high peak occurred at fractions 24-33

that could be assigned to the large MBP-tag (42 kDa). This peak fused into a shoulder peak which turned out to be the PKD domain (~10 kDa). Hence, conducting a gel filtration did not allow to separate those proteins by pooling specific fractions since it seems to elute from the Superose 6 column at similar time points.

This was very unexpected since two proteins with this great difference in sizes should easily be separated by gel filtration. A hypothesis explaining this phenomenon could be that the PKD domain 1 of *PKD1* is forming oligomeres. By the attachment of four domains, a size of ~40 kDa would be achieved which would explain that this formed tetramere is eluting at the same time from the column as the 42 kDa MBP protein. In the following SDS gel this tetramerization is then again dissolved because of the denaturing effect of SDS hence resulting in PKD domain monomeres with its original size of ~10 kDa. Conduction of a cross-linking experiment would give new insights in a potential oligomerization of the domain. By a hanging-drop assay where glutaraldehyde is placed in a dish under a cover slip where a protein droplet is hanging upside down fumes arising from this aggressive carbonyl reagent are cross-linking primary amines and/ or lysines in the protein by the carbonyl group thereby building bonds stable under denaturing conditions. If the domain was oligomerizing under native conditions glutaraldehyde would be able to visualize this in a SDS gel. Regrettably, this hypothesis could not be tested because the remaining MBP-tag would always marginally mask a tetramerization of the domains in a polyacrylamide gel.

Nevertheless, it would be very interesting to find out more about this observation. This could be investigated by replacing the MBP-tag by another affinity tag like the 30 kDa glutathione-S transferase-tag (GST). Here, the gel filtration column must be chosen carefully to ensure a sharp separation of GST and the PKD domain otherwise overlapping elution time points would also exacerbate protein separation.

Even though it was not possible to remove the remaining MBP-tag completely from the purified *PKD1* PKD domain 1, it was still possible to conduct NMR measurements since a purity of ~90 % is recommended. This purity was achieved by the additional His-tag that was introduced into the expression vector. By a following purification with Ni-NTA, most of the remaining MBP and also the TEV protease could successfully be extracted as depicted in fig. 3.6. This allowed the following HSQC NMR measurements with unlabeled or ^{15}N-labeled PKD domain 1 of polycystin-1.

4.1.2 NMR measurements of unlabeled or ^{15}N-labeled PKD domain 1 of polycystin-1

The 2D-HSQC spectra that were conducted by Prof. Dr. Remco Sprangers all displayed a dot plot with clearly separated dots each representing interactions of protons with ^{15}N-labeled amino groups that are separated by one bond (see figs. 3.10,3.11). This indicated a great resolution of the protein structure. Interestingly, a comparison of spectra of ^{15}N-labeled PKD domain 1 that was not incubated with urine with the spectra of the domain either incubated with patient urine or control urine did not show alterations. On the one hand, this shows that the protein domain showed no unexpected problems like denaturing events caused by urea after addition of urine but furthermore, on the other hand, this also suggests that the investigated PKD domain 1 might not be involved in ligand-binding since the protein resonances remained on the same graph coordinates independent on urine incubation.

The fact that we could not detect differences in the NMR spectra could also have several other reasons. Marginal shifts, as seen in the spectra, could be due to differences in the measurement buffer by alterations in pH and/or concentration of both urine samples. An executed washing step after the protein was incubation with the urine was intended to circumvent severe alterations in the final buffer but this could also have led to an undesired side effect. By this washing process, putative weak ligand-binding interactions could have been detached so that the compound in the urine that might have been bound to the domain before was washed-off and was lost in the 3 MWCO filter in the following re-concentration step of the sample. This would result in the same spectrum as a measurement of the PKD domain 1 that has not been incubated with urine as implied in our findings. Next, the incubation of the PKD domain with urine and the actual measurement were conducted on different days with a freezing step in between which might have also caused bond-destabilization and ligand-release so that shifts in the NMR spectra would become undone. This is why the incubation experiment and the NMR measurement should be conducted subsequently on the same day.

Another possibility is that the urine volumes used for the incubation with the *PKD1* PKD domain 1 were too low so that the compound presumably binding to domain 1 was not concentrated high enough. Normally, ~170 L of primary urine are passing the tubule system of the kidney per day that is finally concentrated to 1.7 L which corresponds to a concentration of 100x. In the experiments conducted here, only 12 mL of urine were incubated with PKD domain 1 which correspond to $1/142^{\text{th}}$ of the urine volume that is actually passing the tubules. Shifts in the NMR spectra are only detectable when the protein-ligand interaction reaches a saturation of ~50 %. If this saturation level was not reached e.g. by fewer compounds present in the smaller urine volumes, spectra would also display identical dot plots before

and after urine incubation. Further experiments could be conducted with higher volumes of urine that were concentrated beforehand. Therefore, special urine concentration filters with a higher volume capacity should be used.

Furthermore, the ADPKD patient that donated the urine was not genotyped beforehand so that the mutation causing the disease is unknown. Theoretically, most of the patients show mutations in the *PKD1* gene (85 %) but it is also possible that this gene was unaffected in this patient and he/she suffered from a mutation in the *PKD2* gene. In this case it can be assumed that polycystin-1 and its domains can fulfill its ligand-binding tasks and that substances in the primary urine are filtered out to the same extend as in a healthy state (control urine) and that compounds that might bind to *PKD1* PKD domain 1 are not excreted with the urine. This would again lead to identical NMR spectra of not incubated and incubated *PKD1* PKD domain 1 samples. Consequently, it would be interesting to repeat this experiment with urine of an ADPKD patient with a known mutation located in the PKD domain 1 of the *PKD1* gene.

Aside from that, it is also possible that the artificial expression of *PKD1* PKD domain 1 *in vitro* resulted in an oligomerization, as discussed above. This oligomerization could have led to interactions with other domain 1 molecules that might mask putative binding sites where compounds of the urine would be able to bind under physiological conditions. Again, no shifts in the NMR spectra would be identifiable as ligand-binding would be prevented by the molecular interactions. Since polycystin-1 does not form oligomeres under physiological conditions we may not come to the conclusion that the PKD domain 1 cannot bind ligands present in the urine but by future efforts to handle the protein under denaturing conditions it might be possible to prevent oligomerization, hence facilitating ligand-binding. Here, it has to be kept in mind that it is a very thin line between preventing oligomerization and disrupting the tertiary structure of the protein. Necessary to that end is a confirmation of the hypothesis of a presumptive oligomerization of the domain as already debated above. However, due to the limited time, this could no longer be checked.

Even though the presented data suggest that the PKD domain 1 of polycystin-1 may not interact with compounds in the urine, all the arguments just mentioned are intended to make it clear that no hasty conclusions can be drawn here and future experiments could help to exclude the listed aspects that might have influenced our results. In addition, it must be noted that the experiments were only conducted once and it has to be considered that only one of the 16 domains was examined here. Measurements of other and/or combined PKD domains might lead to a ligand-binding phenomenon whereas the single expression of PKD domain 1 might have not been sufficient. A putative candidate is proposed to be domain 10 since this domain shows the highest sequence conservation among species (Bycroft, 1999).

During this thesis, this domain was also expressed and purified but regrettably, the resulting concentration was very low due to protein precipitation after TEV protease cleavage with a lot of MBP fusion protein remaining. After this problem occurred the focus was only set on PKD domain 1. The precipitation of domain 10 might be prevented by a combined expression and subsequent purification with other domains which will be tested in our lab in the future. These upcoming assays could further elucidate a potential ligand-binding of the PKD domains.

4.2 Investigation of the channel properties of polycystin-2$^{\mathbf{poreL1}}$

On the other hand, calcium conductivity of polycystin-2 was tested when the pore region was exchanged with that of the closely related polycystin-2L1 thereby creating the mutant protein polycystin-2^{poreL1} *in vitro* and *in vivo*.

4.2.1 Comparison of wild-type polycystin-2 and mutant polycystin-2$^{\mathbf{poreL1}}$ *in vitro*

At the beginning, inducible LtTA-2,22 cells deriving from the porcine cell line LLC-PK$_1$ were stably transfected with a vector comprising the polycystin2^{poreL1} mutation controlled by the tetracycline transactivator (tTA). By removing doxycycline from the medium, the TetO operator sequences which are located downstream of the gene promoter is liberated from a repressor leading to expression of the downstream gene. After selecting clones by limiting dilution, the clone #59 was tested by immunofluorescence to ensure the right localization pattern when compared to wild-type polycystin-2 and also protein levels were verified by western blot to check protein induction by comparison of LtTA-2,22/PKD2(hPoreL1),HA with and without doxycycline. Both screenings showed that clone #59 was suitable for further experiments because not only the expected localization in primary cilia and the endoplasmic reticulum could be verified but also the expression of polycystin-2^{poreL1} could be regulated by the removal or addition of doxycycline. This inducibility is a great advantage because by simply adding doxycycline to the medium a trustworthy negative control is available. Since cells could undergo different evolutionary events during their cultivation, there is a great advantage in using a Tet-off system. This guarantees that those events do not affect protein synthesis because cells are cultivated without doxycycline where protein synthesis is prevented. As soon as an experiment was started, doxycycline was removed and the cells that were compared went through the same processes during cultivation up to that moment. All differences that were then detectable were caused by induction of the protein synthesis.

Western blot analysis indicated that protein levels of induced LtTA-2,22/PKD2(hPoreL1),HA cells seemed to be lower than those of induced LtTA-2,22/PKD2,HA cells (see fig. 3.13). When observing the cell growth of both cell lines, differences in proliferation could be identified with a twice as fast cell division in the wild-type cell line which could not be explained. This was unlikely due to higher passaging numbers because both cell lines were thawed and cultivated simultaneously and a contamination with *Mycoplasma* could also be neglected since periodic PCR tests always showed negative results. The observation of an enhanced proliferation rate was detected in a study of different kidney cell lines over-expressing wild-type *PKD2* and a mutant form of *PKD2* where the authors saw increased proliferation in those lines over-expressing a mutant form of *PKD2* (Felekkis et al., 2008) but a decreased proliferation rate in mutant *PKD2* cells was never observed so far. By the fact that western blot analysis was conducted prior to protein level adjustment as implemented in later experiments, both cell lines were induced for an equal amount of days, suggesting that the reduced protein levels detected in LtTA-2,22/PKD2(hPoreL1),HA cells might be due to reduced cell numbers based on a slower proliferation rate when lysates were made. Another explanation could also be that these observed differences were caused by clonal variation. Since cell viability and phenotype did also not exhibit any abnormalities both cell lines were then further on used to investigate whether lower protein levels could also be due to different half lives of both protein variants.

Lower protein levels could lead to problems in detection of the protein's half life in western blots which was then circumvented by adjusting the induction time of both cell lines to ensure visualization of protein degradation over time. Since three days of induction of wild-type cells resulted in protein levels that could be easily detected in western blot, cells producing the mutant polycystin-2^{poreL1} were induced for different time spans to find the right induction time to have equivalent protein levels. This showed that an induction of six days is sufficient to have equal protein levels (see fig. 3.13).

After this adjustment, treatment with cycloheximide had to be defined. By testing different concentrations of cycloheximide for different time spans in both cell lines (see fig. 3.14), treatment concentration was defined to be 100 µg/mL. Interestingly, after 4 h of treating LtTA-2,22/PKD2(hPoreL1),HA cells with the highest dose of cycloheximide, protein levels seem to initially increase before a final decrease followed. Normally, cycloheximide is instantly blocking the ribosome thereby initiating a very fast translational blockade after application. In a publication from Wang et al. (2015) it was shown that in a melanoma cell line 4 hours were also sufficient to reduce wild-type polycystin-2 drastically when treated with only 50 µg/mL cycloheximide so it could be rejected that incubation time was not long enough. Nevertheless, it should be noted that the effects of cycloheximide are cell-type

specific and every cell line probably reacts differently to this reagent. One phenomenon that was observed when treated with 300 µg/mL was that cells already started to detach after 4 h which progressed continuously until 24 h after application which strongly suggests cell viability issues. Due to a putative toxic effect of high doses of cycloheximide, normal cell processes might be dysregulated which could also lead to a sudden disturbance of protein levels as seen in the western blot. Why this was only observed in the mutant polycystin-2^{poreL1} cell line and not in the cell line producing the wild-type polycystin-2 is a fact that we couldn't explain. Because of the impaired cell viability when applying 300 µg/mL the focus was set on the two other tested concentrations. Those only showed minor differences in their effect of blocking the translation so it was favorable to choose the lower dose of 100 µg/mL.

Under those experimental conditions protein degradation of polycystin-2 and polycystin-2^{poreL1} was then compared. This showed a stronger decline in protein levels of wild-type polycystin-2 compared to protein levels of mutant polycystin-2^{poreL1} in the first 10 h after cycloheximide application. This strong decrease was then attenuated in the further course of the experiment resulting in overall higher protein levels of wild-type polycystin-2 compared to mutant polycystin-2^{poreL1}after 24 h after addition of cycloheximide. This initial severe drop in the protein level of wild-type polycystin-2 is also reflected in the half life of the protein suggesting a shorter half life of 6.8 h of wild-type polycystin-2 and a longer half life of 9.4 h of mutant polycystin-2^{poreL1}. These findings reject the hypothesis of a more unstable mutant polycystin-2^{poreL1}with a higher degradation rate but rather indicates that protein levels of mutant polycystin-2^{poreL1}might be lower compared to protein levels of wild-type polycystin-2 *in vitro*.

Another observation was that the mutant polycystin-2^{poreL1} resulted in double bands in the western blot. Here, an additional band of a marginally smaller size could be observed in western blots. One plausible explanation could be that parts of the mutant protein with its substituted pore region are modified differently after translation, hence migrating slower in the SDS-gel. For example by phosphorylation or glycosylation at one or more amino acid residues proteins with a higher molecular weight could arise that are then displayed in bands of a lower molecular weight in a western blot. Whether this could due to different phosphorylation events could be tested by substituting amino acids at putative phosphorylation sites to detect if this might result in a double band in a following western blot as seen in the mutant situation. It is also possible to use phosphatases and compare both wild-type and mutant polycystin-2 after phosphatase treatment in a western blot. If a different phosphorylation pattern is the cause of this double band, both samples should show the same pattern in the blot after phosphatase treatment. An altered glycosylation pattern could further be investigated by an enzymatic deglycosylation of mutant polycystin-2^{poreL1} for example by PNGase F which

cleaves off N-linked oligosaccharides from glycoproteins. Whether this then leads to altered properties of the protein would have to be tested since it is known that post-translational modification is important for stability and correct localization of polycystin-2 (Streets et al., 2006; Hofherr et al., 2014). Interestingly, no phosphorylation or glycosylation sites were reported in the sequence of polycystin-2L1 so far that was introduced into polycystin-2 (amino acids 618-658). As depicted in fig. 1.11, one tyrosine (Y646) as a putative phosphorylation site and two asparagines (N647, N651) as putative glycosylation sites were introduced into the mutant protein polycystin-2^{poreL1}that could lead to post-translational modifications. These positions would serve as the starting point for the proposed experiments. Since the underlying mechanisms of the resulting double band observed in the mutant protein polycystin-2^{poreL1} were not relevant for the further experiments in this work, no experiments were conducted to elucidate this observation. However, it would be very interesting to identify the underlying mechanisms and the suggested experiments could provide more information on that.

4.2.2 Investigation of ciliary length in primary cilia with wild-type polycystin-2 versus mutant polycystin-2^{poreL1} *in vitro*

Since function and stability of primary cilia are crucial in normal kidney development and maintenance (reviewed in Bisgrove and Yost, 2006), changes in primary ciliary length are considered as an initial step in cystogenesis of certain diseases, including ADPKD. The localization of both *PKD* proteins, polycystin-1 and polycystin-2, to primary cilia was suggested to be an important connection between primary cilia and renal cysts (Yoder, 2002). Alteration of those proteins was previously shown to result in cilia length variances as described in a preprint of a research group that observed an elongation of cilia when polycystin-2 expression was inhibited by siRNA in LLC-PK1 cells (Perez et al., 2020). Even though we only exchanged the pore region of polycystin-2 with that of polycystin-2L1 thereby expecting to create a functional cation channel with altered channel properties it was interesting to investigate whether our mutant also comprises disturbances in cilia length.

To conduct those experiments, experimental conditions had to be determined. For instance it was important to investigate optimal induction conditions with doxycycline to have an adequate number of cilia for the following length measurements not only showing the ciliary marker acetylated tubulin but also a positive signal for polycystin-2. Thus, different time spans before seeding the required amount of cells and time spans afterwards were tested and subsequently counted for cilia with a positive polycystin-2 signal in the primary cilia. This exhibited that only a minor number of cilia were polycystin-2-positive which verified the published data that the main portion of polycystin-2 is retained in the endoplasmic reticulum (Cai et al., 1999) and only a small portion of polycystin-2 localizes to primary cilia (Pazour

et al., 2002), which is also for sure due to the limited space of a cilium. By unbiased counting of cilia with a weak and strong signal of polycystin-2 the best induction time span seemed to be 7 days pre- and post-seeding to obtain. Since not only cilia number is important for measurements but also an adequate length for measurements should be given in the initial situation, cells were induced for 7 days with doxycycline pre-seeding and were further on induced for 1, 3, 5 and 7 days to ascertain also the best conditions for a maximum in cilia length. Even though maximum cilia length could be measured after 5 days this condition also showed the highest variability in length so that it was decided to induce for further 7 days after 7 days of induction pre-seeding.

After establishing optimal conditions for having a high number of polycystin-2- positive cilia with an adequate length, the main experiment was conducted by comparing induced with non-induced cells of the established cell line LtTA-2,22/PKD2(hPoreL1), HA to investigate whether the induced expression of mutant polycystin-2^{poreL1} resulted in alteration in the length of polycystin-2-positive primary cilia. As length measurements showed no significant difference in cilia length could be identified when the mutant protein polycystin-2^{poreL1} was expressed. Non-induced cells showed a high variability in cilia length which could not be ascribed to the clonal variation which is often an inevitable effect of stable cell lines but since we use an inducible cell line this effect should be averaged in the investigated cell population. The fact that no significant difference in length was observed between not-induced and induced could be due to the effect that the created mutant protein is not an up- or down-regulation of polycystin-2 hence resulting in a dose-dependend effect but a functioning protein solely comprising diverse channel properties. As immunofluorescence pictures showed, the mutant protein is still localized in the primary cilium obviously accomplishing its function as a non-selective cation channel there thus not resulting in cilia length alterations *in vitro*. The fact that we see ciliary length alterations in our PKD-mouse line *in vivo* but not in the investigated cell lines *in vitro* could be due to the higher complexity of a living being where changes in polycystin-2 might have more influence on the ciliary length whereas in a simplified organization like a cell line this might have less or no influence on the ciliary length.

4.2.3 Investigation of mutant polycystin-2^{poreL1} *in vivo*

After establishing a homozygous polycystin-2^{poreL1} knock-in mouse line in our lab it was also very interesting to closer investigate the mutant protein *in vivo*. Kidney cysts could already be observed in mice at the age of 4 weeks in a 129/Sv background and particularly in collecting ducts wider luminal diameters were found. To analyze the underlying mechanisms of this phenotype mRNA levels were checked in both wild-type and homozygous polycystin-2^{poreL1}

knock-in mice to examine whether this was due to reduced levels of the mutant *Pkd2*^{poreL1}. This hypothesis could be disproved by showing that mRNA levels were even significantly increased in mice with a homozygous polycystin-2^{poreL1} knock-in. Regrettably, western blots with lysates of isolated kidneys of wild-type and polycystin-2^{poreL1} mice conducted with different antibodies to investigate *Pkd2*^{poreL1} on the protein level did not obtain results yet. Our working group is still endeavored that results could be obtained soon.

Immunofluorescent staining of 4 days cultured primary collecting duct cells showed a weak but present localization of polycystin-2 in primary cilia of homozygous knock-in mice even though not comparable in signal strength of primary collecting duct cells from wild-type mice. Here, it could be arguable that the mutant protein might be expressed weaker in primary cilia but this could also be due to the fact that primary collecting duct cells showed a loss of aquaporin-2 signal after a few days of cultivation. Aquaporin-2, whose localization and incorporation at the apical membrane is under control of the peptide vasopressin, is responsible for water permeability in the terminal part of the renal tubule (Gash, 1987) so it is used as a marker for collecting ducts thereby corroborating a normal cell physiology. The loss of aquaporin-2 signal first occurred at the periphery of the cell patch and continued to spread into the center after 3-4 days (data not shown). This speaks for a dedifferentiation event of those cells when cultivated *ex vivo* so antibody stainings of tissue sections from homozygous polycystin-2^{poreL1} knock-in mice and wild-type mice would be the better protein verification. Unfortunately, also here our lab struggled with reliable antibody signals with different antibodies tested but again the working group is confident to resolve this problem in the future.

Notwithstanding the mutant protein polycystin-2^{poreL1} could only be detected in the endoplasmic reticulum but not in the primary cilia of kidney sections of knock-in mice in our hands so far, our working group not only detected focal cystogenesis in kidney sections but also significantly increased ciliary length in electron microscopy recordings of homozygous knock-in mice. By investigating three putative ciliary length-regulating genes, indications to the underlying mechanisms of the observed ciliary elongation could be unraveled. Even though qPCR analyses of Dynll1 did non result in statistical significant differences most likely due to the high variance seen in the tested individuals, the investigation of two other genes that were published to be involved in ciliary length regulation, Foxj1(Cruz et al., 2010) and Nde1(Inaba et al., 2016), suggest to confirm their contribution to cilia elongation in this PKD mouse model.

4.2.4 Examination of calcium conductance of the mutant protein polycystin-2^{poreL1}

Before calcium measurements were conducted, first establishments of stimulation conditions unveiled that vasopressin did not induce a calcium response in *ex vivo* cultivated collecting duct cells whereas ATP responses were increasing with ascending concentrations. As already described above, aquaporin-2 signal decreased over cultivation time speaking for a dedifferentiation of those cells. Since vasopressin stimulation showed no response in those cultures it could be speculated that the vasopressin receptor V2R got lost during the dedifferentiation event. This would furthermore explain the loss of aquaporin-2 signal because normally the water channel is incorporated into the apical membrane when the ligand vasopressin binds to its receptor V2R (Nielsen et al., 1995) which was obviously not feasible in *ex vivo* cultures any more. However, purinergic receptors seemed to be not affected by the dedifferentiation of the cultured cells since a stimulation with ATP resulted in calcium responses.

Continuing measurements of cultivated collecting duct cells stimulated with ATP revealed marginally higher intracellular calcium levels in cultivated collecting duct cells of homozygous polycystin-2^{poreL1} mice compared to wild-type mice, even though the difference did not reach statistical significance (see fig. 3.24). This suggests either a higher expression level of polycystin-2^{poreL1} which could not be investigated so far in our lab or a higher calcium conductivity in the knock-in mice which might have been enabled by the substitution of the pore region. To exclude dedifferentiation effects in those measurements freshly isolated collecting ducts from the whole kidney were analyzed. In those structures vasopressin did show calcium responses after application which again confirms the hypothesis of a dedifferentiation in the beforehand-measured cultivated collecting ducts. Regrettably, we were not able to produce responses by applying different concentrations of ATP which we could not explain so that we only focused on a stimulation with vasopressin. This displayed calcium responses that were significantly higher in freshly isolated collecting ducts from homozygous polycystin-2^{poreL1} mice compared to wild-type mice which corroborates the anteriorly *ex vivo* data. These results were also verified when imaging buffer without calcium was used to exclude an influx of extracellular calcium after stimulant application. Although total calcium levels were lower in both tested genotypes, calcium responses were significantly increased in freshly isolated collecting ducts of homozygous knock-in mice.

Isolated collecting ducts from the whole kidney were chosen by their characteristic cobblestone pattern and their unique branching. When branched ducts from the whole kidney were measured it could not be properly allocated which tubule was a connection of the distal part of the nephron to the collecting duct and which was a branch of two fusing

collecting ducts as located in the papillary regions of the kidney. To exclude undesirable side effects, only freshly isolated collecting ducts deriving from the beforehand separated papilla of homozygous polycystin-2^{poreL1} knock-in mice and polycystin-2 wild-type mice were measured. The regions of interest were furthermore specified by only measuring the central 50 % of tubules that had a minimum length of 100 µm to also exclude unpredictable effects arising at the ends of the fragments where the epithelial sheath may be harmed by the preparation. Measurements of those collecting ducts could be conducted with both ATP and vasopressin and both stimulants suggested higher calcium responses in papillary collecting ducts of homozygous polycystin-2^{poreL1} knock-in mice compared to those of wild-type mice although statistical difference was not reached in either case. The fact that the statistical significant difference was not achieved between the genotypes might probably be due to the high variability among the tested individuals which is implied by the high error bars in the graph. All these data suggest a higher conductance of calcium when the pore region of polycystin-2 was exchanged with that of polycystin-2L1. This conclusion is further supported by observations published in a previous study which used the opposite approach (Shen et al., 2016). In that study it was shown that replacing the pore region of polycystin-2L1 by that of polycystin-2 significantly reduced the permeability of the polycystin-2L1 mutant channel to Ca^{2+} ions.

Upon closer inspections of the pore regions of the investigated proteins, we found interesting differences which could explain this data outcome. Homology models of polycystin-2 and polycystin-2L1, which were kindly provided by Dr. Gregor Madej from the department of structural biology of the University of Regensburg, were based on recently published cryo-EM data (Wilkes et al., 2017; Su et al., 2018; Hulse et al., 2018) yielding a predicted structure of the pore region of our mutant protein polycstin-2^{poreL1}. This data supported a wider pore diameter in polycystin-2^{poreL1} compared to polycystin-2 hence suggesting the experimental observations obtained in our PKD mouse model. By plotting the pore radius of wild-type polycystin-2, polycystin-2L1 and mutant polycystin-2^{poreL1}along the ion-conduction axis it was suggested that the pore region of polycystin-2 comprises the greatest constrictions and since the mutant pore region is more similar to polycystin-2L1 according to *in silico* predictions it is agreed to accept a higher calcium conductivity of the mutant protein polycystin-2^{poreL1}. When smaller cations like potassium were included in those predictions it was shown that this cation could easily pass the selectivity filter of either pore loop whereas calcium was only able to pass through the selectivity filter of polycystin-2L1 which implied that this was also true for the similar selectivity filter of polycystin-2^{poreL1}.

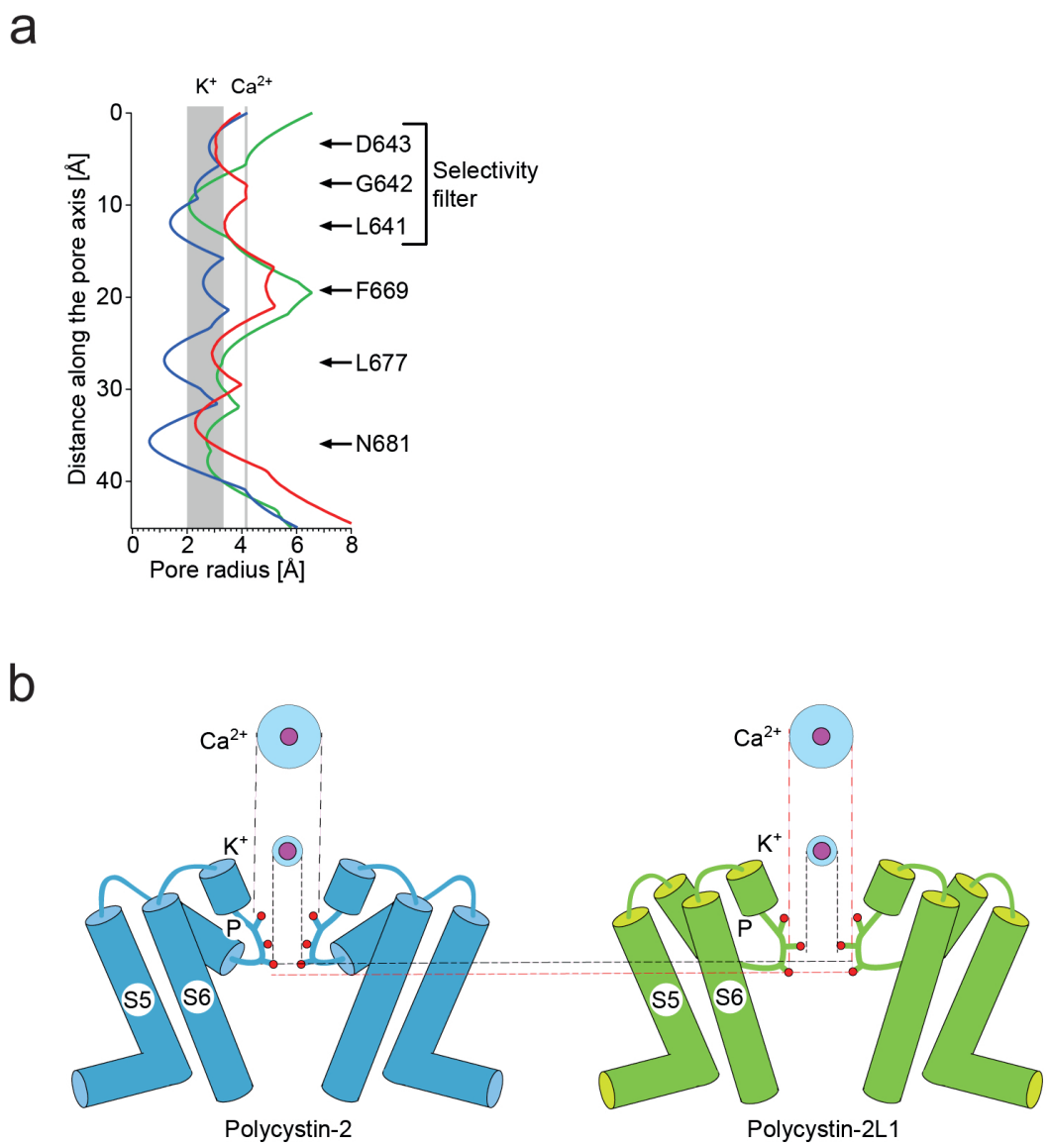

Figure 4.1: **Structural modeling of polycystin-2^{poreL1}.** The pore radius is plotted along the ion-conduction axis together with the residues lining the pore. As depicted, most prominent constrictions are present in wild-type polycystin-2 (blue line) whereas the pore shows a wider diameter in polycystin-2L1 (green line). The structure of polycystin-2^{poreL1} (red line) is closer to that of polycystin-2L1. Shaded regions indicate the radius of hydrated K^+ and of hydrated Ca^{2+} ions (a). Displayed are the transmembrane segments S5 and S6 of polycystin-2 and polycystin-2L1 together with the intervening pore loop (P). By the red circles the amino acids in the selectivity filter of polycystin-2 (D643, G642 and L641, top to bottom) and of polycystin-2L1 (D523, G522 and L521, top to bottom) are depicted with the outer circles of each ion indicating the radii of the hydrated ions and the inner circles representing the ionic radii. It is suggested that e.g. hydrated K^+ ions can pass through the selectivity filter of either pore loop but Ca^{2+} ions will only be able to pass through the selectivity filter of polycystin-2L1 (provided by Dr. Gregor Madej).

The observed second smaller peak after the first calcium response induced by ATP is a known phenomenon due to a re-influx of calcium from the extracellular space. After stores were depleted calcium is rapidly transported out of the cell to re-establish a calcium homeostasis since this second messenger is involved in many pathways (reviewed in Blaustein, 1985) which would otherwise be affected. This is enabled by the store-operated calcium entry (SOCE) causing a calcium re-filling of the endoplasmic reticulum (Smyth et al., 2010) which is beforehand detectable in a second smaller peak caused by a fluorescence shift of the calcium-sensor Fura-2 in the intracellular space.

When analyzing mice with the collecting duct specific knock-out of polycystin-2 compared to wild-type mice, no differences in calcium response were expected since polycystin-2 was suggested to be unable to conduct calcium according to the results discussed above. Indeed, measurements in freshly isolated collecting ducts of whole kidneys did not show significant differences in calcium responses but indicated a marginally weaker calcium response in mice where polycystin-2 was supposed to be absent in collecting ducts compared to *Pkd2*$^{lox/lox}$-mice resembling the wild-type situation. This indicated difference could be due to the high variability among measured individuals as implied by the high error bars.

Another explanation could be that the used method of gene editing by the Cre-loxP system did not result in a complete knock-out of polycystin-2 in collecting ducts. The lower response in the "knock-out" mice could reflect a decreased but remaining level of polycystin-2. Even if polycystin-2 should not be able to conduct calcium by itself it should be kept in mind that the channel might still be of importance for calcium release by interaction with other calcium permeable channels situated in the membrane of the endoplasmic/sarcoplasmic reticulum like IP_3R and RyR2 (Li et al., 2005; Anyatonwu et al., 2007). This indirect calcium release would then result in weaker calcium levels in mice with lower polycystin-2 levels (*Pkhd1*::Cre-mice) compared to the investigated *Pkd2*$^{lox/lox}$-mice with normal levels of polycystin-2 as seen in our findings. This hypothesis was then confirmed by a western blot with lysates from isolated papilla from *Pkd2*$^{lox/lox}$ and *Pkhd1*::Cre;*Pkd2*$^{lox/lox}$ mice conducted and kindly provided by Prof. Dr. Silke Härteis' research group from the department of molecular and cellular anatomy of the University of Regensburg. As figure 4.2 showed, protein levels of *Pkhd1*::Cre mice were only reduced but not absent compared to *Pkd2*$^{lox/lox}$ mice which corroborated the findings of the calcium measurements conducted in those mice.

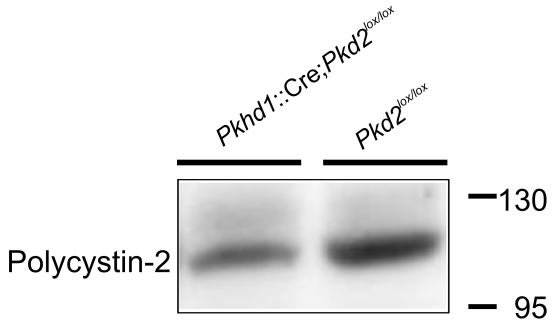

Figure 4.2: **Western blot of *Pkhd1*::Cre;*Pkd2*$^{lox/lox}$ and *Pkd2*$^{lox/lox}$ mice.** For lysates, 6 papilla were isolated and pooled from 4 weeks old animals of the respective genotype. After loading 100 µg lysate per lane bands were detected by an antibody against polycystin-2 (rabbit-anti PC2C1) showing the expected size of ~110 kDa. The expected absence of a signal from lysates of pooled papilla from *Pkhd1*::Cre;*Pkd2*$^{lox/lox}$ mice was not given and only a reduction in protein levels could be detected in those mice compared to the signal of pooled papilla from *Pkd2*$^{lox/lox}$ mice. The numbers on the right of the blots give the size of the molecular weight standard in kDa (provided by Prof. Dr. Silke Härteis).

To ensure a complete reduction of polycystin-2 in collecting ducts, another mouse line should be generated. Again the Cre-loxP system could be used for another try of a complete tissue-specific knock-out. Furthermore, the recently established method of gene editing by CRISPR/Cas9 showed some pioneer experiments were tissue specific knock-out could be introduced in *Drosophila* (Meltzer et al., 2019) and zebrafish (Ablain and Zon, 2016) but with some limitations. Poor gene targeting and mosaicism inside the tissue often occurred which was suggested to be either due to a bad intrinsic quality of guide RNAs (gRNAs) or weak promoter activity. It will probably still take some time until science has made some progress here to overcome those problems and to successfully introduce those methods after improvement in the more complex mouse model system on a tissue-specific level. In the last year, first approaches already showed some promising results in lung-, spleen- and liver-targeted lipid nanoparticles that are used in different gene editing techniques including CRISPR/Cas (Cheng et al., 2020). These obtained results might further aid the development of gene editing also in other targeted tissues.

5 Summary

The autosomal-dominant polycystic kidney disease (ADPKD) is the most common monogenic kidney disease caused by mutations in the genes *PKD1* or *PKD2.*

In 85 %, patients show mutations in *PKD1* which encodes for a ~4300 amino acid protein with 11 transmembrane domains located in the primary cilium and the plasma membrane in ductal epithelial cells of many tissues e.g. the kidney. Polycystin-1 is probably involved in signal sensing by its large extracellular domain. In this domain several motifs are present all comprising different functions. The repetitive sixteen PKD domains with one occurring separately and fifteen further domains located more downstream are likely to be important in signal sensing since similar structures were found in protein-protein and protein-carbohydrate interactions. Interestingly, only less information was published about this hypothesis yet. In 1999, Bycroft identified a novel protein family in those PKD domains by a structural analysis with a suggested role as a cell-surface protein.

To test the hypothesis of a putative ligand-binding function, one domain of those PKD domains of polycystin-1 was introduced in an expression vector for the synthesis of pure *PKD1* PKD domain 1. This domain was chosen because of its separate occurrence in the extracellular domain which might speak for a certain importance. The idea was to measure the domain in a nuclear magnetic resonance analysis prior to an incubation of the domain with urine samples of either an ADPKD-patient with an unknown mutation or a healthy person to identify afterwards putative shifts in the NMR spectra. This should exhibit whether components of the patient's urine are binding to this domain which are not present any more in the urine of a healthy person due to a filtration by polycystin-1 beforehand. After establishing optimal conditions to ensure solubility of the protein in a small scale we went on in upscaling expression volumes to reach an appropriate concentration with a purity of >90 % for a following NMR analysis. Since a first spectrum of unlabeled protein showed a nice resolution, a subsequent expression of ^{15}N-labeled protein was conducted. Here, 2D-HSQC NMR spectra suggested that the PKD domain 1 of polycystin-1 is not involved in ligand-binding since spectra of urine-incubated and not incubated domain samples did not show peak alterations. Since a lot of circumstances might have influenced these findings, more experiments have to be conducted in the future to verify the results.

Polycystin-1 is capable to interact with polycystin-2, the protein encoded by the gene *PKD2* responsible for the remaining 15 % of ADPKD cases when mutations originate. This reported interaction via their C-termini furthermore speaks for a sensory function of polycystin-1 leading to downstream changes in polycystin-2. This protein is mainly located in the endoplasmic reticulum and primary cilia and its 968 amino acids are forming six transmembrane domains with a suggested function of a non-selective cation channel. Lately, it was disputed about the capability of a calcium conductance of polycystin-2 with more data recently speaking against this ability. By exchanging the pore region of polycystin-2 with that of the closely related polycystin-2L1 we created a mutant but functional channel with altered conduction properties - polycystin-2^{poreL1}. After establishing a stable cell line inducible for the expression of the mutant polycystin-2^{poreL1}, we could identify a proper localization pattern of the protein encouraging to proceed with those cells. A western blot of wild-type polycystin-2 and mutant polycystin-2^{poreL1} exhibited reduced protein levels in the mutant cell line leading us to test the protein stability of both wild-type and mutant protein. Those experiments suggested an even more stable polycystin-2^{poreL1} protein when compared to the half life of wild-type polycystin-2 and so the reduced amount of mutant protein in the western blot is more likely due to lower levels of mutant protein, per se, or a slower doubling rate of the cells.

Next, the phenomenon of alterations in the length of primary cilia, which was reported in different cases of ADPKD, should be investigated by comparing ciliary length in non-induced and induced cells of the mutant cell line LtTA-2,22/PKD2(hPoreL1),HA. However, this observation of altered ciliary length could not be verified in our cell line with an altered pore region.

By the following comparisons of wild-type polycystin-2 and mutant polycystin-2^{poreL1} *in vitro* and *in vivo*, we wanted to identify possible changes in the channel's calcium response after applying different stimulants like ATP or vasopressin. In first approaches, we wanted to investigate our mutant polycystin-2^{poreL1} protein *in vivo*. By analysis of isolated collecting ducts from wild-type polycystin-2 and homozygous polycystin-2^{poreL1} knock-in mice by quantitative PCR, a detectable increase in mRNA levels of $Pkd2^{poreL1}$ compared to wild-type *Pkd2* was exhibited. A subsequent investigation of the localization pattern of the mutant protein in primary collecting duct cells showed a weak but correct signal in immunofluorescence suggesting a correct localization in primary cilia. This verification was the basis for further qPCR analyses. Since our lab detected elongated primary cilia in homozygous polycystin-2^{poreL1} knock-in mice when compared to wild-type polycystin-2 mice in electron micrographs, we were interested to investigate genes that might be putative contributors to those length alterations. By this, we were able to identify two genes that are

suggested to be involved in the detected elongation of primary cilia, FoxJ1 and Nde1.

In the following, primary collecting duct cells were used for first measurements of intracellular calcium levels. Here we found a marginally higher calcium response in primary collecting duct cells isolated from homozygous polycystin-2^{poreL1} mice compared to those isolated from wild-type mice. To exclude *ex vivo* impacts like dedifferentiation events in the cultivated primary cells we also measured freshly isolated collecting ducts from both wild-type and homozygous knock-in mice either from whole kidneys or from priorly separated papilla which also showed a higher calcium response in collecting ducts isolated from homozygous knock-in mice, even though statistical significance was only reached in collecting ducts isolated from whole kidneys. This corroborated our findings from the primary collecting duct cells. Hence, all these data suggest that wild-type polycystin-2 has no or minor impact on the intracellular calcium homeostasis by a direct conductance. This moreover speaks for the recent findings doubting polycystin-2 to be a calcium-permeable cation channel.

However, investigation of a collecting duct-specific *Pkd2*-floxed mouse line showed that polycystin-2 might still be somehow involved in calcium conduction since isolated collecting ducts from wild-type mice had a marginally but not significantly higher calcium response compared to mice where *Pkd2* should be absent in collecting ducts. This difference should not be observed when polycystin-2 would not be able to conduct calcium. Unfortunately, it was shown afterwards that the Cre-*lox* method did not seem to have worked completely in this mouse line since a weaker but prominent band was detectable in a western blot of isolated papilla from those mice. Nevertheless, even though the presented data suggest that polycystin-2 is probably not involved in a direct calcium conductance it is still possible that the channel is important for indirect calcium conductance by e.g. interaction with other calcium-permeable channels.

References

Aanstad, P., Santos, N., Corbit, K. C., Scherz, P. J., Trinh, L. A., Salvenmoser, W., Huisken, J., Reiter, J. F. and Stainier, D. Y. (2009). The Extracellular Domain of Smoothened Regulates Ciliary Localization and Is Required for High-Level Hh Signaling. Current Biology *19*, 1034–1039.

Ablain, J. and Zon, L. (2016). Tissue-specific gene targeting using CRISPR/Cas9. In Methods in Cell Biology pp. 189–202. Elsevier.

Anyatonwu, G. I., Estrada, M., Tian, X., Somlo, S. and Ehrlich, B. E. (2007). Regulation of ryanodine receptor-dependent calcium signaling by polycystin-2. Proceedings of the National Academy of Sciences of the United States of America *104*, 6454–6459.

Babich, V., Zeng, W.-Z., Yeh, B.-I., Ibraghimov-Beskrovnaya, O., Cai, Y., Somlo, S. and Huang, C.-L. (2004). The N-terminal Extracellular Domain Is Required for Polycystin-1-dependent Channel Activity. Journal of Biological Chemistry *279*, 25582–25589.

Baccetti, B. and Afzelius, B. A. (1976). The biology of the sperm cell.

Barr, M. M. and Sternberg, P. W. (1999). A polycystic kidney-disease gene homologue required for male mating behaviour in C. elegans. Nature *401*, 386–389.

Bisgrove, B. W. and Yost, H. J. (2006). The roles of cilia in developmental disorders and disease. Development *133*, 4131–4143.

Bisswanger, H. (2017). Enzyme Kinetics. Wiley-VCH GmbH.

Blaustein, M. P. (1985). Intracellular Calcium as a Second Messenger. In Calcium in Biological Systems pp. 23–33. Springer US.

Boehlke, C., Kotsis, F., Patel, V., Braeg, S., Voelker, H., Bredt, S., Beyer, T., Janusch, H., Hamann, C., Goedel, M., Mueller, K., Herbst, M., Hornung, M., Doerken, M., Koettgen, M., Nitschke, R., Igarashi, P., Walz, G. and Kuehn, E. W. (2010). Primary cilia regulate mTORC1 activity and cell size through Lkb1. Nature Cell Biology *12*, 1115–1122.

Brasier, J. L. and Henske, E. P. (1997). Loss of the polycystic kidney disease (PKD1) region of chromosome 16p13 in renal cyst cells supports a loss-of-function model for cyst pathogenesis. The Journal of clinical investigation *99*, 194–199.

Bycroft, M. (1999). The structure of a PKD domain from polycystin-1: implications for polycystic kidney disease. The EMBO Journal *18*, 297–305.

Cai, Y., Anyatonwu, G., Okuhara, D., Lee, K.-B., Yu, Z., Onoe, T., Mei, C.-L., Qian, Q., Geng, L., Wiztgall, R., Ehrlich, B. E. and Somlo, S. (2004). Calcium dependence of polycystin-2 channel activity is modulated by phosphorylation at Ser812. The Journal of biological chemistry *279*, 19987–19995.

Cai, Y., Maeda, Y., Cedzich, A., Torres, V. E., Wu, G., Hayashi, T., Mochizuki, T., Park, J. H., Witzgall, R. and Somlo, S. (1999). Identification and Characterization of Polycystin-2, the PKD2 Gene Product. Journal of Biological Chemistry *274*, 28557–28565.

Chang, M.-Y. and Ong, A. C. (2012). Mechanism-Based Therapeutics for Autosomal Dominant Polycystic Kidney Disease: Recent Progress and Future Prospects. Nephron Clinical Practice *120*, c25–c35.

Chen, X.-Z., Vassilev, P. M., Basora, N., Peng, J.-B., Nomura, H., Segal, Y., Brown, E. M., Reeders, S. T., Hediger, M. A. and Zhou, J. (1999). Polycystin-L is a calcium-regulated cation channel permeable to calcium ions. Nature *401*, 383–386.

Cheng, Q., Wei, T., Farbiak, L., Johnson, L. T., Dilliard, S. A. and Siegwart, D. J. (2020). Selective organ targeting (SORT) nanoparticles for tissue-specific mRNA delivery and CRISPR-Cas gene editing. Nature nanotechnology *15*, 313–320.

Collins, A. J., Foley, R. N., Chavers, B., Gilbertson, D., Herzog, C., Johansen, K., Kasiske, B., Kutner, N., Liu, J., Peter, W. S., Guo, H., Gustafson, S., Heubner, B., Lamb, K., Li, S., Li, S., Peng, Y., Qiu, Y., Roberts, T., Skeans, M., Snyder, J., Solid, C., Thompson, B., Wang, C., Weinhandl, E., Zaun, D., Arko, C., Chen, S.-C., Daniels, F., Ebben, J., Frazier, E., Hanzlik, C., Johnson, R., Sheets, D., Wang, X., Forrest, B., Constantini, E., Everson, S., Eggers, P. and Agodoa, L. (2012). US Renal Data System 2011 Annual Data Report. American Journal of Kidney Diseases *59*, A7.

Cosens, D. J. and Manning, A. (1969). Abnormal Electroretinogram from a Drosophila Mutant. Nature *224*, 285–287.

Cruz, C., Ribes, V., Kutejova, E., Cayuso, J., Lawson, V., Norris, D., Stevens, J., Davey, M., Blight, K., Bangs, F., Mynett, A., Hirst, E., Chung, R., Balaskas, N., Brody, S. L., Marti, E. and Briscoe, J. (2010). Foxj1 regulates floor plate cilia architecture and modifies the response of cells to sonic hedgehog signalling. Development *137*, 4271–4282.

Davis, E. E., Brueckner, M. and Katsanis, N. (2006). The Emerging Complexity of the Vertebrate Cilium: New Functional Roles for an Ancient Organelle. Developmental Cell *11*, 9–19.

Delling, M., Indzhykulian, A. A., Liu, X., Li, Y., Xie, T., Corey, D. P. and Clapham, D. E. (2016). Primary cilia are not calcium-responsive mechanosensors. Nature *531*, 656–660.

Delmas, P., Nauli, S. M., Li, X., Coste, B., Osorio, N., Crest, M., Brown, D. A. and Zhou, J. (2004). Gating of the polycystin ion channel signaling complex in neurons and kidney cells. The FASEB Journal *18*, 740–742.

Delmas, P., Nomura, H., Li, X., Lakkis, M., Luo, Y., Segal, Y., FernÃ¡ndez-FernÃ¡ndez, J. M., Harris, P., Frischauf, A.-M., Brown, D. A. and Zhou, J. (2002). Constitutive activation of G-proteins by polycystin-1 is antagonized by polycystin-2. The Journal of biological chemistry *277*, 11276–11283.

Doyle, D. A., Morais Cabral, J., Pfuetzner, R. A., Kuo, A., Gulbis, J. M., Cohen, S. L., Chait, B. T. and MacKinnon, R. (1998). The structure of the potassium channel: molecular basis of K+ conduction and selectivity. Science (New York, N.Y.) *280*, 69–77.

Ezratty, E. J., Stokes, N., Chai, S., Shah, A. S., Williams, S. E. and Fuchs, E. (2011). A Role for the Primary Cilium in Notch Signaling and Epidermal Differentiation during Skin Development. Cell *145*, 1129–1141.

Felekkis, K. N., Koupepidou, P., Kastanos, E., Witzgall, R., Bai, C.-X., Li, L., Tsiokas, L., Gretz, N. and Deltas, C. (2008). Mutant polycystin-2 induces proliferation in primary rat tubular epithelial cells in a STAT-1/p21-independent fashion accompanied instead by alterations in expression of p57KIP2 and Cdk2. BMC nephrology *9*, 10.

Gabow, P. A. (1993). Autosomal Dominant Polycystic Kidney Disease. New England Journal of Medicine *329*, 332–342.

Gallagher, A. R., Hoffmann, S., Brown, N., Cedzich, A., Meruvu, S., Podlich, D., Feng, Y., Koenecke, V., de Vries, U., Hammes, H.-P., Gretz, N. and Witzgall, R. (2006). A Truncated Polycystin-2 Protein Causes Polycystic Kidney Disease and Retinal Degeneration in Transgenic Rats. Journal of the American Society of Nephrology *17*, 2719–2730.

Gash, D. (1987). Vasopressin : Principles and Properties. Springer US, Boston, MA.

Gaudet, R. (2008). TRP channels entering the structural era. The Journal of Physiology *586*, 3565–3575.

Geng, L. (2006). Polycystin-2 traffics to cilia independently of polycystin-1 by using an N-terminal RVxP motif. Journal of Cell Science *119*, 1383–1395.

Geng, L., Segal, Y., Peissel, B., Deng, N., Pei, Y., Carone, F., Rennke, H. G., Gluecksmann-Kuis, A. M., Schneider, M. C., Ericsson, M., Reeders, S. T. and Zhou, J. (1996). Identification and localization of polycystin, the PKD1 gene product. Journal of Clinical Investigation *98*, 2674–2682.

Gonzalez-Perrett, S., Kim, K., Ibarra, C., Damiano, A. E., Zotta, E., Batelli, M., Harris, P. C., Reisin, I. L., Arnaout, M. A. and Cantiello, H. F. (2001). Polycystin-2, the protein mutated in autosomal dominant polycystic kidney disease ADPKD, is a Ca2+-permeable nonselective cation channel. Proceedings of the National Academy of Sciences *98*, 1182–1187.

Grantham, J. J., Torres, V. E., Chapman, A. B., Guay-Woodford, L. M., Bae, K. T., King, B. F., Wetzel, L. H., Baumgarten, D. A., Kenney, P. J., Harris, P. C., Klahr, S., Bennett, W. M., Hirschman, G. N., Meyers, C. M., Zhang, X., Zhu, F. and Miller, J. P. (2006). Volume Progression in Polycystic Kidney Disease. New England Journal of Medicine *354*, 2122–2130.

Grieben, M., Pike, A. C. W., Shintre, C. A., Venturi, E., El-Ajouz, S., Tessitore, A., Shrestha, L., Mukhopadhyay, S., Mahajan, P., Chalk, R., Burgess-Brown, N. A., Sitsapesan, R., Huiskonen, J. T. and Carpenter, E. P. (2016). Structure of the polycystic kidney disease TRP channel Polycystin-2 (PC2). Nature Structural & Molecular Biology *24*, 114–122.

Guo, L., Schreiber, T. H., Weremowicz, S., Morton, C. C., Lee, C. and Zhou, J. (2000). Identification and characterization of a novel polycystin family member, polycystin-L2, in mouse and human: sequence, expression, alternative splicing, and chromosomal localization. Genomics *64*, 241–251.

Habbig, S., Bartram, M. P., Mueller, R. U., Schwarz, R., Andriopoulos, N., Chen, S., Saegmueller, J. G., Hoehne, M., Burst, V., Liebau, M. C., Reinhardt, H. C., Benzing, T. and Schermer, B. (2011). NPHP4, a cilia-associated protein, negatively regulates the Hippo pathway. The Journal of Cell Biology *193*, 633–642.

Haimo, L. T. and Rosenbaum, J. L. (1981). Cilia, flagella, and microtubules. The Journal of Cell Biology *91*, 125s–130s.

Han, S. J., Jang, H.-S., Kim, J. I., Lipschutz, J. H. and Park, K. M. (2016). Unilateral nephrectomy elongates primary cilia in the remaining kidney via reactive oxygen species. Scientific reports *6*, 22281.

Hanaoka, K., Qian, F., Boletta, A., Bhunia, A. K., Piontek, K., Tsiokas, L., Sukhatme, V. P., Guggino, W. B. and Germino, G. G. (2000). Co-assembly of polycystin-1 and -2 produces unique cation-permeable currents. Nature *408*, 990–994.

Hardie, R. C. and Minke, B. (1992). The trp gene is essential for a light-activated Ca2+ channel in Drosophila photoreceptors. Neuron *8*, 643–651.

Hellmich, U. A. and Gaudet, R. (2014). Structural biology of TRP channels. Handbook of experimental pharmacology *223*, 963–990.

Hildebrandt, F., Benzing, T. and Katsanis, N. (2011). Ciliopathies. New England Journal of Medicine *364*, 1533–1543.

Hofherr, A., Wagner, C., Fedeles, S., Somlo, S. and Koettgen, M. (2014). N-glycosylation determines the abundance of the transient receptor potential channel TRPP2. The Journal of biological chemistry *289*, 14854–14867.

Hong, S.-K. and Dawid, I. B. (2009). FGF-dependent left-right asymmetry patterning in zebrafish is mediated by Ier2 and Fibp1. Proceedings of the National Academy of Sciences *106*, 2230–2235.

Huang, A. L., Chen, X., Hoon, M. A., Chandrashekar, J., Guo, W., TrÃ€nkner, D., Ryba, N. J. P. and Zuker, C. S. (2006). The cells and logic for mammalian sour taste detection. Nature *442*, 934–938.

Hughes, J., Ward, C. J., Peral, B., Aspinwall, R., Clark, K., Millán, J. L. S., Gamble, V. and Harris, P. C. (1995). The polycystic kidney disease 1 (PKD1) gene encodes a novel protein with multiple cell recognition domains. Nature Genetics *10*, 151–160.

Hulse, R. E., Li, Z., Huang, R. K., Zhang, J. and Clapham, D. E. (2018). Cryo-EM structure of the polycystin 2-l1 ion channel. eLife *7*.

Inaba, H., Goto, H., Kasahara, K., Kumamoto, K., Yonemura, S., Inoko, A., Yamano, S., Wanibuchi, H., He, D., Goshima, N., Kiyono, T., Hirotsune, S. and Inagaki, M. (2016). Ndel1 suppresses ciliogenesis in proliferating cells by regulating the trichoplein–Aurora A pathway. Journal of Cell Biology *212*, 409–423.

Ishimaru, Y., Inada, H., Kubota, M., Zhuang, H., Tominaga, M. and Matsunami, H. (2006). Transient receptor potential family members PKD1L3 and PKD2L1 form a candidate sour taste receptor. Proceedings of the National Academy of Sciences of the United States of America *103*, 12569–12574.

Kawaguchi, H., Yamanaka, A., Uchida, K., Shibasaki, K., Sokabe, T., Maruyama, Y., Yanagawa, Y., Murakami, S. and Tominaga, M. (2010). Activation of polycystic kidney disease-2-like 1 (PKD2L1)-PKD1L3 complex by acid in mouse taste cells. The Journal of biological chemistry *285*, 17277–17281.

Keeler, J. K. (2010). Understanding NMR Spectroscopy. John Wiley and Sons.

Kim, K., Drummond, I., Ibraghimov-Beskrovnaya, O., Klinger, K. and Arnaout, M. A. (2000). Polycystin 1 is required for the structural integrity of blood vessels. Proceedings of the National Academy of Sciences of the United States of America *97*, 1731–1736.

Kim, S., Zaghloul, N. A., Bubenshchikova, E., Oh, E. C., Rankin, S., Katsanis, N., Obara, T.

and Tsiokas, L. (2011). Nde1-mediated inhibition of ciliogenesis affects cell cycle re-entry. Nature Cell Biology *13*, 351–360.

Koettgen, M., Buchholz, B., Garcia-Gonzalez, M. A., Kotsis, F., Fu, X., Doerken, M., Boehlke, C., Steffl, D., Tauber, R., Wegierski, T., Nitschke, R., Suzuki, M., Kramer-Zucker, A., Germino, G. G., Watnick, T., Prenen, J., Nilius, B., Kuehn, E. W. and Walz, G. (2008). TRPP2 and TRPV4 form a polymodal sensory channel complex. The Journal of cell biology *182*, 437–447.

Koettgen, M., Hofherr, A., Li, W., Chu, K., Cook, S., Montell, C. and Watnick, T. (2011). Drosophila Sperm Swim Backwards in the Female Reproductive Tract and Are Activated via TRPP2 Ion Channels. PLoS ONE *6*, e20031.

Koulen, P., Cai, Y., Geng, L., Maeda, Y., Nishimura, S., Witzgall, R., Ehrlich, B. E. and Somlo, S. (2002). Polycystin-2 is an intracellular calcium release channel. Nature Cell Biology *4*, 191–197.

Langman, J. (1975). Medical embryology; human development-normal and abnormal., vol. 186,. Williams and Wilkins, Baltimore.

Li, Y., Wright, J. M., Qian, F., Germino, G. G. and Guggino, W. B. (2005). Polycystin 2 interacts with type I inositol 1,4,5-trisphosphate receptor to modulate intracellular Ca2+ signaling. The Journal of biological chemistry *280*, 41298–41306.

Liu, X., Vien, T., Duan, J., Sheu, S.-H., DeCaen, P. G. and Clapham, D. E. (2018). Polycystin-2 is an essential ion channel subunit in the primary cilium of the renal collecting duct epithelium. eLife *7*.

Long, S. B., Campbell, E. B. and Mackinnon, R. (2005). Crystal structure of a mammalian voltage-dependent Shaker family K+ channel. Science (New York, N.Y.) *309*, 897–903.

Long, S. B., Tao, X., Campbell, E. B. and MacKinnon, R. (2007). Atomic structure of a voltage-dependent K+ channel in a lipid membrane-like environment. Nature *450*, 376–382.

Lu, H., Toh, M. T., Narasimhan, V., Thamilselvam, S. K., Choksi, S. P. and Roy, S. (2015). A function for the Joubert syndrome protein Arl13b in ciliary membrane extension and ciliary length regulation. Developmental Biology *397*, 225–236.

Lu, W., Peissel, B., Babakhanlou, H., Pavlova, A., Geng, L., Fan, X., Larson, C., Brent, G. and Zhou, J. (1997). Perinatal lethality with kidney and pancreas defects in mice with a targetted Pkd1 mutation. Nature genetics *17*, 179–181.

McLafferty, E., Johnstone, C., Hendry, C. and Farley, A. (2014). The urinary system. Nursing Standard *28*, 43–50.

Meijer, E. and Gansevoort, R. T. (2020). Vasopressin V2 receptor antagonists in autosomal dominant polycystic kidney disease: efficacy, safety, and tolerability. Kidney international *98*, 289–293.

Meijer, E., Gansevoort, R. T., de Jong, P. E., van der Wal, A. M., Leonhard, W. N., de Krey, S. R., van den Born, J., Mulder, G. M., van Goor, H., Struck, J., de Heer, E. and Peters, D. J. M. (2011). Therapeutic potential of vasopressin V2 receptor antagonist in a mouse model for autosomal dominant polycystic kidney disease: optimal timing and dosing of the drug. Nephrology Dialysis Transplantation *26*, 2445–2453.

Meltzer, H., Marom, E., Alyagor, I., Mayseless, O., Berkun, V., Segal-Gilboa, N., Unger, T., Luginbuhl, D. and Schuldiner, O. (2019). Tissue-specific (ts)CRISPR as an efficient strategy for in vivo screening in Drosophila. Nature Communications *10*.

Mochizuki, T., Wu, G., Hayashi, T., Xenophontos, S. L., Veldhuisen, B., Saris, J. J., Reynolds, D. M., Cai, Y., Gabow, P. A., Pierides, A., Kimberling, W. J., Breuning, M. H., Deltas, C. C., Peters, D. J. M. and Somlo, S. (1996). PKD2, a Gene for Polycystic Kidney Disease That Encodes an Integral Membrane Protein. Science *272*, 1339–1342.

Montell, C. and Rubin, G. M. (1989). Molecular characterization of the Drosophila trp locus: a putative integral membrane protein required for phototransduction. Neuron *2*, 1313–1323.

Murakami, M., Ohba, T., Xu, F., Shida, S., Satoh, E., Ono, K., Miyoshi, I., Watanabe, H., Ito, H. and Iijima, T. (2004). Genomic Organization and Functional Analysis of Murine PKD2L1. Journal of Biological Chemistry *280*, 5626–5635.

Nielsen, S., Chou, C. L., Marples, D., Christensen, E. I., Kishore, B. K. and Knepper, M. A. (1995). Vasopressin increases water permeability of kidney collecting duct by inducing translocation of aquaporin-CD water channels to plasma membrane. Proceedings of the National Academy of Sciences of the United States of America *92*, 1013–1017.

Niemczyk, M., Niemczyk, S. and Paczek, L. (2009). Autosomal dominant polycystic kidney disease and transplantation. Annals of transplantation *14*, 86–90.

Nilius, B. and Owsianik, G. (2011). The transient receptor potential family of ion channels. Genome Biology *12*, 218.

Nishio, S., Tian, X., Gallagher, A. R., Yu, Z., Patel, V., Igarashi, P. and Somlo, S. (2009). Loss of Oriented Cell Division Does not Initiate Cyst Formation. Journal of the American Society of Nephrology *21*, 295–302.

Nobakht, N., Hanna, R. M., Al-Baghdadi, M., Ameen, K. M., Arman, F., Nobahkt, E.,

Kamgar, M. and Rastogi, A. (2020). Advances in Autosomal Dominant Polycystic Kidney Disease: A Clinical Review. Kidney Medicine *2*, 196–208.

Nonaka, S., Tanaka, Y., Okada, Y., Takeda, S., Harada, A., Kanai, Y., Kido, M. and Hirokawa, N. (1998). Randomization of Left-Right Asymmetry due to Loss of Nodal Cilia Generating Leftward Flow of Extraembryonic Fluid in Mice Lacking KIF3B Motor Protein. Cell *95*, 829–837.

Owsianik, G., D'hoedt, D., Voets, T. and Nilius, B. (2006). Structure-function relationship of the TRP channel superfamily. Reviews of physiology, biochemistry and pharmacology *156*, 61–90.

Pattenden, L. K. and Thomas, W. G. (2008). Amylose affinity chromatography of maltose-binding protein: purification by both native and novel matrix-assisted dialysis refolding methods. Methods in molecular biology (Clifton, N.J.) *421*, 169–189.

Pavel, M. A., Lv, C., Ng, C., Yang, L., Kashyap, P., Lam, C., Valentino, V., Fung, H. Y., Campbell, T., Møller, S. G., Zenisek, D., Holtzman, N. G. and Yu, Y. (2016). Function and regulation of TRPP2 ion channel revealed by a gain-of-function mutant. Proceedings of the National Academy of Sciences *113*, E2363–E2372.

Pazour, G. J., Agustin, J. T. S., Follit, J. A., Rosenbaum, J. L. and Witman, G. B. (2002). Polycystin-2 localizes to kidney cilia and the ciliary level is elevated in orpk mice with polycystic kidney disease. Current Biology *12*, R378–R380.

Pedersen, L. B., Schrøder, J. M., Satir, P. and Christensen, S. T. (2011). The ciliary cytoskeleton, vol. 2,. Wiley Online Library.

Pei, Y., Obaji, J., Dupuis, A., Paterson, A. D., Magistroni, R., Dicks, E., Parfrey, P., Cramer, B., Coto, E., Torra, R., Millan, J. L. S., Gibson, R., Breuning, M., Peters, D. and Ravine, D. (2008). Unified Criteria for Ultrasonographic Diagnosis of ADPKD. Journal of the American Society of Nephrology *20*, 205–212.

Perez, P. L., Scarinci, N., Cantiello, H. F. and del Rocio Cantero, M. (2020). Polycystin-2 (trpp2) regulates primary cilium length in llc-pk1 renal epithelial cells.

Pfaffl, M. W. (2001). A new mathematical model for relative quantification in real-time RT-PCR. Nucleic Acids Research *29*, 45e–45.

Ponting, C. P., Hofmann, K. and Bork, P. (1999). A latrophilin/CL-1-like GPS domain in polycystin-1. Current biology : CB *9*, R585–R588.

Praetorius, H. and Spring, K. (2001). Bending the MDCK Cell Primary Cilium Increases Intracellular Calcium. Journal of Membrane Biology *184*, 71–79.

Qian, F., Boletta, A., Bhunia, A. K., Xu, H., Liu, L., Ahrabi, A. K., Watnick, T. J., Zhou, F. and Germino, G. G. (2002). Cleavage of polycystin-1 requires the receptor for egg jelly domain and is disrupted by human autosomal-dominant polycystic kidney disease 1-associated mutations. Proceedings of the National Academy of Sciences *99*, 16981–16986.

Qian, F., Germino, F. J., Cai, Y., Zhang, X., Somlo, S. and Germino, G. G. (1997). PKD1 interacts with PKD2 through a probable coiled-coil domain. Nature Genetics *16*, 179–183.

Rayner, H., Thomas, M. and Milford, D. (2015). Kidney Anatomy and Physiology. In Understanding Kidney Diseases pp. 1–10. Springer International Publishing.

Reeders, S. T. (1992). Multilocus polycystic disease. Nature Genetics *1*, 235–237.

Reif, G. A., Yamaguchi, T., Nivens, E., Fujiki, H., Pinto, C. S. and Wallace, D. P. (2011). Tolvaptan inhibits ERK-dependent cell proliferation, Cl- secretion, and in vitro cyst growth of human ADPKD cells stimulated by vasopressin. American Journal of Physiology-Renal Physiology *301*, F1005–F1013.

Rohatgi, R., Milenkovic, L. and Scott, M. P. (2007). Patched1 Regulates Hedgehog Signaling at the Primary Cilium. Science *317*, 372–376.

Roitbak, T., Ward, C. J., Harris, P. C., Bacallao, R., Ness, S. A. and Wandinger-Ness, A. (2004). A Polycystin-1 Multiprotein Complex Is Disrupted in Polycystic Kidney Disease Cells. Molecular Biology of the Cell *15*, 1334–1346.

Saito, S., Tampe, B., Mueller, G. A. and Zeisberg, M. (2015). Primary cilia modulate balance of canonical and non-canonical Wnt signaling responses in the injured kidney. Fibrogenesis and tissue repair *8*, 6.

Sandford, R., Sgotto, B., Aparicio, S., Brenner, S., Vaudin, M., Wilson, R. K., Chissoe, S., Pepin, K., Bateman, A., Chothia, C., Hughes, J. and Harris, P. (1997). Comparative Analysis of the Polycystic Kidney Disease 1 (PKD1) Gene Reveals an Integral Membrane Glycoprotein with Multiple Evolutionary Conserved Domains. Human Molecular Genetics *6*, 1483–1489.

Scheffers, M. S., van der Bent, P., Prins, F., Spruit, L., Breuning, M. H., Litvinov, S. V., de Heer, E. and Peters, D. J. (2000). Polycystin-1, the product of the polycystic kidney disease 1 gene, co-localizes with desmosomes in MDCK cells. Human molecular genetics *9*, 2743–2750.

Schmidt, R. F., Lang, F. and Heckmann, M. (2011). Physiologie des Menschen. Springer-Verlag GmbH.

Schneider, L., Clement, C. A., Teilmann, S. C., Pazour, G. J., Hoffmann, E. K., Satir, P. and Christensen, S. T. (2005). PDGFR-alpha Signaling Is Regulated through the Primary Cilium in Fibroblasts. Current Biology *15*, 1861–1866.

Shamshirsaz, A., Bekheirnia, R. M., Kamgar, M., Johnson, A. M., Mcfann, K., Cadnapaphornchai, M., Haghighi, N. and Schrier, R. W. (2005). Autosomal-dominant polycystic kidney disease in infancy and childhood: Progression and outcome11See Editorial by Steinman, p. 2398. Kidney International *68*, 2218–2224.

Sharman, A. and Low, J. (2008). Vasopressin and its role in critical care. Continuing Education in Anaesthesia Critical Care and Pain *8*, 134–137.

Shen, P. S., Yang, X., DeCaen, P. G., Liu, X., Bulkley, D., Clapham, D. E. and Cao, E. (2016). The Structure of the Polycystic Kidney Disease Channel PKD2 in Lipid Nanodiscs. Cell *167*, 763–773.e11.

Smyth, J. T., Hwang, S.-Y., Tomita, T., DeHaven, W. I., Mercer, J. C. and Putney, J. W. (2010). Activation and regulation of store-operated calcium entry. Journal of cellular and molecular medicine *14*, 2337–2349.

Streets, A. J., Moon, D. J., Kane, M. E., Obara, T. and Ong, A. C. M. (2006). Identification of an N-terminal glycogen synthase kinase 3 phosphorylation site which regulates the functional localization of polycystin-2 in vivo and in vitro. Human molecular genetics *15*, 1465–1473.

Su, Q., Hu, F., Ge, X., Lei, J., Yu, S., Wang, T., Zhou, Q., Mei, C. and Shi, Y. (2018). Structure of the human PKD1-PKD2 complex. Science *361*, eaat9819.

Torres, V. E., Chapman, A. B., Devuyst, O., Gansevoort, R. T., Grantham, J. J., Higashihara, E., Perrone, R. D., Krasa, H. B., Ouyang, J. and Czerwiec, F. S. (2012). Tolvaptan in Patients with Autosomal Dominant Polycystic Kidney Disease. New England Journal of Medicine *367*, 2407–2418.

Tsiokas, L., Arnould, T., Zhu, C., Kim, E., Walz, G. and Sukhatme, V. P. (1999). Specific association of the gene product of PKD2 with the TRPC1 channel. Proceedings of the National Academy of Sciences *96*, 3934–3939.

Valente, E. M., Rosti, R. O., Gibbs, E. and Gleeson, J. G. (2013). Primary cilia in neurodevelopmental disorders. Nature Reviews Neurology *10*, 27–36.

Verani, R. R. and Silva, F. G. (1988). Histogenesis of the renal cysts in adult (autosomal dominant) polycystic kidney disease: a histochemical study. Modern pathology : an official journal of the United States and Canadian Academy of Pathology, Inc *1*, 457–463.

Wallingford, J. B. and Mitchell, B. (2011). Strange as it may seem: the many links between Wnt signaling, planar cell polarity, and cilia. Genes & Development *25*, 201–213.

Wang, Q., Zheng, W., Wang, Z., Yang, J., Hussein, S., Tang, J. and Chen, X.-Z. (2015). Filamin-A Increases the Stability and Plasma Membrane Expression of Polycystin-2. PLOS ONE *10*, e0123018.

Wang, Z., Ng, C., Liu, X., Wang, Y., Li, B., Kashyap, P., Chaudhry, H. A., Castro, A., Kalontar, E. M., Ilyayev, L., Walker, R., Alexander, R. T., Qian, F., Chen, X.-Z. and Yu, Y. (2019). The ion channel function of polycystin-1 in the polycystin-1/polycystin-2 complex. EMBO reports *20*.

Wanner, A., Salathé, M. and O'Riordan, T. G. (1996). Mucociliary clearance in the airways. American Journal of Respiratory and Critical Care Medicine *154*, 1868–1902.

Wei, W., Hackmann, K., Xu, H., Germino, G. and Qian, F. (2007). Characterization of cis-autoproteolysis of polycystin-1, the product of human polycystic kidney disease 1 gene. The Journal of biological chemistry *282*, 21729–21737.

Wilkes, M., Madej, M. G., Kreuter, L., Rhinow, D., Heinz, V., Sanctis, S. D., Ruppel, S., Richter, R. M., Joos, F., Grieben, M., Pike, A. C. W., Huiskonen, J. T., Carpenter, E. P., Kuehlbrandt, W., Witzgall, R. and Ziegler, C. (2017). Molecular insights into lipid-assisted Ca2+ regulation of the TRP channel Polycystin-2. Nature Structural & Molecular Biology *24*, 123–130.

Williams, S. S., Cobo-Stark, P., Hajarnis, S., Aboudehen, K., Shao, X., Richardson, J. A., Patel, V. and Igarashi, P. (2014). Tissue-specific regulation of the mouse Pkhd1 (ARPKD) gene promoter. American Journal of Physiology-Renal Physiology *307*, F356–F368.

Witt, M. (2007). Anatomie – GK 1. Springer Medizin Verlag Heidelberg, Berlin, Heidelberg.

Wu, G., D'Agati, V., Cai, Y., Markowitz, G., Park, J. H., Reynolds, D. M., Maeda, Y., Le, T. C., Hou, H., Kucherlapati, R., Edelmann, W. and Somlo, S. (1998). Somatic inactivation of Pkd2 results in polycystic kidney disease. Cell *93*, 177–188.

Wu, G., Markowitz, G. S., Li, L., D'Agati, V. D., Factor, S. M., Geng, L., Tibara, S., Tuchman, J., Cai, Y., Park, J. H., van Adelsberg, J., Hou, H., Kucherlapati, R., Edelmann, W. and Somlo, S. (2000). Cardiac defects and renal failure in mice with targeted mutations in Pkd2. Nature Genetics *24*, 75–78.

Yamaguchi, T., Nagao, S., Wallace, D. P., Belibi, F. A., Cowley, B. D., Pelling, J. C. and Grantham, J. J. (2003). Cyclic AMP activates B-Raf and ERK in cyst epithelial cells from autosomal-dominant polycystic kidneys. Kidney International *63*, 1983–1994.

Yamaguchi, T., Wallace, D. P., Magenheimer, B. S., Hempson, S. J., Grantham, J. J. and Calvet, J. P. (2004). Calcium Restriction Allows cAMP Activation of the B-Raf/ERK Pathway, Switching Cells to a cAMP-dependent Growth-stimulated Phenotype. Journal of Biological Chemistry *279*, 40419–40430.

Yoder, B. K. (2002). The Polycystic Kidney Disease Proteins, Polycystin-1, Polycystin-2, Polaris, and Cystin, Are Co-Localized in Renal Cilia. Journal of the American Society of Nephrology *13*, 2508–2516.

Yu, Y., Ulbrich, M. H., hui Li, M., Buraei, Z., Chen, X.-Z., Ong, A. C., Tong, L., Isacoff, E. Y. and Yang, J. (2010). Structural and Molecular Basis of the Assembly of the TRPP2/PKD1 Complex. Biophysical Journal *98*, 344a.

Zhou, J. (2009). Polycystins and Primary Cilia: Primers for Cell Cycle Progression. Annual Review of Physiology *71*, 83–113.

Zoetis, T. and Hurtt, M. E. (2003). Species comparison of anatomical and functional renal development. Birth Defects Research Part B: Developmental and Reproductive Toxicology *68*, 111–120.

List of abbreviations

A	
aa	Amino acid
Amp	Ampicillin
APS	Ammonium persulfate
Arl13B	ADP-ribosylation factor-like protein 13B
ATP	Adenosine-5'-triphosphate
B	
BSA	Bovine serum albumin
*Bam*H	*Bacillus amyloliquefaciens* H
C	
Ca^{2+}	Calcium
$CaCl_2$	Calcium chloride
Cam	Chloramphenicol
Carb	Carbenicillin
cDNA	Complementary DNA
$CoCl_2$	Cobalt chloride
$CuCl_2$	Copper chloride
D	
DAPI	4',6-Diamidin-2-phenylindol
dd	Double distilled
DMEM	Dulbecco's modified eagle medium
DMSO	Disodium hydrogen phosphate dihydrate
DNA	Desoxyribonucleic acid
dNTPs	Desoxynukleosidtriphosphate
DOX	Doxycycline
DTT	Dithiothreitol

E

E. coli	*Escherichia coli*
EDTA	Ethylenediaminetetraacetic acid
EGTA	Ethylene glycol-bis(2-aminoethylether)-N,N,N´,N´-tetraacetic acid
et al.	latin: *et alia*, and others
etc.	latin *et ceterea,* and so on
EtOH	Ethanol

F

FCS	Fetal calf serum
$FeCl_3$	Iron chloride

H

h	Human *(homo sapiens)*
H_2O	Water
H_3BO_3	Boric acid
HA	Human influenza hemagglutinin
HEPES	4-(2-Hydroxyethyl)piperazine-1-ethanesulfonic acid
HF	High fidelity
*Hin*d	*Haemophilus influenzae* d
HRP	Horseradish peroxidase

I

ICC	Immunocytochemistry
IPTG	Isopropyl β-*D*-1-thiogalactopyranoside

K

kb/ kbp	Kilo base/ kilo base pairs
KCl	Potassium chloride
kg	kilogram
KH_2PO_4	Potassium dihydrogen phosphate

L

L	Liter
LB medium	Luria Bertoni- medium

M

µg	Microgram
µL	Microliter
µM	Micromolar
M	Molar
$MgCl_2$	Magnesium chloride
$MgSO_4$	Magnesium sulfate
min	Minute
mg	Miligram
mL	Milliliter
mM	Milimolar
MOPS	3-(N-morpholino)propanesulfonic acid

N

n. s.	Not significant
N	Nitrogen
NaCl	Sodium chloride
Na_2EDTA	Disodium ethylenediaminetetraacetate
ng	Nanogram
Na_2HPO_4	Disodium hydrogen phosphate
NaH_2PO_4	Sodium dihydrogen phosphate
NaP_i	Sodium phosphate
NH_4Cl	Ammonium chloride

O

o/n	Over night
OD	Optical density

P

PAGE	Polyacrylamide gel electrophoresis
PBS	Phosphate buffered saline
PCR	Polymerase chain reaction
PEI	Polyethylenimine
PFA	Paraformaldehyde
PIPES	Piperazine-N,N´-bis(2-ethanesulfonic acid)
PKD	Polycystic kidney disease
PLL	Poly-L-lysine
PMSF	Phenylmethylsulfonyl fluoride

PVDF	Polyvinylidene fluoride

R

RbCl	Rubidium chloride
RT	Room temperature

S

Sac	*Streptomyces achromogenes*
SD	Standard deviation
SDS	Sodium dodecyl sulfate

T

TAE	Tris, acetic acid, EDTA
Taq	*Thermus aquaticus*
TE	Tris-EDTA
TEMED	N,N,N,N'-Tetramethylethylenediamine
TEV	Tobacco Etch Virus
TBS	Tris buffered saline
TBS-T	Tris buffered saline, supplemented with 0.1 % Tween 20
TRP(P)	Transient receptor potential (polycystic)

U

U	Units

W

WB	Western blot
WT	Wild-type

Z

$ZnCl_2$	Zinc chloride

Appendix

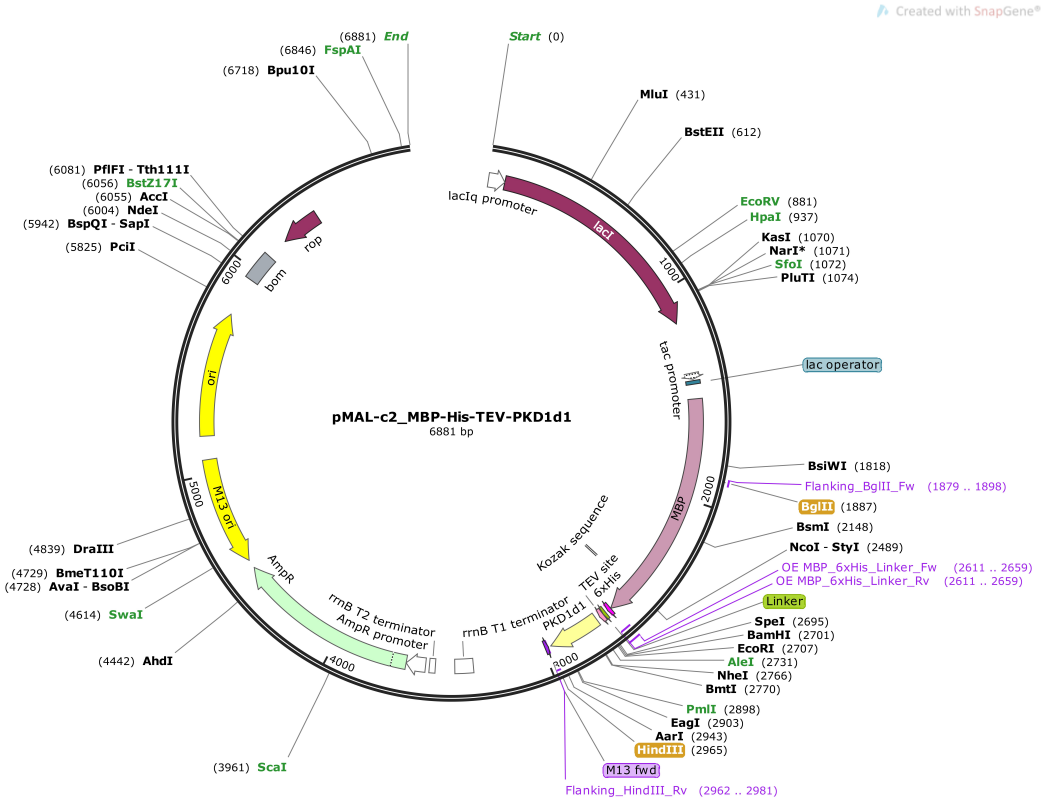

Figure 5.1: **Map of the expression vector 'pMAL-c2/MBP-His-TEV-PKD1d1'.** The constructed vector with a size of ~6.9 kb contains an MBP-tag followed by a 6x His-tag, a linker, a TEV cleavage site and the *PKD1* domain 1. For selection, an ampicillin resistance is present and induction is enabled through the lacI-repressor gene that can be inhibited by applying the artificial sugar IPTG thereby inducing a conformational change to activate the lac operator. This further on enables a binding of the T7 RNA polymerase to start transcription of the fusion protein.

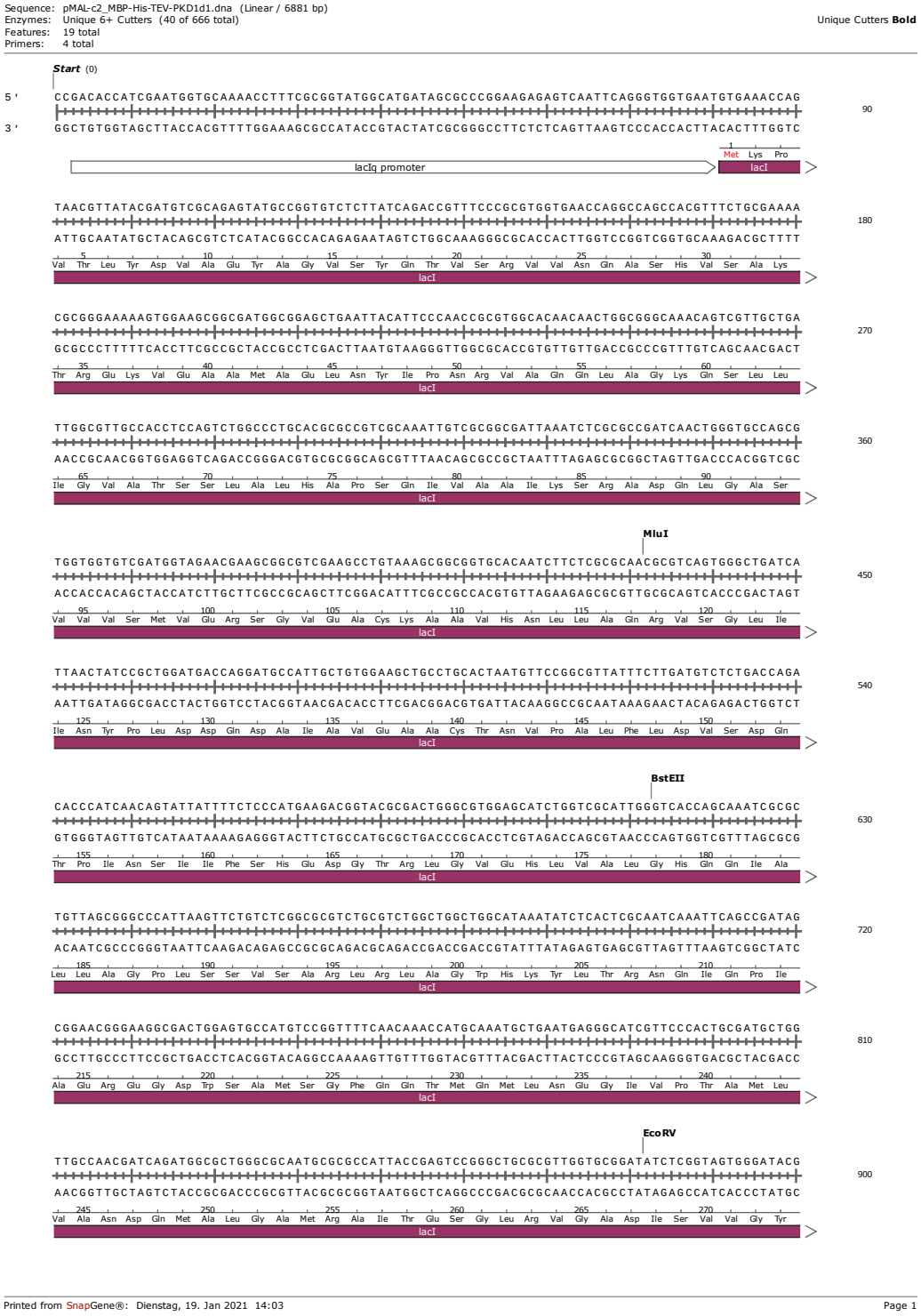

Figure 5.2: **Sequence of the 'pMAL-c2/MBP-His-TEV-PKD1d1' vector (Part I).**

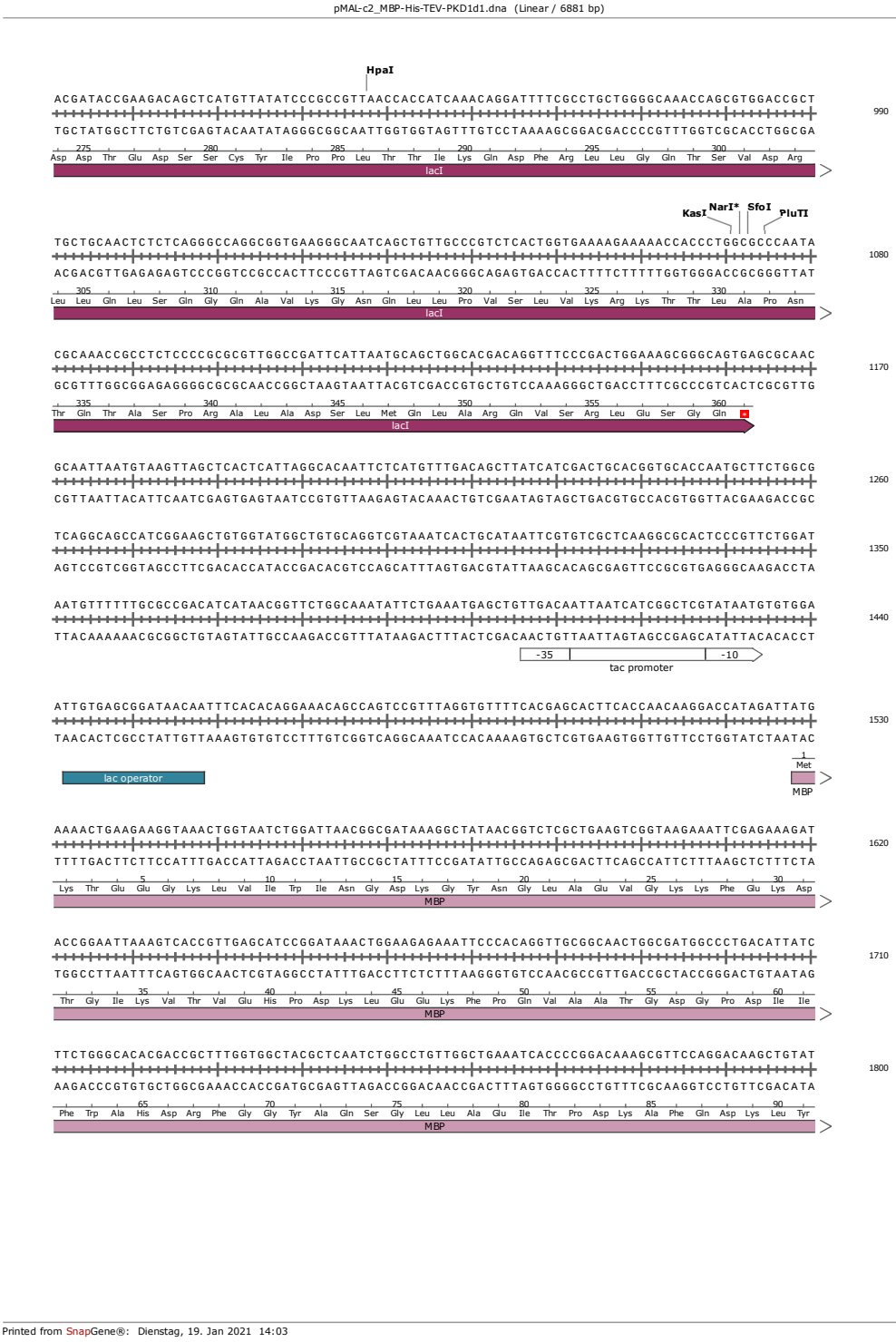

Figure 5.3: **Sequence of the 'pMAL-c2/MBP-His-TEV-PKD1d1' vector (Part II).**

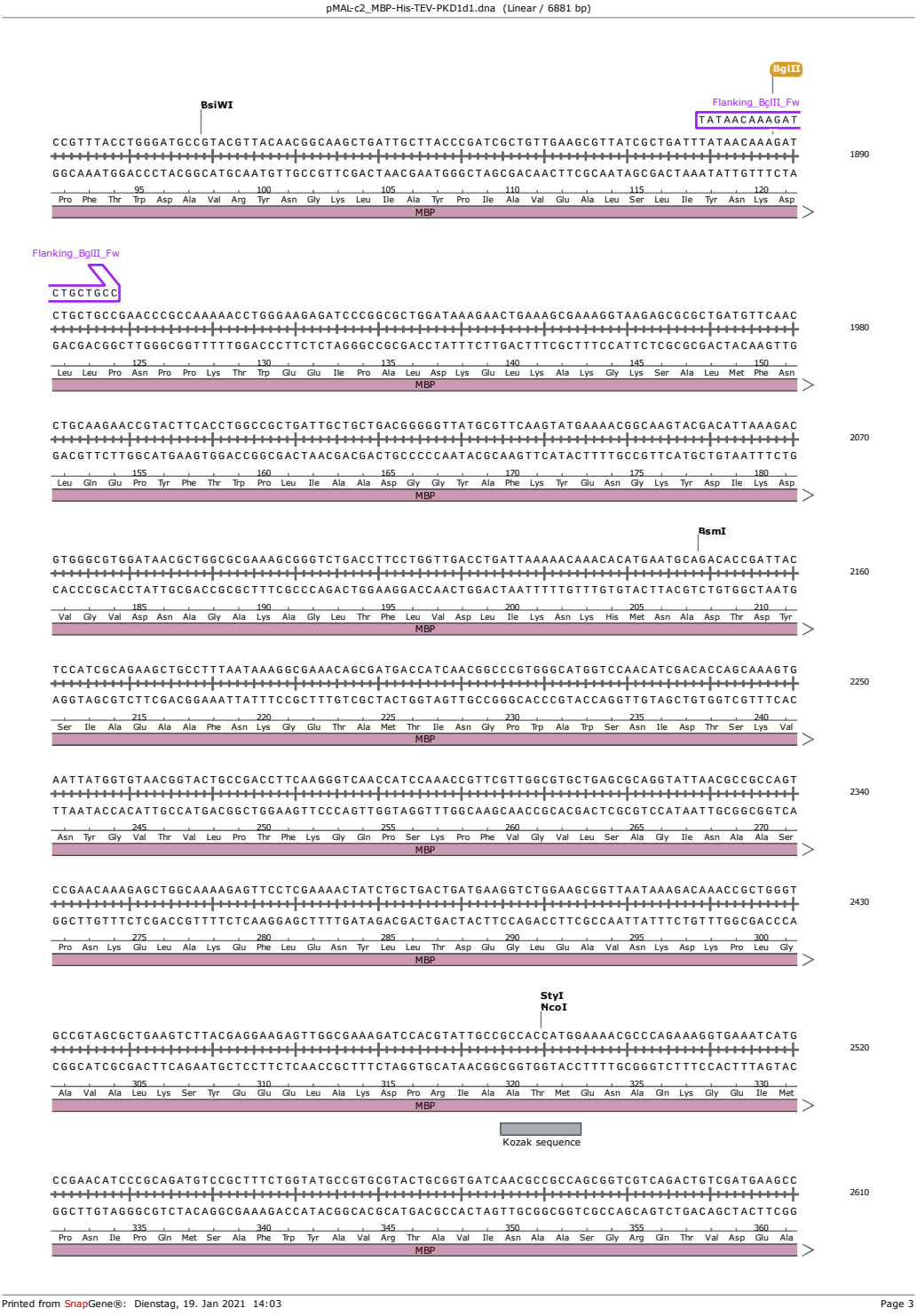

Figure 5.4: **Sequence of the 'pMAL-c2/MBP-His-TEV-PKD1d1' vector (Part III).**

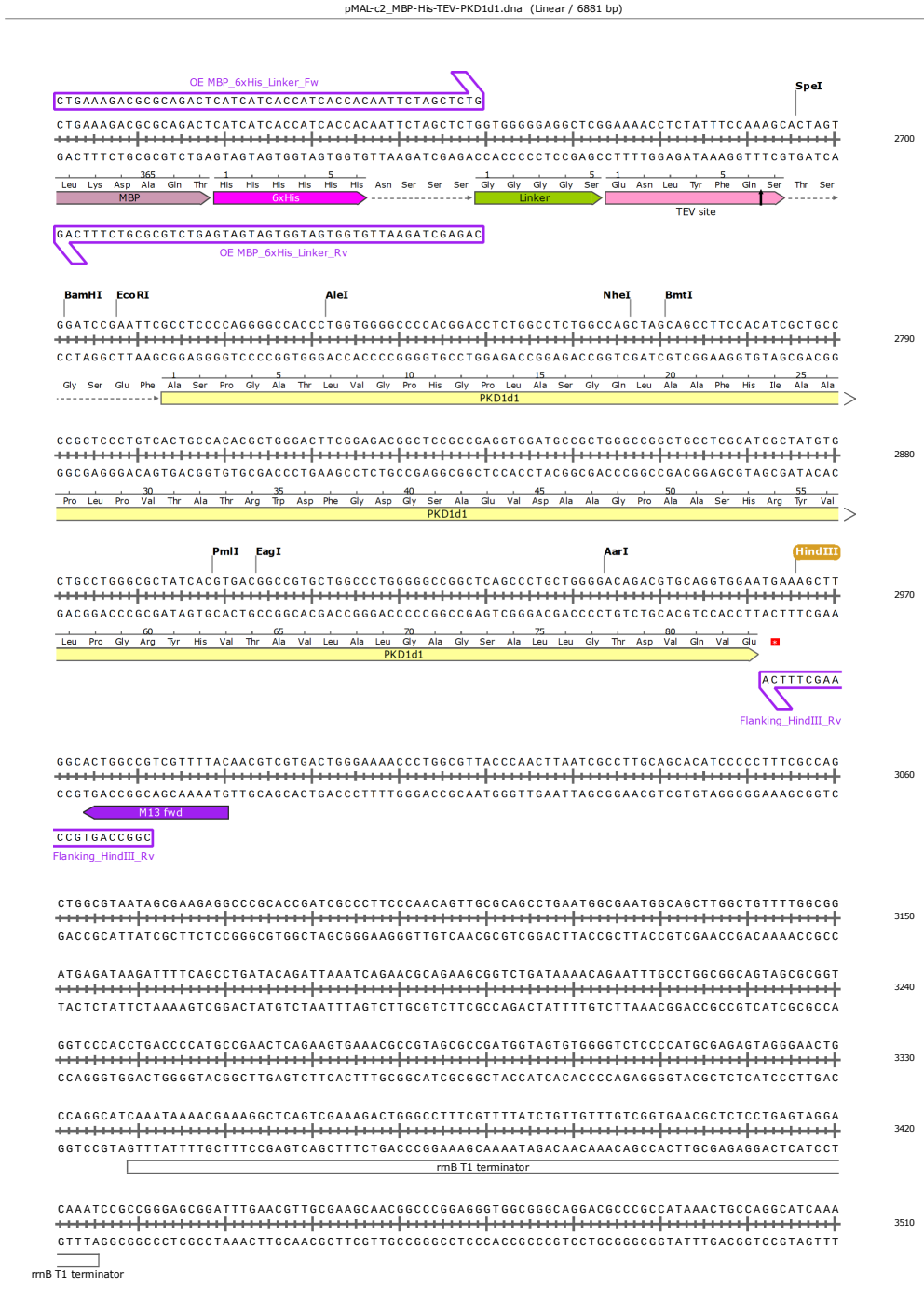

Printed from SnapGene®: Dienstag, 19. Jan 2021 14:03 Page 4

Figure 5.5: **Sequence of the 'pMAL-c2/MBP-His-TEV-PKD1d1' vector (Part IV).**

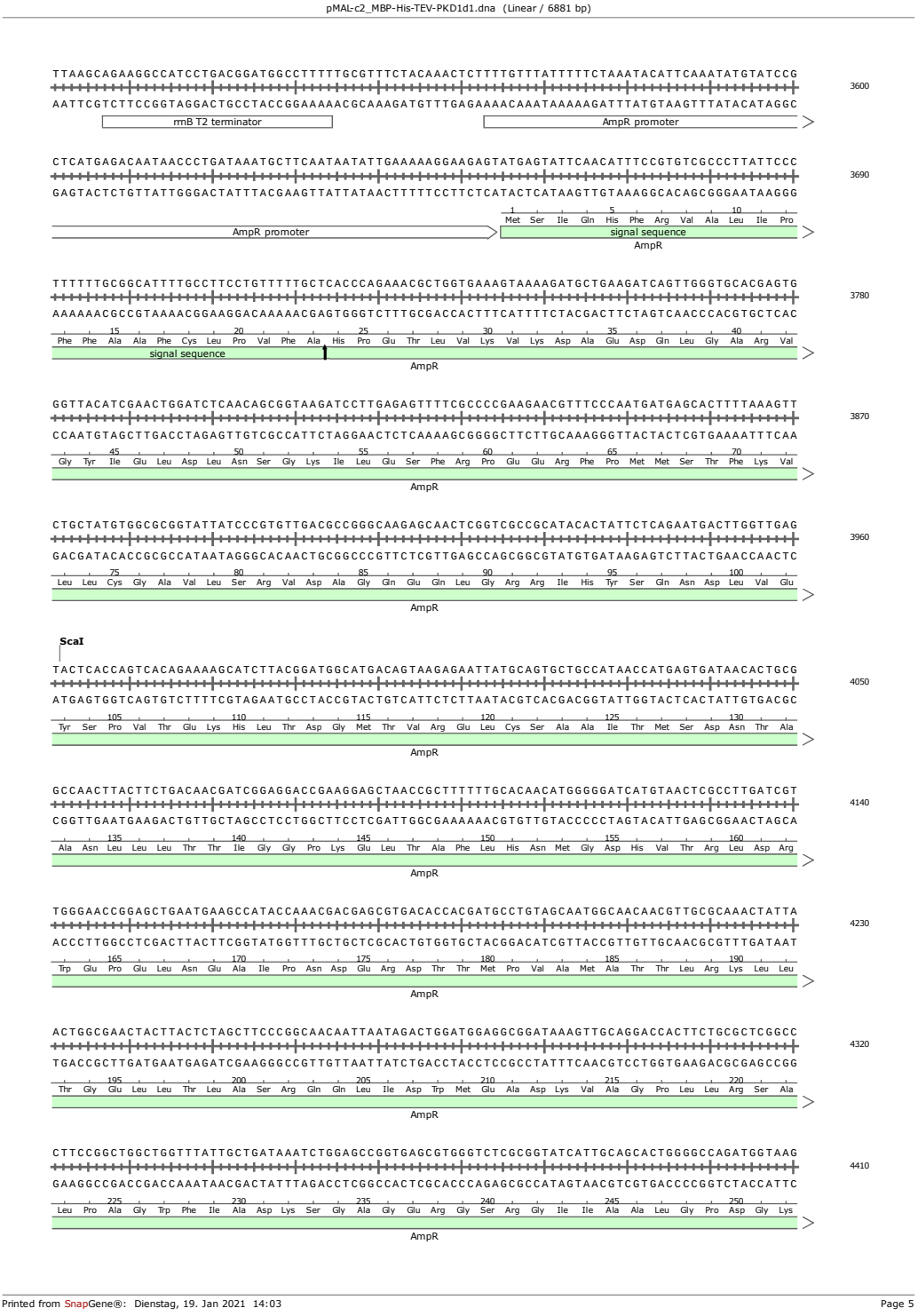

Figure 5.6: **Sequence of the 'pMAL-c2/MBP-His-TEV-PKD1d1' vector (Part V).**

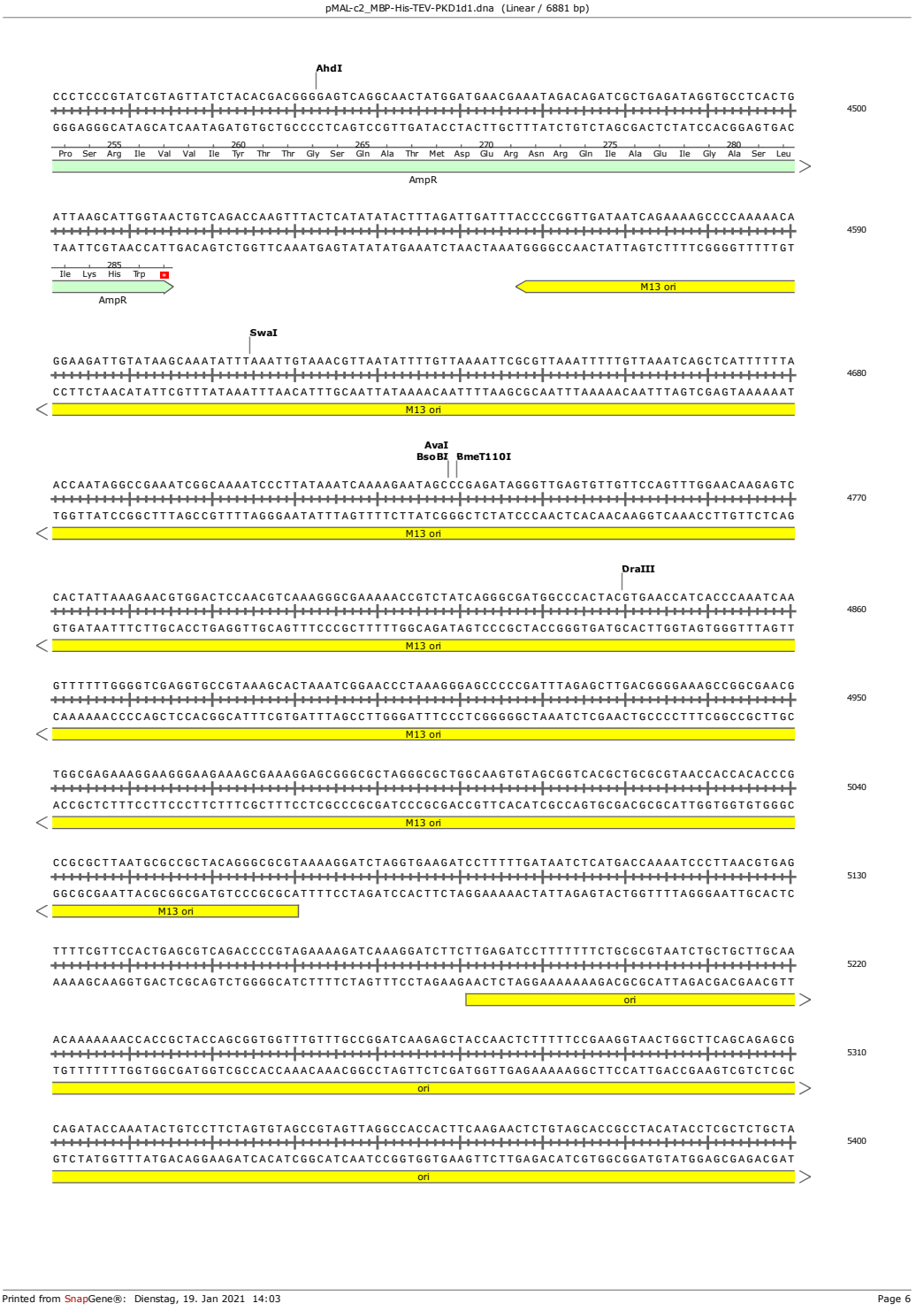

Figure 5.7: **Sequence of the 'pMAL-c2/MBP-His-TEV-PKD1d1' vector (Part VI).**

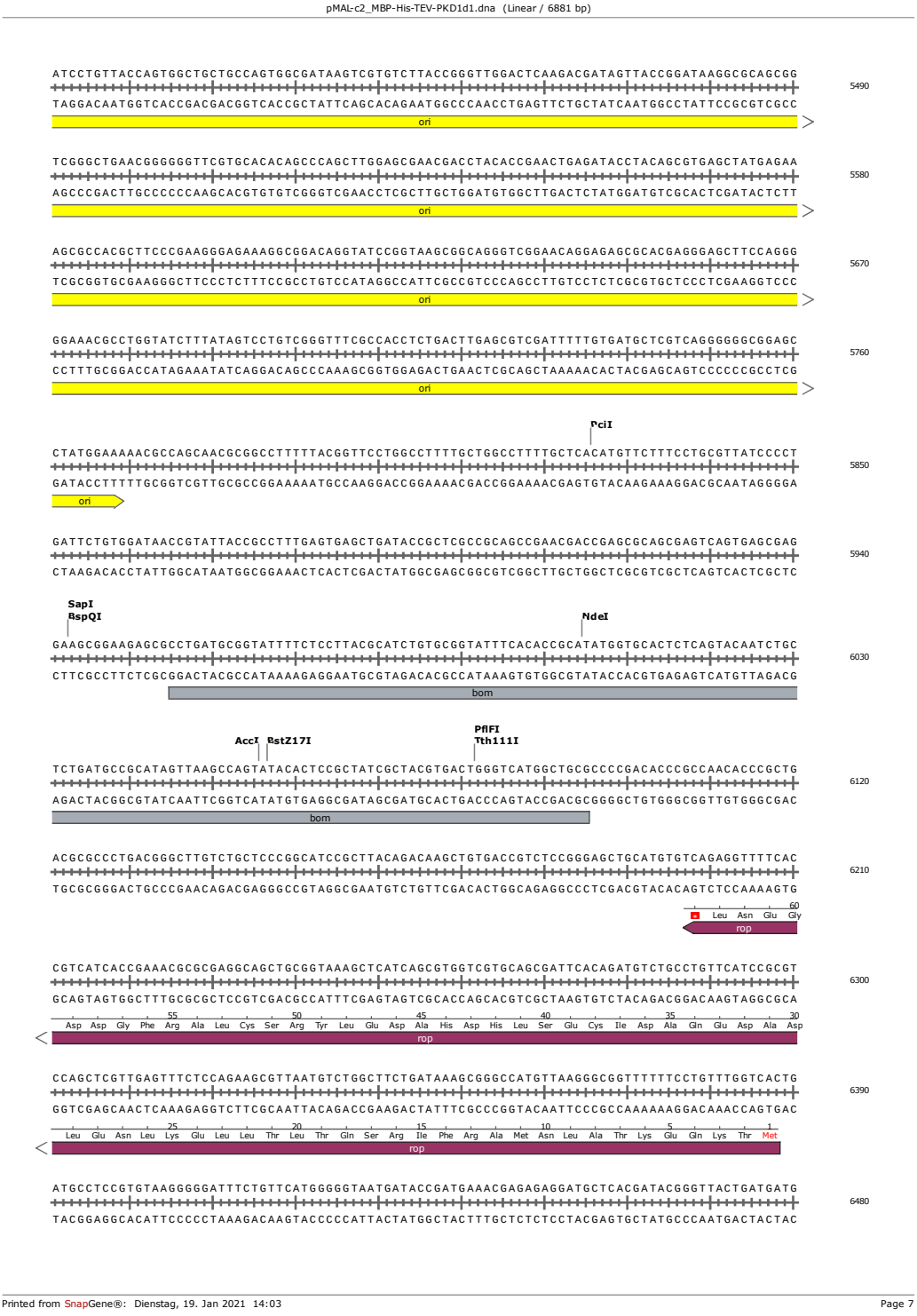

Figure 5.8: **Sequence of the 'pMAL-c2/MBP-His-TEV-PKD1d1' vector (Part VII).**

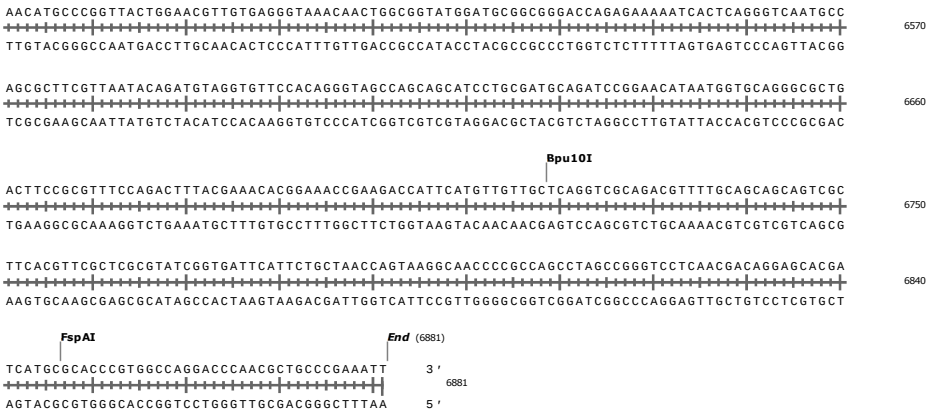

Figure 5.9: **Sequence of the 'pMAL-c2/MBP-His-TEV-PKD1d1' vector (Part VIII).**

Acknowledgements

In the last four years during my dissertation I was able to get to know many great people, whom I would like to thank in this way.

First, I would like to thank my doctoral supervisor and mentor Prof. Dr. Ralph Witzgall, whose expertise was invaluable in formulating the research questions and methodology and who has always encouraged me in my work. His informative feedback always pushed me to review and sharpen my thinking and thereby brought my work to another level.

I would like to acknowledge my mentors Prof. Dr. Christine Ziegler and Prof. Dr. Michael Wiesener for their valuable guidance throughout my studies. In addition, I would like to thank Prof. Dr. Remco Sprangers for answering all my questions and conducting the NMR measurements.

Furthermore, a huge thanks goes out to my colleagues in the lab where I always found a sympathetic ear for all major and minor problems. I was able to find not only great colleagues, but also friends who supported me in this important chapter of my life. I will always remember great sessions at lunch time where we laughed a lot while eating pizza. Along these lines I would like to address a special thanks to Dr. Lisa Lucke, Sandra Meisinger, Korbinian Bürger, Jasmin Karreis, Markus Setzer, Julia Dörr and Tim Braun.

Not to forget all the members of the working group, that supported my experiments mentally and physically: Dr. Melanie Grosch for answering all the questions that came to my mind. We helped each other wherever we could which was a great gift during this time. Dr. Kerstin Schmid, Dr. Melanie Zaparty, Prof. Dr. Silke Härteis and Prof. Dr. Reinhard Rachel for giving important advice for experiments and for the lab life. I would also like to thank Uwe deVries who measured and calculated lots of data for me, Marion Kubitza and Lucia Denk who helped enormously when preparing and collecting these tiny little collecting ducts, Larissa Osten for always offering a helping hand when needed, Felix Fischer from Prof. Dr. Ziegler's lab for conducting size exclusion chromatography and Helga Othmen for having exhilarative talks in the Thermo-Room when I was measuring calcium levels while she was recording electron micrographs. Furthermore, I'd like to thank my students that contributed to this work: Marie-Sophie Dürr, Regina Hüttner and Thi Truc Quynh Nguyen for doing a great job in the lab.

I would also like to thank my husband Matthias (DPS god), my friends and my family who have always been there for me during this intense but interesting time.

These four years will always be an unforgettable experience in this chapter of my life.

Eidesstattliche Erklärung

Ich, Katrin Brunner, geb. Pohl, erkläre hiermit an Eides statt, dass ich die vorliegende Arbeit ohne unzulässige Hilfe Dritter und ohne Benutzung anderer als der angegebenen Hilfsmittel angefertigt habe. Die aus anderen Quellen direkt oder indirekt übernommenen Daten und Konzepte sind unter Angabe des Literaturzitats gekennzeichnet.

Bei der Auswahl und Auswertung folgenden Materials haben mir keine zusätzlichen Personen in der jeweils beschriebenen Weise entgeltlich/unentgelt-lich geholfen.

Weitere Personen waren an der inhaltlich-materiellen Herstellung der vorliegenden Arbeit nicht beteiligt. Insbesondere habe ich hierfür nicht die entgeltliche Hilfe eines Promotionsberaters oder anderer Personen in Anspruch genommen. Niemand hat von mir weder unmittelbar noch mittelbar geldwerte Leistungen für Arbeiten erhalten, die im Zusammenhang mit dem Inhalt der vorgelegten Dissertation stehen.

Die Arbeit wurde bisher weder im In- noch im Ausland in gleicher oder ähnlicher Form einer anderen Prüfungsbehörde vorgelegt.

Unterschrift: